

INFORMATION TO USERS

This manuscript has been reproduced from the microfilm master. UMI films the text directly from the original or copy submitted. Thus, some thesis and dissertation copies are in typewriter face, while others may be from any type of computer printer.

The quality of this reproduction is dependent upon the quality of the copy submitted. Broken or indistinct print, colored or poor quality illustrations and photographs, print bleedthrough, substandard margins, and improper alignment can adversely affect reproduction.

In the unlikely event that the author did not send UMI a complete manuscript and there are missing pages, these will be noted. Also, if unauthorized copyright material had to be removed, a note will indicate the deletion.

Oversize materials (e.g., maps, drawings, charts) are reproduced by sectioning the original, beginning at the upper left-hand corner and continuing from left to right in equal sections with small overlaps. Each original is also photographed in one exposure and is included in reduced form at the back of the book.

Photographs included in the original manuscript have been reproduced xerographically in this copy. Higher quality 6" x 9" black and white photographic prints are available for any photographs or illustrations appearing in this copy for an additional charge. Contact UMI directly to order.

UMI

A Bell & Howell Information Company
300 North Zeeb Road, Ann Arbor MI 48106-1346 USA
313/761-4700 800/521-0600

**EXPERIMENTAL AND COMPUTATIONAL
INVESTIGATIONS OF THE STABILITY AND DYNAMICS OF
CYTOCHROME b₅**

by

Elizabeth Marie Storch

A dissertation submitted in partial fulfillment of the
requirements for the degree of

Doctor of Philosophy

University of Washington

1998

Approved by William M. Atkins
Chairpersons of Supervisory Committee

Valerie Laggett

Program Authorized
to Offer Degree Medicinal Chemistry

Date March 3, 1998

UMI Number: 9826368

**Copyright 1998 by
Storch, Elizabeth Marie**

All rights reserved.

**UMI Microform 9826368
Copyright 1998, by UMI Company. All rights reserved.**

**This microform edition is protected against unauthorized
copying under Title 17, United States Code.**

UMI
300 North Zeeb Road
Ann Arbor, MI 48103

© Copyright 1998

Elizabeth Marie Storch

Doctoral Dissertation

In presenting this dissertation in partial fulfillment of the requirements for the Doctoral degree at the University of Washington, I agree that the Library shall make its copies freely available for inspection. I further agree that extensive copying of this dissertation is allowable only for scholarly purposes, consistent with "fair use" as prescribed in the U.S. Copyright Law. Requests for copying or reproduction of this dissertation may be referred to University Microfilms, 1490 Eisenhower Place, P.O. Box 975, Ann Arbor, MI 48106, to whom the author has granted "the right to reproduce and sell (a) copies of the manuscript in microform and/or (b) printed copies of the manuscript made from microform."

Signature *Elizabeth Marie Spach*
Date 3-3-98

University of Washington

Abstract

**EXPERIMENTAL AND COMPUTATIONAL INVESTIGATIONS OF
THE STABILITY AND DYNAMICS OF CYTOCHROME b_5**

by Elizabeth Marie Storch

Chairpersons of the Supervisory Committee: Associate Professor William M. Atkins and
Associate Professor Valerie Daggett
Department of Medicinal Chemistry

Both computational and experimental approaches were used to study cytochrome b_5 . The goal was to investigate protein dynamics and how they may relate to stability and biological function.

Computational studies used molecular dynamics simulations to model the solution structure of cytochrome b_5 . Simulations revealed conformational changes on the protein surface that resulted in the periodic formation of a large cleft. The cleft was located near acidic residues implicated in electrostatic-based protein-protein recognition and complex formation.

Simulations of rat and bovine apocytochrome b_5 were performed to investigate structural consequences of heme removal and the effects of species sequence differences. The simulated rat apoprotein was in good agreement with experimental data, while the variant residues were responsible for the simulated bovine apoprotein deviations from rat experimental data. In both proteins, core 1 exhibited increased mobility, and loss of secondary structure, while core 2 was well maintained and retained native-like structure.

Based on the results from the holocytochrome b_5 simulations, S18D and S18C/R47C mutant proteins were modeled, constructed using site-directed mutagenesis, and then experimentally tested to determine if mutations spanning the cleft region could affect the predicted dynamics.

Thermodynamic stability of the proteins in the presence of increasing urea or temperature was studied using absorbance and fluorescence spectroscopies. The mutations had modest effects on heme binding; however, they had pronounced effects on the conformational dynamics prior to heme release. The two spectroscopies supported a complex, three-state denaturation pathway, in contrast to the currently proposed two-state model.

Fluorescence was used to determine mutational effects on protein dynamics. Steady-state measurements showed blue-shifted spectra for the mutants. Acrylamide quenching revealed decreased K_{SV} values in the mutants, particularly for S18C/R47C at 50 °C. Bimolecular rate constants were calculated from life-time measurements, and at 50 °C, S18C/R47C had a lower rate constant relative to wild-type.

Observations from the computational and experimental studies showed the two techniques to be complementary, and the final results would not have been achieved using one technique over the other. Observed differences between the proteins were consistent with the hypothesis that rationally designed mutations may affect localized dynamics and stability in cytochrome b_5 .

TABLE OF CONTENTS

LIST OF FIGURES	iv
LIST OF TABLES	vi
CHAPTER 1: INTRODUCTION.....	1
1.1 Introduction	1
1.2 Cytochrome b ₅ Background.....	2
1.3 Molecular Dynamics and Fluorescence Spectroscopy.....	4
1.3.1 Molecular Dynamics Background	4
1.3.2 Fluorescence Spectroscopy Background	8
1.4 Thesis Outline.....	15
CHAPTER 2: MOLECULAR DYNAMICS SIMULATION OF	
 CYTOCHROME b₅: IMPLICATIONS FOR PROTEIN-	
 PROTEIN RECOGNITION.....	16
2.1 Introduction	16
2.2 Methods.....	20
2.3 Results	22
2.3.1 Overall Structure.....	22
2.3.2 Internal Motion.....	24
2.3.3 Secondary Structure.....	26
2.3.4 NOE Connectivities	28
2.3.5 Protein Surface.....	29
2.4 Discussion.....	36

CHAPTER 3: STRUCTURAL CONSEQUENCES OF HEME REMOVAL: MOLECULAR DYNAMICS SIMULATIONS OF RAT AND BOVINE APOCYTOCHROME b₅	44
3.1 Introduction	44
3.2 Methods.....	48
3.3 Results	49
3.3.1 Rat Apocytochrome b ₅ : Tertiary Structure.....	49
3.3.2 Secondary Structure.....	54
3.3.3 Bovine Apocytochrome b ₅ : Tertiary Structure	58
3.3.4 Secondary Structure.....	59
3.3.5 Structural Effects of Variant Residues	60
3.4 Discussion.....	62
3.4.1 Rat Apocytochrome b ₅	63
3.4.2 Bovine Apocytochrome b ₅ and Structural Effects of the Variant Residues	65
3.5 Conclusions	67
CHAPTER 4: ENGINEERING OUT MOTION: INTRODUCTION OF A <i>DE NOVO</i> DISULFIDE BOND AND A SALT BRIDGE DESIGNED TO CLOSE A PUTATIVE DYNAMIC CLEFT ON THE SURFACE OF CYTOCHROME b₅	69
4.1 Introduction	69
4.2 Materials and Methods	73
4.3 Results	78
4.3.1 Molecular Dynamics Characterization of Wild-type and Mutant Proteins	78

4.3.2	Experimental Characterization of Oxidized and Reduced Forms of the Disulfide Mutant	81
4.3.3	Urea and Thermal Denaturation Detected by Heme Absorbance	83
4.3.4	Urea and Thermal Denaturation Detected by Tryptophan Fluorescence	86
4.4	Discussion	92
4.4.1	MD Simulations	93
4.4.2	Experimental Mutational Effects on Heme Binding	94
4.4.3	Experimental Mutational Effects at the Interface of Cores 1 and 2	95
4.4.4	Differences Between Absorbance and Fluorescence Results Prior to Heme Release	96
4.5	Conclusions	97
CHAPTER 5: PROBING THE DYNAMICS OF A CLEFT ON THE SURFACE OF CYTOCHROME b_5 THROUGH STEADY-STATE AND TIME-RESOLVED FLUORESCENCE		100
5.1	Introduction	100
5.2	Materials and Methods	104
5.3	Results	106
5.3.1	Steady-State Fluorescence and Acrylamide Quenching	106
5.3.2	Fluorescence Lifetimes	109
5.4	Discussion	112
5.5	Conclusions	115
BIBLIOGRAPHY		116

LIST OF FIGURES

1.1	Ribbon diagram of holocytochrome b_5	3
1.2	Protein in a box of water	6
1.3	Jablonski diagram.....	8
1.4	Modified Jablonski diagram depicting solvent relaxation	10
1.5	Modified Jablonski diagram depicting quenching.....	11
1.6	Frequency-domain fluorescence schematic	14
1.7	Time-domain fluorescence schematic.....	14
2.1	Ribbon diagram of holocytochrome b_5	19
2.2	C_α RMS deviation of holocytochrome b_5 from crystal structure.....	23
2.3	Contour plot of C_α RMS deviation of holocytochrome b_5	23
2.4	Mainchain traces from holocytochrome b_5 MD simulation and C_α RMS fluctuations plot.....	25
2.5	Space-filling snapshots from holocytochrome b_5 MD simulation highlighting acidic residues	31
2.6	Space-filling snapshots from holocytochrome b_5 MD simulation highlighting cleft formation.....	32
2.7	Distance between Ser 18 and Ala 50 during holocytochrome b_5 MD simulation	33
2.8	Stereo diagram of C_α backbone of crystal structure and 1.66 ns MD simulation snapshot.....	43
3.1	Ribbon diagram of apocytochrome b_5 with variant rat and bovine residues	45
3.2	C_α RMS deviation of rat and bovine apocytochrome b_5 from crystal structure	50
3.3	Contour plot of C_α RMS deviation of apocytochrome b_5	51
3.4	C_α RMS fluctuations of apocytochrome b_5	51

3.5	Mainchain traces from rat and bovine holocytochrome b ₅ MD simulations	53
3.6	Space-filling snapshots highlighting variant residues.....	62
4.1	Ribbon diagram of cytochrome b ₅ with Ser 18, Trp 22, Arg 47, and heme displayed	70
4.2	Space-filling representations depicting control of the “opened” and “closed” conformations of the cleft in the wild-type, S18D, S18C/R47C _{ox} , and S18C/R47C _{red} MD simulations	71
4.3	Mainchain C _α RMS fluctuation traces from 25 °C and 50 °C MD simulations of wild-type, S18D, S18C/R47C _{ox} , and S18C/R47C _{red}	80
4.4	Positive-ion MALDI mass spectra of S18C/R47C.....	82
4.5	Urea and temperature denaturation as a function of absorbance.....	84
4.6	Steady-state fluorescence emission spectra	86
4.7	Urea denaturation as a function of fluorescence.....	89
4.8	Temperature denaturation as a function of fluorescence.....	90
4.9	Mainchain C _α traces of wild-type cytochrome b ₅ along the denaturation pathway: A three-state model.....	98
5.1	Ribbon diagram of cytochrome b ₅ with Ser 18, Trp 22, Arg 47, and heme displayed	102
5.2	Space-filling representations depicting the “opened” and “closed” conformations of the cleft in the wild-type MD simulation	102
5.3	Normalized steady-state fluorescence emission spectra of wild-type, S18D, S18C/R47C _{ox} , and S18C/R47C _{red}	107
5.4	Stern-Volmer plots at 5 °C, 35 °C, and 50 °C	108
5.5	Phase and modulation data for wild-type and S18C/R47C _{ox} at 50 °C.....	110

LIST OF TABLES

2.1	Secondary structure content of holocytochrome b_5 as a function of time	27
2.2	Change in solvent-exposed surface area of residues located in cleft region.....	35
3.1	Secondary structure content of apocytochrome b_5 during MD simulations	56
4.1	Thermodynamic parameters for urea and thermal denaturation determined by absorbance spectroscopy	85
4.2	Thermodynamic parameters for urea and thermal denaturation determined by fluorescence spectroscopy	91
5.1	Acrylamide quenching parameters for cytochrome b_5	109
5.2	Fluorescence lifetime data analysis	111

ACKNOWLEDGMENTS

I sincerely thank the following people who aided in my graduation education and research and provided an enjoyable environment which I will certainly miss: Dr. Darwin O.V. Alonso, Andrew Bird, Michael Dabrowski, Dr. Eric Dietze, Steven Kazmirski, Luke Koenigs, Dr. Keith Laidig, Dr. Aijun Li, and Dr. Raimund Peter. I would like to give special thanks to my advisors, Dr. Bill Atkins and Dr. Valerie Daggett, for their enthusiasm and guidance.

DEDICATION

To my parents, Adam and Maria Storch,

and David Goldberg

whose never ending emotional support made this all possible.

CHAPTER 1

INTRODUCTION

1.1 Introduction

Computer simulations have become a popular method to investigate the dynamic behavior and conformational transitions of proteins in aqueous environments. More specifically, molecular dynamics (MD) simulations are used to describe the motion of all the atoms of a protein as a function of time at a specified temperature. This method can be very powerful because it provides a picture of all atomic interactions -- something that is often obscured in experimental work. MD, however, is not without weaknesses, and it is necessary to provide experimental data for verification of the results. This dependency makes the experimental and computational methods very complementary. Computer technology has advanced to the point where we are now making predictions from MD simulations and testing them experimentally in the lab. The thesis presented here began with an MD computer simulation of a protein, cytochrome b_5 , in a box of water, that led to predictions which were tested experimentally. Furthermore, additional computer simulations and modeling studies were used to aid in interpretation of the experimental results. The following pages of the introduction are intended to provide background information on cytochrome b_5 . In addition, the predominant techniques used, MD simulations and fluorescence spectroscopy, are discussed in detail, as they relate to protein dynamics.

1.2 Cytochrome b_5 Background

Cytochrome b_5 is a heme containing protein that accepts and transfers electrons with a variety of redox protein partners (Figure 1.1). It naturally occurs in both soluble and membrane bound forms. The soluble form is found in erythrocytes and functions to reduce hemoglobin (Hultquist et al., 1974; Hultquist and Passon, 1971). The membrane bound form is located in the endoplasmic reticulum (ER) or mitochondria. In the ER, ferric cytochrome b_5 is reduced by either NADH-cytochrome b_5 reductase or NADPH-cytochrome P450 reductase. The ferrous form of the protein reduces various fatty acyl coenzyme A desaturases for the biosynthesis of selected lipids (Okayasu et al., 1977; Strittmatter et al., 1974) and donates the second electron to certain P450s in their catalytic reaction cycle (Okayasu et al., 1977; Strittmatter et al., 1974). In the mitochondria, cytochrome b_5 participates in electron transfer from NADH to cytochrome c oxidase via cytochrome c (Bernardi and Azzone, 1981). Cytochrome b_5 has been most extensively studied as a soluble tryptic fragment. This form of the protein retains the heme and transfers electrons, *in vitro*, with both physiological and non-physiological redox partners. For example, ferricytochrome b_5 receives electrons from tryptic-solubilized NADH-cytochrome b_5 reductase (Dailey and Strittmatter, 1979) and the ferrous protein transfers electrons to cytochrome c (Ng et al., 1977; Stonehuerner et al., 1979; Strittmatter, 1964). Because cytochrome b_5 participates in electron-transfer reactions with a variety of different proteins, it is of great interest to determine how this protein might discern between structurally varied proteins.

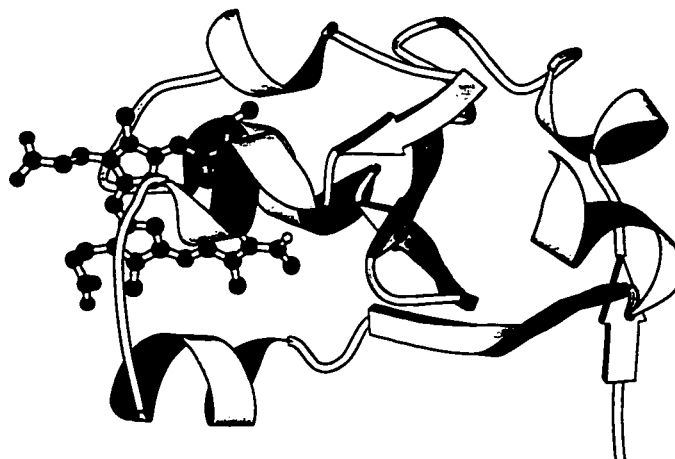


Figure 1.1: Ribbon diagram of the crystal structure of cytochrome b₅ including the prosthetic heme group (Mathews et al., 1972). The residues involved in secondary structure are given in the following figures (Figure 2.1, Figure 3.1, Figure 4.1, and Figure 5.1).

The solution structure of tryptic-solubilized cytochrome b₅ has been studied experimentally both with and without the prosthetic heme group. Two- and three-dimensional NMR studies of the holoprotein suggest that the solution structure closely resembles the crystal structure, although it is more dynamic in character [ferroprotein: (Guiles et al., 1990; Guiles et al., 1992); ferriprotein: (Muskett et al., 1996)]. Using one- and two-dimensional NMR, Moore and Lecomte found a stable hydrophobic cluster in apocytochrome b₅ -- a key structural element of the second core (Moore and Lecomte, 1990). In the apoprotein, core 1 is only partially “structured” and fluctuates between

several conformations (Falzone et al., 1996; Moore et al., 1991; Moore and Lecomte, 1993; Storch and Daggett, 1996).

The equilibrium conformational stability of tryptic-solubilized ferri- and ferrocycytochrome b_5 has previously been studied. Pfeil and Bendzko (Pfeil and Bendzko, 1980) investigated the thermal stability of the ferriprotein by scanning calorimetry, circular dichroism, and absorption spectroscopy. In addition, thermal unfolding of the ferriprotein was probed with resonance Raman and absorption spectroscopy by Kitagawa and others (Kitagawa et al., 1982). Using absorption spectroscopy and NMR methods, Newbold and others determined that ferrocycytochrome b_5 has a T_m 6 °C higher than the ferric protein (Hewson et al., 1993; Newbold et al., 1992; Newbold and Whitford, 1997). In all cases, the previous investigators determined the thermodynamic stability of cytochrome b_5 based on structural changes that occurred in the vicinity of the prosthetic heme group.

1.3 Molecular Dynamics and Fluorescence Spectroscopy

Because MD and fluorescence spectroscopy are the predominant techniques utilized in this thesis, a review of their theory and practice is provided in the following sections.

1.3.1 Molecular Dynamics Background

MD is a method in which a trajectory describing the motion of a molecule is determined mathematically. The positions of each of the atoms are based on the results from classical mechanics equations and, hence, no covalent bonds are formed or broken during the simulation. The physical properties of each of the atoms and their interactions with water determine the behavior of the molecule in solution. Important noncovalent

interactions that contribute to the trajectory include hydrogen bonding, van der Waals, and electrostatic. Before an MD simulation of a protein can be successfully performed, a starting structure, potential energy function (U), or force field, and experimental data for comparison are needed. The three-dimensional coordinates of the protein are usually obtained from the X-ray crystal structure or NMR-derived model of the solution structure and used as the starting position for the simulation. The potential function describes the potential energy of a protein as a function of the atomic positions, and is generally described by the following bonded and nonbonded terms:

$$U = \sum K_b(b-b_0)^2 + \sum K_\theta(\Theta-\Theta_0)^2 + \sum K_\phi[1-\cos(n(\phi-\phi_0))] + \sum A/r^{12}-B/r^6 + \sum q_1q_2/r$$

bond	bond	torsion	nonbonded	partial
lengths	angles	angles	pairs	charges

The potential function accounts for changes in bond lengths, bond angles, torsion angles, and interatomic distances. The first three terms describe bonded interactions (i.e. atoms that are separated by up to three bonds), while the last two terms describe nonbonded interactions. For the first two terms, b_0 and Θ_0 are ideal bond lengths and angles. These two functions are each represented by a quadratic function with force constant K . The third term, is represented by a cosine function with barrier height K_ϕ , periodicity n , and minimum angle ϕ_0 . The fourth term describes the van der Waal's interactions as described by the Lennard-Jones potential. In this function there is a short-range repulsive term, A/r^{12} , and a long-range term, B/r^6 , describing weak attraction between atoms. The last nonbonded term is represented by Coulomb's Law and accounts for electrostatic

interactions. The charges, q , separated by a distance, r , can be any combination of positive and negative charges describing both attractive and repulsive interactions. A more detailed, technical description is available elsewhere (Levitt, 1989; Levitt et al., 1995; Levitt et al., 1997; Levitt and Meirovitch, 1983). Correlation of MD with experimental data determines the reliability or validity of an MD simulation. Typically, experimental data describe the properties or behavior of proteins in solution and are usually obtained by such methods as NMR, CD, differential scanning calorimetry, absorbance and fluorescence spectroscopy. Additionally, analysis of the simulation may rely on comparison to the X-ray crystal structure.

A simulation is begun by solvating the three-dimensional starting structure in a box of water molecules 8 Å or more from any protein atom (Figure 1.2).

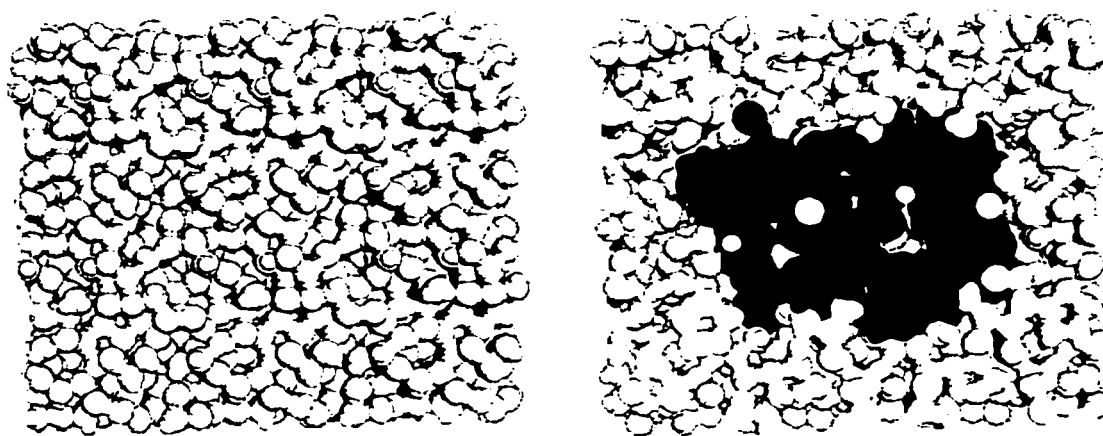


Figure 1.2: The box of water that is constructed upon solvation of a protein molecule. On the right, a slice of the box is removed in order to show the protein, depicted in blue.

The velocities of the atoms are slowly increased from zero to values corresponding to a specified temperature defined by the user. The initial velocities are assigned from a Maxwellian distribution. The velocities, v , are related to the absolute temperature, T , by the equipartition theorem:

$$1/2 m v^2 = 3/2 N k_B T$$

The force, F , on each atom is determined by taking the derivative of the potential energy function, U , with respect to position, x . By integrating Newton's second law, the acceleration, a , is related to the position of the atoms, x . The masses of the atoms are known, and therefore the acceleration can be determined. This is described by the following equations:

$$F = -\delta U / \delta x$$

$$F = m a$$

$$F = m \delta v / \delta t$$

$$F = m d^2 x / dt^2$$

The equations of motion are integrated using a modified Beeman algorithm (Levitt and Meirovitch, 1983) to determine the new positions and velocities of all the atoms as a function of time. In order to minimize error in the calculated trajectory, the time step must be very small. Typically a value of 2 fs or less is used. For the exact equations used refer to Levitt (Levitt and Meirovitch, 1983). The eventual outcome is a set of molecular conformations that represent the protein motion in water at a specified temperature.

1.3.2 Fluorescence Spectroscopy Background

Proteins often contain only one or a small number of tryptophan residues, the most fluorescent amino acid. The indole ring of tryptophan is very sensitive to environmental changes, such as solvent polarity (Herskovits and Sorensen, 1968; Williams et al., 1965) and can provide information regarding protein conformational changes. Quenching, or energy transfer from the excited-state to a small molecule acceptor, can also reveal details about solvent accessibility of tryptophan. The underlying theory of steady-state fluorescence, quenching of fluorescence, and time-resolved fluorescence is discussed in more detail below along with a summary of how each provides information about proteins in solution.

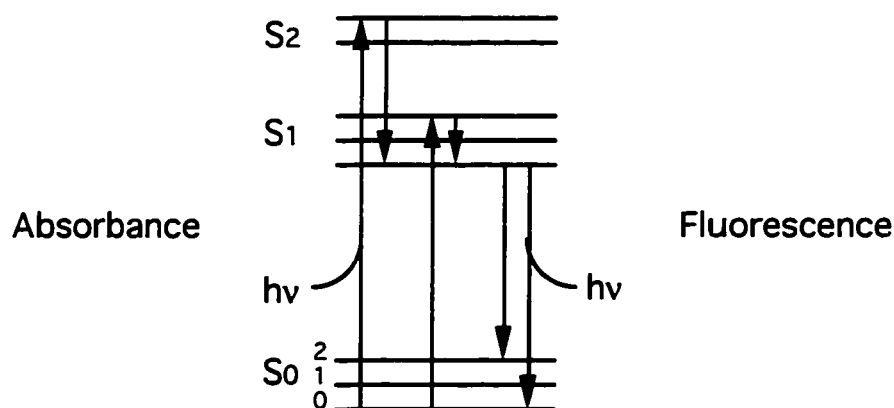


Figure 1.3: Jablonski diagram depicting ground-state and excited-state electronic levels (S_0 , S_1 , S_2) and vibrational levels (0, 1, 2). A hypothetical scenario of light absorption and fluorescence is shown by arrows.

Fluorescence is due to the emission of photons from the electronically excited-states of the delocalized electrons. The Jablonski diagram describes the process of light absorption and emission in fluorescence (Figure 1.3)(Jablonski, 1935). In the ground-state, S_0 , the electrons can exist in a number of vibrational energy levels, 0, 1, 2, etc. When light absorption occurs (10^{-15} sec), $h\nu_A$, the electrons are excited to higher electronic levels (S_1 or S_2) and immediately (10^{-12} sec) relax to the lowest vibrational level of the lowest excited-state, S_1 . The excited-state fluorophore returns to the ground-state through photon emission or radiationless decay (10^{-8} sec). The efficiency of the above process, which is the ratio of the number of photons emitted to the number absorbed is known as the quantum yield. Relative to absorbance, fluorescence emission occurs on a slower time scale and can be influenced by solvent effects and quenching. For protein molecules in solution, the emission wavelength is longer relative to the absorption wavelength. This loss of energy, known as Stokes' shift, is the result of different dynamic processes such as interactions of the fluorophores dipole moments with the surrounding solvent (Stokes, 1852). Upon absorption of a photon, the electronically excited-state of tryptophan instantaneously creates a dipole moment that is larger than in the ground-state. This newly created dipole perturbs the solvent environment surrounding the fluorophore. The solvent then reorganizes or relaxes around the fluorophore and lowers the energy of the excited-state electronic level (Figure 1.4). The solvent interactions can therefore result in spectral emission shifts.

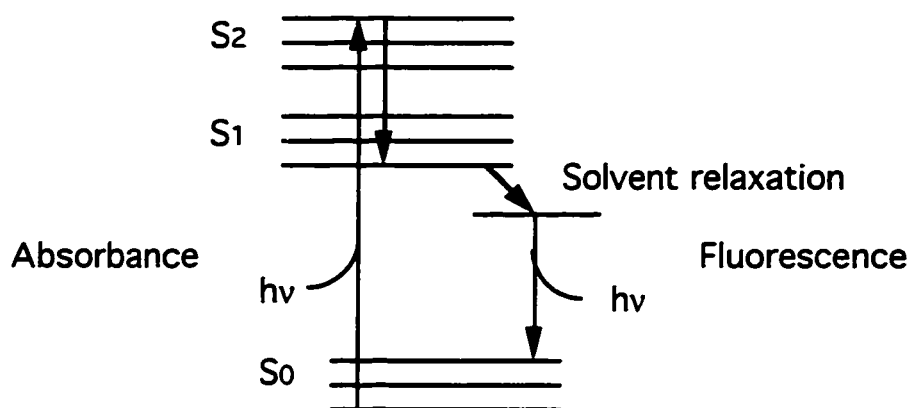


Figure 1.4: A modified Jablonski diagram depicting solvent relaxation effects on the excited-state electronic levels.

Typically, fluorescence emission (λ_{max}) of tryptophan in native proteins ranges from 325 to 350 nm. A relationship exists between λ_{max} and tryptophan exposure to solvent (Burstein et al., 1973; Teale, 1959). Simply stated, as a buried residue is exposed to a polar solvent, its fluorescence shifts to longer wavelengths (red shifts). However, it is also possible that a tryptophan in a rigid environment may fluorescence at longer wavelengths, even if the surrounding environment is polar. Such circumstances may be the result of specific interactions between the indole ring and neighboring polar groups on the protein, or the presence of buried water molecules. Therefore, steady-state fluorescence spectra alone cannot conclusively determine the extent of a residue's solvent accessibility. For this reason, processes such as quenching are exploited.

Quenching is the process by which fluorescence intensity or lifetime is decreased by the physical contact of a small molecule with the excited-state fluorophore (Lakowicz, 1983). The reaction can be described by the following scheme and Figure 1.5:

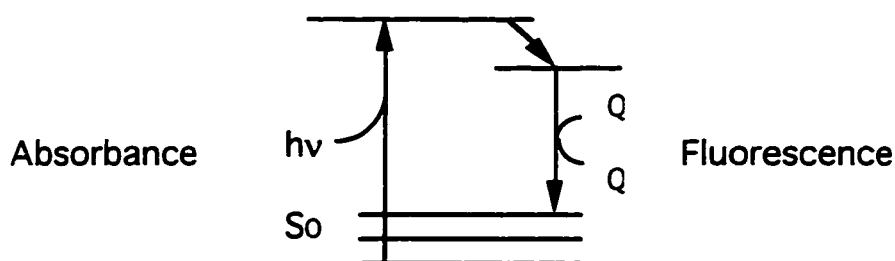
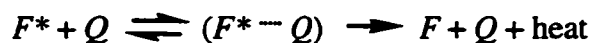


Figure 1.5: A modified Jablonski diagram depicting the interaction of a quencher (Q) with the excited-state electronic level.

The complex, $(F^* \cdots Q)$, is formed by physical encounter between the excited-state fluorophore and the quencher and the rate of formation is diffusion controlled (k_d). The complex will dissipate the electronic excited-state energy as heat. The apparent rate constant for the bimolecular quenching process is given by:

$$k_q = \gamma k_d$$

The efficiency, γ , describes how often an encounter between the quencher and the excited-state fluorophore results in deactivation. If the efficiency is equal to one, then k_q equals k_d . The Stern-Volmer equation relates the decrease in fluorescence intensity (F_0/F) to the concentration of quencher (Q):

$$F_0/F = 1 + K_{sv}[Q] = 1 + k_q\tau_0[Q]$$

From this equation, the Stern-Volmer constant (K_{SV}) is calculated. When excited-state lifetimes (τ_o) are obtained, the bimolecular quenching constant (k_q) can be determined.

Quenching processes can be more completely described by including both “collisional” and “static” components. The former has just been described. The latter is described by considering a randomly distributed solution in which quencher and chromophore molecules are very close at the moment the chromophore becomes excited. The probability for quenching in this case is so high that it occurs almost instantaneously or “statically.” The two processes can be distinguished by excited-state lifetime measurements, absorption spectra of the fluorophore-quencher complex, or increasing the temperature of steady-state fluorescence experiments. In all cases, the methods take advantage of the fact that static quenching only affects the ground-state and not the excited-state complex. Except for rare occasions, dynamic quenching will dominate over the static process (Eftink and Ghiron, 1981).

There are a number of different molecules and ions capable of quenching tryptophan fluorescence. Acrylamide, molecular oxygen, bromide and iodide ions are just a few of the commonly used quenchers. Acrylamide is neutral and may penetrate into the interior of proteins, and is therefore useful in probing the degree of solvent exposure of tryptophan residues (Eftink and Ghiron, 1976). The anions, however, are charged, heavily hydrated, and quench only surface tryptophan residues (Burstein et al., 1973; Eftink and Ghiron, 1976; Lehrer, 1971). The degree to which a residue is quenched depends solely on how frequently it physically encounters a quencher molecule. In the case of a buried tryptophan, surrounding protein segments sterically shield the residue and decrease the frequency of collision. Penetration of the quencher into the interior of a protein will be facilitated by fluctuations in the protein conformation occurring on a nanosecond time scale and are therefore useful for probing protein dynamics.

Time-resolved fluorescence monitors the dynamic events occurring during the lifetime of the excited-state which can range from a few picoseconds to several nanoseconds. During this time period, different physical processes can occur such as protein rotation or tumbling, segmental motion, and single amino acid side chain motion. Through time-resolved fluorescence, detailed information can be obtained about the population distribution of the excited-state species of the emitting fluorophores. This technique is often used to obtain a more complete picture of fluorophore accessibility in conjunction with quenching studies. Two approaches used to obtain fluorophore lifetime distributions are frequency-domain and time-domain fluorescence. In either technique, the distribution of the lifetime decays are recovered by fitting the data using nonlinear least-squares procedures. The objective of both techniques is to recover parameters describing the time-dependent decay of the excited-states. It is typical to have multiple decay constants which may result from a fluorophore being in several distinct environments, and can be described by the multiexponential equation:

$$I(t) = \sum \alpha_i e^{-t/\tau_i}$$

The preexponential factors (α_i) represent the fraction of molecules in each environment with decay times, τ_i .

The frequency-domain approach is summarized in Figure 1.6 (Lakowicz and Gryczynski, 1991). The sample is excited with light that has been modulated sinusoidally (*Exc*). Because of the finite lag time between absorption and emission there is a phase shift, ϕ_ω , and the emission (*Em*) is delayed in time relative to the modulated excitation. The finite time response of the sample results in demodulation of the emission by a factor m_ω .

These parameters are measured over a wide range of frequencies making up the frequency response function. The shape of this function is determined by the number of decay times.

In the time-domain method, the sample is excited with an infinitely short pulse of light (on the experimental time scale) as described in Figure 1.7 (Birch and Imhof, 1991). In theory, each fluorophore absorbs one photon instantaneously resulting in a population of excited-states. The time-dependent decay is recorded by measuring the time delays of individual fluorescence photons with respect to the excitation pulse. The fractions and lifetimes of the individual species are then calculated. Exhaustive accounts of both time-domain and frequency-domain methods may be found elsewhere.

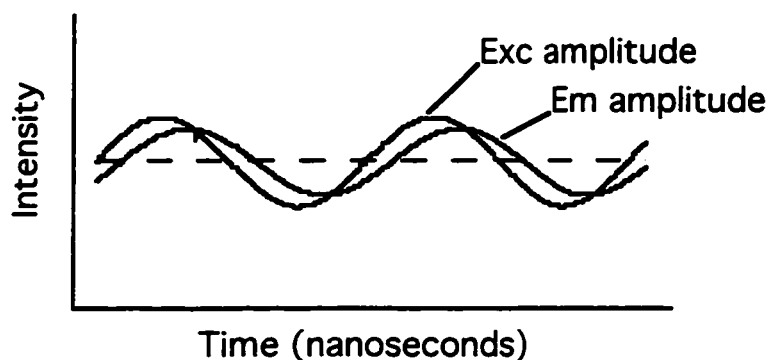


Figure 1.6: Frequency-domain fluorescence. The phase shift, ϕ_w , is defined as the difference between the excitation and emission curves at half-maximum. The response function is constructed after the collection of measurements at several frequencies.



Figure 1.7: Time-domain fluorescence.

1.4 Thesis Outline

The thesis project has been divided into four parts. The first two parts involved MD simulations of cytochrome b_5 . The initial holocytochrome b_5 simulation served as a control for future simulations and was used to test how well the simulated solution model of holocytochrome b_5 agreed with experiment (Chapter 2). In addition, the results provided structural data to aid experimental interpretation. The second part of the MD simulation study describes simulations of rat and bovine apocytochrome b_5 (Chapter 3). Apocytochrome b_5 is an experimentally isolable intermediate along the cytochrome b_5 denaturation pathway. The purpose of this MD study was to provide a molecular model of the apoprotein and test the effects of variant residues on the intermediate state. The last two parts of the thesis describe experimental extensions of the computational studies and further simulations to guide the experimental studies. On the basis of the holoprotein MD observations, experiments were designed to study the stability and dynamics of cytochrome b_5 by introducing mutations in the area of putative cleft mobility (Chapter 4). The dynamics of the putative cleft were addressed as explored through differences in steady-state and time-resolved fluorescence of the wild-type and mutant proteins (Chapter 5).

CHAPTER 2

MOLECULAR DYNAMICS SIMULATION OF CYTOCHROME b_5 : IMPLICATIONS FOR PROTEIN-PROTEIN RECOGNITION

2.1 *Introduction*

The link between structure and function of proteins relies heavily on the detailed information provided by high-resolution X-ray crystallography experiments. This information allows direct visualization of the structure of a protein and may reveal details of biological relevance. Motion, however, is implicated in biological function and the crystal structure of a protein represents an average conformation. Some or all of the residues may have a variety of preferred conformations that would not be captured in a single static depiction (Smith et al., 1986). In addition, studies have also revealed that structures of proteins (or portions of a protein) in solution and in a crystalline environment can be quite different (Clare et al., 1987; Housset et al., 1991; Hua and Weiss, 1990; Kline et al., 1988; Pflugrath et al., 1986; Urbanova et al., 1991; Weiss et al., 1989; Wittekind et al., 1992). Proteins exhibit a variety of complex motions even in their resting states. The magnitude of the motion experienced by the protein can increase dramatically during binding, catalytic, and signal transduction events. A recent study suggests that normal room temperature movements of proteins in solution can span up to ~ 15 Å (Careaga and Falke, 1992). The picture is complicated further in light of Frauenfelder and co-workers' suggestions that native proteins can occupy numerous distinct conformational substates that

perform the same function but at different rates and that thermal energy and environmental conditions determine which of these states is preferred (Hong et al., 1990).

Experimental studies generally only yield limited amounts of information of the actual molecular details of the motion experienced by a protein. Molecular dynamics simulations provide a way of analyzing motion at the atomic level as a function of time and of obtaining a physical description of protein behavior. Through such simulations, the motions that are inferred by nuclear magnetic resonance (NMR) relaxation and crystalline B-factors can be investigated. Hence, the simulations should be consistent with the physical picture provided by NMR and crystallography. To date, few studies have compared molecular dynamics generated structures with both crystallographic and structural NMR data, mostly because solution NMR structures are rarely available. Braatz and others (Braatz et al., 1992) made such comparisons for a long simulation (3 ns) of the protein ubiquitin; however, explicit solvent molecules were not included. The properties of interleukin-1 β were investigated in a 550 ps simulation by Chandrasekhar and co-workers (Chandrasekhar et al., 1992). Only a thin shell of waters was added to solvate this protein, but good agreement with experiment was achieved. Brunne and co-workers (Brunner et al., 1993) have described a long simulation (1.4 ns) of bovine pancreatic trypsin inhibitor, which proved to be in good agreement with experiment. Recently, Li and Daggett (Li and Daggett, 1997) made direct comparison between structures determined using X-ray crystallography and 2-D NMR and those generated during a 5.3 ns molecular dynamics simulation of chymotrypsin inhibitor 2 in solution. However, there is still a need to make further comparisons for other systems employing a large number of water molecules and reaching the nanosecond regime to ensure that the simulated structures adequately reflect the structural and dynamical properties of proteins in solution. Cytochrome b₅ is a good system to study with molecular dynamics techniques. The protein is small (85 residues), a high resolution crystal structure is available (1.5 Å, (Mathews et al., 1972)), and the

solution structure has been characterized by 2-D NMR techniques (Guiles et al., 1990; Guiles et al., 1992; Lecomte and Moore, 1991; Moore et al., 1991; Moore and Lecomte, 1990; Veitch et al., 1988).

Cytochrome b_5 is a low-spin hemoprotein that exists in several forms and plays a role as an electron-transfer mediator in a variety of redox (Mathews and Czerwinski, 1976). Of particular interest is its involvement in the drug metabolizing P450-dependent reactions where it transfers the second electron necessary for substrate oxidation ((1993). One naturally occurring soluble form and two membrane bound forms of the protein exist. The soluble form is found in erythrocytes and its role is to reduce methemoglobin (Hegesh et al., 1986). The physiological role of the membrane bound mitochondrial form participates in electron transfer from NADH to cytochrome c oxidase via cytochrome c (Bernardi and Azzone, 1981). A water soluble form of the hepatically bound cytochrome b_5 can be released by lipase or proteolytic solubilization. This fragment contains the heme and retains some activity with respect to protein recognition and electron transfer. The structure of the lipase-solubilized bovine liver cytochrome b_5 has been determined by X-ray crystallography (Mathews et al., 1972) and is used as the starting point for our work.

The structure of hepatic cytochrome b_5 consists of a heme containing region and a hydrophobic tail that anchors the protein to the endoplasmic reticulum. The soluble portion is composed of six α -helices, five strands arranged in a β -sheet, and several β -turns (Figure 2.1). A prosthetic heme group located in the crevice formed by four of the helices ($\alpha 2$ – $\alpha 5$) is partially accessible to the solvent and is coordinated to His 39 and His 63. The crevice is lined with nonpolar residues and constitutes hydrophobic core 1 (Figure 2.1). Another hydrophobic core (core 2) is located on the opposite side of the protein. This core appears to be important in maintaining the structural integrity of the protein (Mathews et al., 1979). It is also an independent structural domain during folding (Moore et al., 1991; Moore and Lecomte, 1993). The results of 2-D NMR experiments suggest that the solution

structure of cytochrome b_5 closely resembles the crystalline structure, although the protein is more dynamic in solution (Guiles et al., 1990; Guiles et al., 1992).

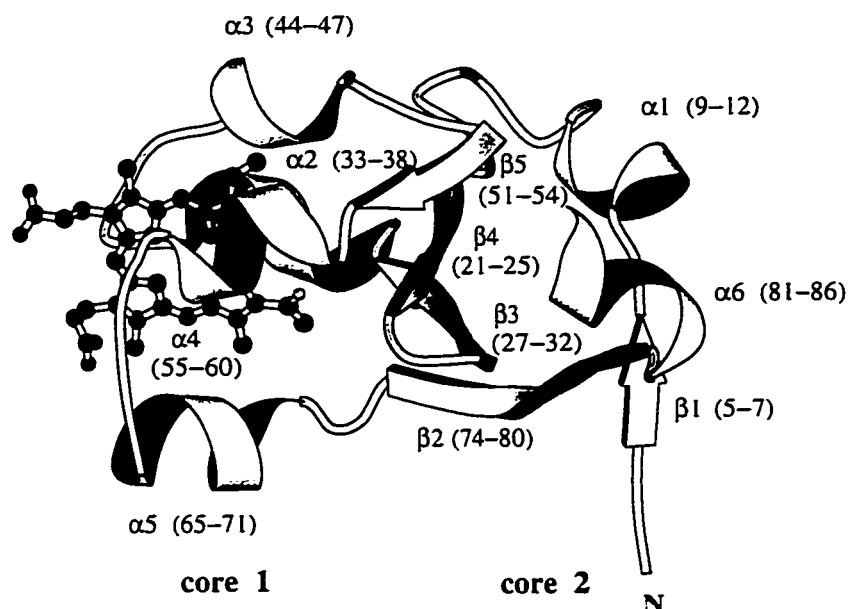


FIGURE 2.1: A ribbon diagram of the crystal structure of cytochrome b_5 including the prosthetic heme group (Mathews et al., 1972). The residues involved in the secondary structure are given in parentheses. The bovine numbering scheme is used. This figure was constructed using the Molscript program (Kraulis, 1991).

Extensive experimental data are available regarding the structural properties of cytochrome b_5 and the potential recognition sites for its interactions with other proteins. The details surrounding macromolecular recognition began to emerge with the computer-generated models of cytochrome b_5 complexed with other proteins. These models focused on protein-protein interactions based on complementary charge pairing at the interface of the complex. An array of acidic residues surrounding the partially buried heme group of cytochrome b_5 was proposed to participate in the formation of cytochrome b_5 -cytochrome c complexes (Mauk et al., 1986; Salemme, 1976; Wendoloski et al., 1987). Models of cytochrome b_5 complexed with methemoglobin (Poulos and Mauk, 1983), metmyoglobin

(Livingston et al., 1985) and cytochrome P-450_{cam} (Stayton et al., 1989) implicated the same or neighboring acidic residues. Using chemical modification, protection experiments, and site-directed mutagenesis studies, the results of the computer models have been largely substantiated (Mauk and Mauk, 1989; Ng et al., 1977; Rodgers et al., 1988; Rodgers and Sligar, 1991; Strittmatter et al., 1990; Tamburini et al., 1985).

Initially we performed the simulation described here as a control for simulation studies of the apo form of the protein, which adopts a partially folded conformation that appears to be an intermediate along the folding pathway (Storch and Daggett, 1996). However, the behavior of the native holo form was unexpected and we became interested in the structural and dynamical characteristics of cytochrome b₅ and their possible relation to macromolecular recognition. To this end, the protein was simulated in water at 298 K and pH 6.9 for 2.5 nanoseconds (ns). This time scale revealed macroscopic conformational changes that would not have been detected in a shorter simulation. The mobility of the protein was mainly localized to two regions and resulted in conformations displaying different patterns of residues on the surface, as well as the periodic formation of a large cleft. The dynamic behavior of cytochrome b₅ observed may be important in influencing the diverse range of protein-protein interactions in which this protein participates.

2.2 Methods

The starting conformation of cytochrome b₅ was obtained from the Brookhaven Protein Data Bank (PDB accession number 3b5c). The structure was determined by Mathews and others (Mathews et al., 1972) to 1.5 Å resolution. The solubilized form of oxidized, bovine liver cytochrome b₅, contains 93 residues. Residues 1–2 and 88–93 were not visible in the electron density maps and were therefore omitted in our starting

structure for the simulation. The potential energy function (Laidig and Daggett, 1996; Levitt, 1989; Levitt et al., 1995; Levitt et al., 1997; Levitt and Meirovitch, 1983) and associated protocols (Daggett and Levitt, 1992) are described in detail elsewhere. The heme parameters of Henry and co-workers were used (Henry et al., 1985). Energy minimization and molecular dynamics were performed using the program ENCAD (Levitt, 1990) on a Silicon Graphics Iris Indigo computer. All atoms were present in the simulation and the system was modeled to mimic an experimental pH of 6.9 (i.e. Lys, Arg, and His 15 were positively charged; His 26, His 80 were neutral; and Glu and Asp were negatively charged). The experimentally determined pK_a values were used in assigning the ionization state of the His residues (Altman et al., 1989). The system consisted of the protein in a rectangular box of water molecules, with walls at least 8.0 Å from any protein atom (3034 water molecules). The water density was set to the experimental value (0.997 g/ml) for 298 K (Kell, 1967) by adjusting the volume of the box.

Initially, conjugate gradient minimization of the protein was carried out for 2000 steps in order to reduce unfavorable contacts. The water molecules were then added, and the water only was minimized for 2000 steps, followed by 2000 steps of molecular dynamics and another 2000 steps of minimization. The protein was subsequently minimized for 2000 steps followed by minimization of the entire system for 2000 steps. After the preparation, the atoms were assigned velocities according to a Maxwellian distribution. The system was brought to the target temperature by adjusting the velocities intermittently until the system reached the desired temperature of 298 K, which occurred in 2–3 ps. After this point, the total energy was constant and no further scaling of velocities was necessary. Periodic boundary conditions were employed and the box volume was held constant during the simulation. Molecular dynamics was performed for 1.25×10^6 steps utilizing a 2 fs time step, resulting in a 2.5 ns trajectory. Structures were saved every

0.2 ps for further analysis (12,500 structures). An 8.0 Å nonbonded cutoff was used and the nonbonded list was updated every 5 steps.

2.3 *Results*

2.3.1 *Overall Structure*

The C $_{\alpha}$ root mean square (RMS) deviation from the crystal structure as a function of time is shown in Figure 2.2. The deviation ranged from 1.3 to 3.0 Å, excluding the first 0.2 ns (200 ps). The first 0.2 ns reflected an equilibration period for the system. The initial 0.5 ns and last 0.6 ns displayed similar average deviations from the crystal structure, approximately 1.5 and 1.8 Å, respectively. The 0.6 ns to 1.9 ns segment showed more dramatic fluctuations. These different segments of the trajectory were chosen for further study and are marked in Figure 2.2.

The deviation from the crystal structure was not distributed uniformly throughout the protein (Figure 2.3). Instead, the mobility was localized to approximately three regions: residues 10–20 (region 1), 40–52 (region 2), and 65–75 (region 3), which comprise a loop, $\alpha 3$ and adjacent loops, and $\alpha 5/\beta 2$, respectively (Figure 2.1). For short periods of time, the C $_{\alpha}$ RMS deviation from the crystal structure in these regions reached distances of > 5.0 Å. Region 1 experienced large scale RMS deviations from 1.2–1.55 ns. Region 2 deviated from the crystal structure for the duration of the simulation after 0.5 ns. Region 3 fluctuated from 0–1.75 ns and then returned to the conformation observed in the crystal structure.

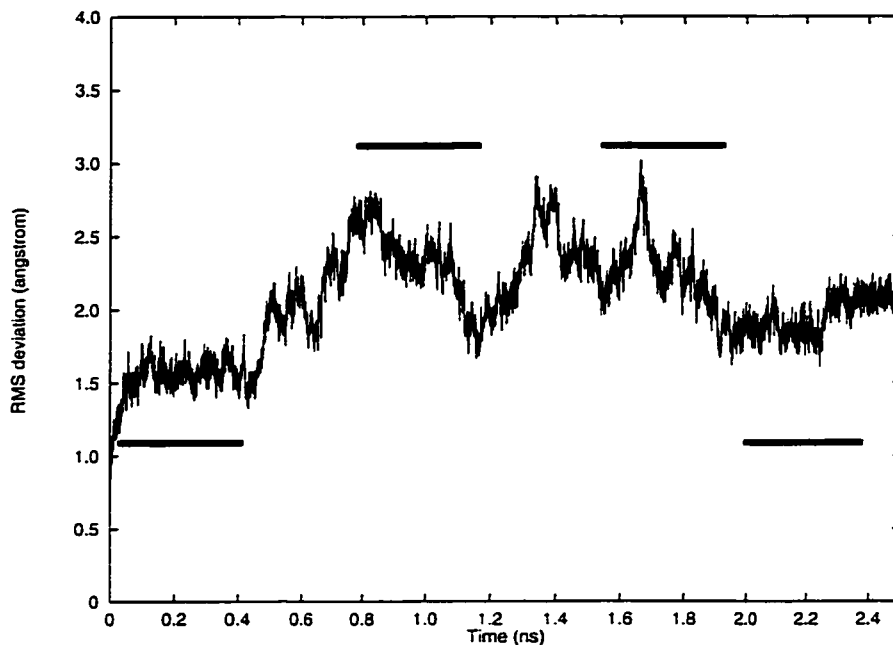


FIGURE 2.2: The C_{α} RMS deviation from the crystal structure as a function of time. Four main regions of the trajectory were analyzed and are indicated by the horizontal bars. The C_{α} RMS deviation was calculated after optimum superposition of the protein coordinates (Kabsch, 1976).

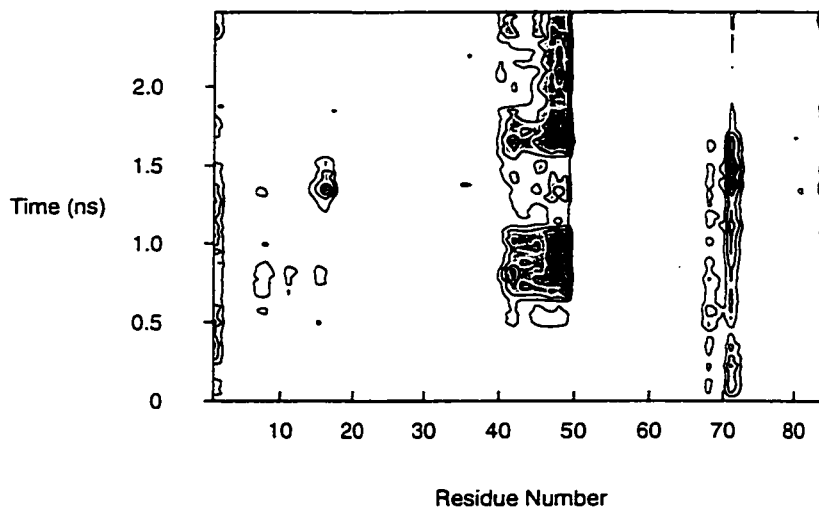


FIGURE 2.3: Contour plot of the C_{α} RMS deviation per residue number as a function of time. Deviations are outlined as follows: ≤ 3.0 Å white; 3.0 Å \leq light gray ≤ 4.0 Å; 4.0 Å \leq gray ≤ 5.0 Å; 5.0 Å \leq dark gray ≤ 6.0 Å; and ≥ 6.0 Å black.

2.3.2 Internal Motion

The C_{α} RMS fluctuations describing the motion about the mean structure were used to determine the distribution of mobility along the sequence as a function of time. The RMS fluctuation for the first 0.4 ns was approximately 0.8 Å. This constancy paralleled the RMS deviation from the crystal structure (Figure 2.2). Throughout the course of the simulation, large RMS fluctuations were localized to the three main regions of the protein described above. Residues 10–20 reached peak fluctuations of 1.5 Å. The RMS fluctuation of residues 40–52 oscillated between 1.0–2.0 Å. The C-terminus (res. 83–86) displayed similar large-scale oscillations. Residues 65–75 remained relatively constant, except from 1.6–2.0 ns. During the last 0.1 ns, the RMS fluctuation for all residues, excluding the C-terminus, remained below 0.8 Å and paralleled the evenness of the RMS deviation from the crystal structure (Figure 2.2).

Overall, the C_{α} fluctuation for the crystal structure is ~0.6 Å as estimated from the experimental B-factors using the following relationship: $C_{\alpha} \text{ fluc} = (3B/8\pi^2)^{1/2}$, which assumes that all motion is internal and that the contribution from lattice disorder is negligible. The corresponding values from the last 0.5 ns of the simulation are displayed in Figure 2.4 for comparison. While the positions of relative mobility are similar (graphics portion of Figure 2.4), the magnitude of the motion in the solution simulation differs from the crystal structure (plot in Figure 2.4). For the three main regions described above and marked in Figure 2.4, the first two show increased motion in both environments. Region 2 is particularly prominent in the simulation, and although relatively mobile in the crystal structure, this portion of the protein appears to be involved in crystal contacts (Plate I, (Mathews et al., 1972)), which may hinder its mobility. Region 3 also appears to be involved in crystal contacts and shows low mobility in the crystal structure. Interestingly, the portions of the protein exhibiting low mobility in the simulation have lower fluctuations

than those estimated from the B-factors (by ~ 0.2 Å), which may indicate the magnitude of the contribution of the lattice disorder. Additionally, the relative number of intraprotein contacts in these regions, although shifted to the right slightly, is higher than those in mobile regions (bar graph, Figure 2.4).

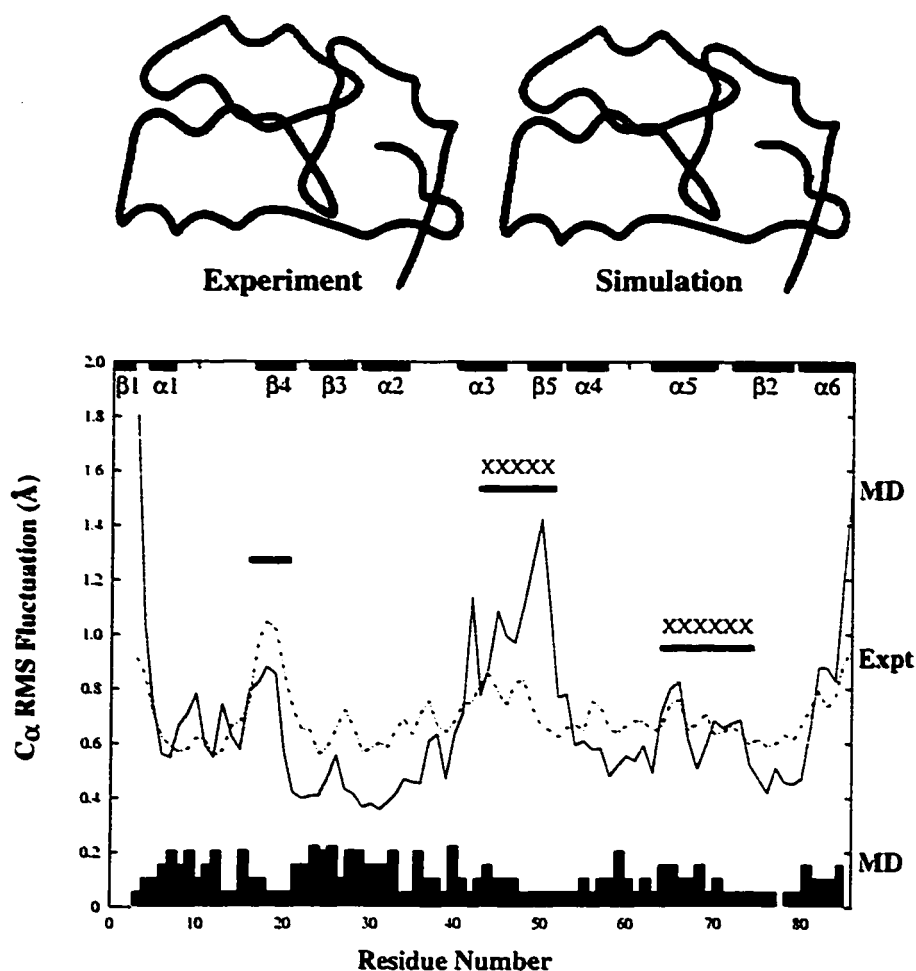


FIGURE 2.4: Top: Mainchain C_{α} traces of cytochrome b_5 depicting the relative mobility from the experimental B-factors (see text) and the C_{α} RMS fluctuation (last 0.50 ns of MD). Structures are colored according low mobility (blue) to high mobility (red). Bottom: C_{α} RMS fluctuation as a function of residue number: experiment (dashed line) and MD (solid line). The observed crystal contacts (Plate I, (Mathews et al., 1972)) are indicated with 'XXX'. The relative number of intraprotein contacts (atoms ≤ 4.5 Å) during the simulation, not including contacts within or between neighboring residues, are indicated by the bar graph at the bottom of the plot. The bar graph is normalized so that 0.2 equals the maximum number (250) of average contacts a residue makes during MD.

2.3.3 Secondary Structure

To determine the origins of the localized mobility detected through the C_α RMS fluctuations and displayed in the mainchain traces, we investigated how the helical and β -content changed with time (Table 2.1). The method used to determine the secondary structure is based on repeating segments of at least 3 residues in succession containing either helical or beta structure, as indicated by (ϕ, ψ) dihedral angles (Daggett et al., 1991; Daggett and Levitt, 1992). The four time periods were chosen to represent the prominent regions of the plot in Figure 2.2: the beginning (0–0.4 ns), the two fluctuating periods (0.6–1.0 ns and 1.4–1.8 ns), and the end (2.0–2.4 ns).

$\alpha 1$ showed a constant average helical content, but experienced large fluctuations with time (note that a 30% standard deviation for this segment corresponds to one residue out of three). $\alpha 2$ exhibited the largest change in helical content during the course of the simulation. During the first 0.4 ns, $\alpha 2$ contained the same helical content as the crystal structure and the helix content increased two-fold during the two fluctuating time periods (0.6–1.0 ns and 1.4–1.8 ns). The dramatic change in helix content of $\alpha 2$ for each time period, coupled with the large standard deviations, indicated that this segment was conformationally heterogeneous. It should be noted that because of its irregular nature, $\alpha 2$ is defined as a series of turns by Mathews and co-workers (Mathews et al., 1972). In contrast, $\alpha 4$ and $\alpha 5$ maintained stable helical structure throughout the simulation. $\alpha 6$ consistently remained below 50%, reaching low points of 0% from 0.7–1.0 ns and 1.2–1.6 ns. These residues make up the carboxy-terminus, which is less constrained than other regions of the protein.

Table 2.1: Secondary Structure Content for Particular Regions of Cytochrome b_5 as a Function of Time^a

Secondary Structure ^b	Crystal Structure	Time (ns)			
		0–0.4	0.6–1.0	1.4–1.8	2.0–2.4
$\alpha 1$ (9–12)	100	87 (33)	84 (37)	82 (38)	81 (39)
$\alpha 2$ (33–38)	33	32 (24)	64 (29)	55 (29)	47 (30)
$\alpha 3$ (44–47)	100	96 (18)	92 (24)	93 (20)	98 (11)
$\alpha 4$ (55–60)	100	98 (7)	98 (7)	99 (6)	98 (8)
$\alpha 5$ (65–71)	100	85 (11)	81 (14)	85 (12)	83 (11)
$\alpha 6$ (81–86)	83	31 (31)	10 (15)	9 (19)	24 (27)
$\beta 1$ (5–7)	100	97 (16)	97 (18)	97 (17)	97 (15)
$\beta 2$ (74–80)	57	20 (23)	14 (20)	10 (19)	13 (19)
$\beta 3$ (27–32)	67	58 (15)	66 (2)	66 (4)	67 (1)
$\beta 4$ (21–25)	100	83 (32)	84 (20)	88 (19)	99 (6)
$\beta 5$ (51–54)	0	0	0	0	0

^a α -helical or β -structure is defined as having at least three consecutive residues with the appropriate (ϕ, ψ) dihedral angles (Daggett and Levitt, 1992). Secondary structure contents are given in percentages, so, for example, 33% of the residues in $\alpha 2$ adopt helical (ϕ, ψ) angles in the crystal structure. The values from the simulation are averages over particular regions of the sequence, in the specified time interval. The standard deviation is given in parentheses alongside each value.

^b The elements of secondary structure are shown in Figure 2.1 and the residue numbers are given in parentheses.

The $i \rightarrow i + 4$ hydrogen bond distances for all six helices were analyzed as another measure of the secondary structure, where a hydrogen bond was defined as having a distance between an amide hydrogen atom and a carbonyl oxygen atom of ≤ 2.6 Å and with a hydrogen bonding ($N-H \cdots O=C$) angle within 45° of linearity. All of the helices

maintained α -helical hydrogen bonding throughout the simulation with the exception of $\alpha 6$ at the carboxy-terminus, whose hydrogen bonding pairs fluctuated about 3.2 Å (data not shown). Even though $\alpha 2$ showed large fluctuations based on repeating structure (Table 2.1), the $i \rightarrow i + 4$ hydrogen bonds were maintained throughout the simulation. In addition, $\alpha 3$ and $\alpha 4$ also showed increased motion (Figure 2.4), but, maintained ideal α -helical hydrogen bonding patterns.

Among the β -strands, $\beta 2$ deviated the most from the crystal structure. $\beta 2$ contained a decreased beta content of less than 20% during the simulation. The first few residues of this region also displayed an increased C_{α} RMS fluctuation relative to other residues in the protein, as mentioned previously. $\beta 5$ never contained beta content according to our definition of repeating structure in either the simulation or crystal structure. The beginning portion of $\beta 5$ contained residues that also displayed large fluctuations. Both $\beta 2$ and $\beta 5$ are defined as irregular in the Brookhaven PDB file. The involvement of $\beta 2$ and $\beta 5$ in the β -sheet will be justified below through NOE connectivities.

2.3.4 NOE Connectivities

Interresidue hydrogen-hydrogen distances were also monitored to compare with experimentally observed nuclear Overhauser enhancement (NOE) connectivities. The predicted NOEs from the simulation were obtained by calculating an average weighted distance ($\langle r^{-6} \rangle^{-1/6}$) between the interacting hydrogens. All of the hydrogen-hydrogen distances corresponding to the experimentally observed NOEs in the β -sheet (Guiles et al., 1990; Moore and Lecomte, 1993) remained below 5.0 Å, which is considered a reasonable cutoff for an NOE (Wüthrich, 1986), throughout the simulation except for the $d_{\alpha N}$ connectivities between 23–51 and 23–52 (data not presented). In addition, the NOEs

between Tyr 30 and Phe 74, forming the connectivities between $\beta 3$ and $\beta 2$ at the back wall of the heme pocket, were also observed (Moore and Lecomte, 1990; Reid et al., 1987). Maximum average distances of 7.6 and 6.8 Å, respectively, were observed for these interactions during the 1.6–1.8 ns time segment, where the values were below 5.0 Å prior to this. Even though these large interresidue distances occurred, the native-like structure was reestablished in the latter part of the simulation and the distances dropped back below 5.0 Å. The connectivities observed in the α -helical regions were also monitored ($d_{\alpha N(i+3)}$) (Guiles et al., 1990; Guiles et al., 1992). All of the appropriate proton pairs remained below 5.0 Å during the simulation (data not shown).

In addition to the mainchain NOEs within secondary structure described above, sidechain NOEs between residues located mainly within core 2 have been determined (Moore and Lecomte, 1990). All hydrogen-hydrogen distances for these core NOEs remained below 5.0 Å, thus demonstrating the integrity of the hydrophobic core. NOEs between the sidechains of residues 26 and 55 (Moore and Lecomte, 1993; Reid et al., 1987), representing the interface of the cores, remained ≤ 4.0 Å during the simulation. Furthermore, although the N-terminus was structurally labile, $\alpha 6$ remained docked to $\beta 1$ as monitored through the observed d_{NN} NOE connectivities between 7–78 and 7–80 (Moore and Lecomte, 1993).

2.3.5 Protein Surface

As discussed above with reference to Figure 2.3 and the C_α RMS fluctuations, three distinct regions of the protein showed high mobility. Region 2 (residues 40–52) comprises $\alpha 3$ and the loop following it (Figure 2.1). Residues in this region occupy the periphery of one side of the heme pocket and are predominantly acidic. The high percentage of acidic residues in cytochrome b₅, 11 glutamates and 6 aspartates, made assignment of the

sidechain conformations in this region by 2-D NMR nearly impossible (Guiles et al., 1990). Space-filling representations highlighting some of these acidic residues (Glu 37, Glu 38, Glu 43, Glu 44, and Glu 48) and Arg 47, which is involved in a salt bridge (Veitch et al., 1990) illustrate that distinct surfaces were displayed at different time points during the simulation (Figure 2.5, the orientation of the protein has been changed to better illustrate the surface of interest).

The charged residues initially occurred as three groups in the crystal structure: Glu 44/Glu 48, Glu 43/Arg 47, and Glu 37/Glu 38. Glu 44 and Glu 48 ultimately moved apart during the simulation as compared to the crystal structure, where they are nestled next to each other (Figure 2.5). The distances between the ϵ -amino hydrogen of Arg 47 and the carboxylate oxygen of Glu 43 and Glu 37 were monitored during the simulation as a probe of the surface changes. At approximately 1.4 ns, the salt bridge present in the crystal structure between Glu 43 and Arg 47 (2.4 Å) broke but reformed by 1.8 ns (~3.4 Å). Glu 37 and Glu 38 fluctuated greatly during the simulation: at 1.7 ns, they were separated by a distance of ~12.0 Å, as compared to 6.0 Å in the crystal structure. By 1.8 ns, Glu 37 also formed a salt bridge with Arg 47, with an average distance of 1.6 Å. Throughout the simulation, all of the residues remained exposed on the surface of the protein.

Regions 1 (residues 10–20) and 2 (residues 40–52), are also depicted through space-filling representations in Figure 2.6 (same orientation as Figure 2.5). Various structures from the simulation illustrate that the movement of these regions alternately exposed and buried a hydrophobic core, comprised of Thr 21, Leu 23, Leu 32, Leu 46, and Ala 54 (Figure 2.6). The opening and closing of the cleft occurred in intervals of 0.3 to 0.6 ns. The maximum dimensions of the cleft were 15.2 Å x 10.5 Å x 11.5 Å (length by width by depth) and the corresponding dimensions in the crystal structure are 16.5 Å x 4.7 Å x 5.7 Å.

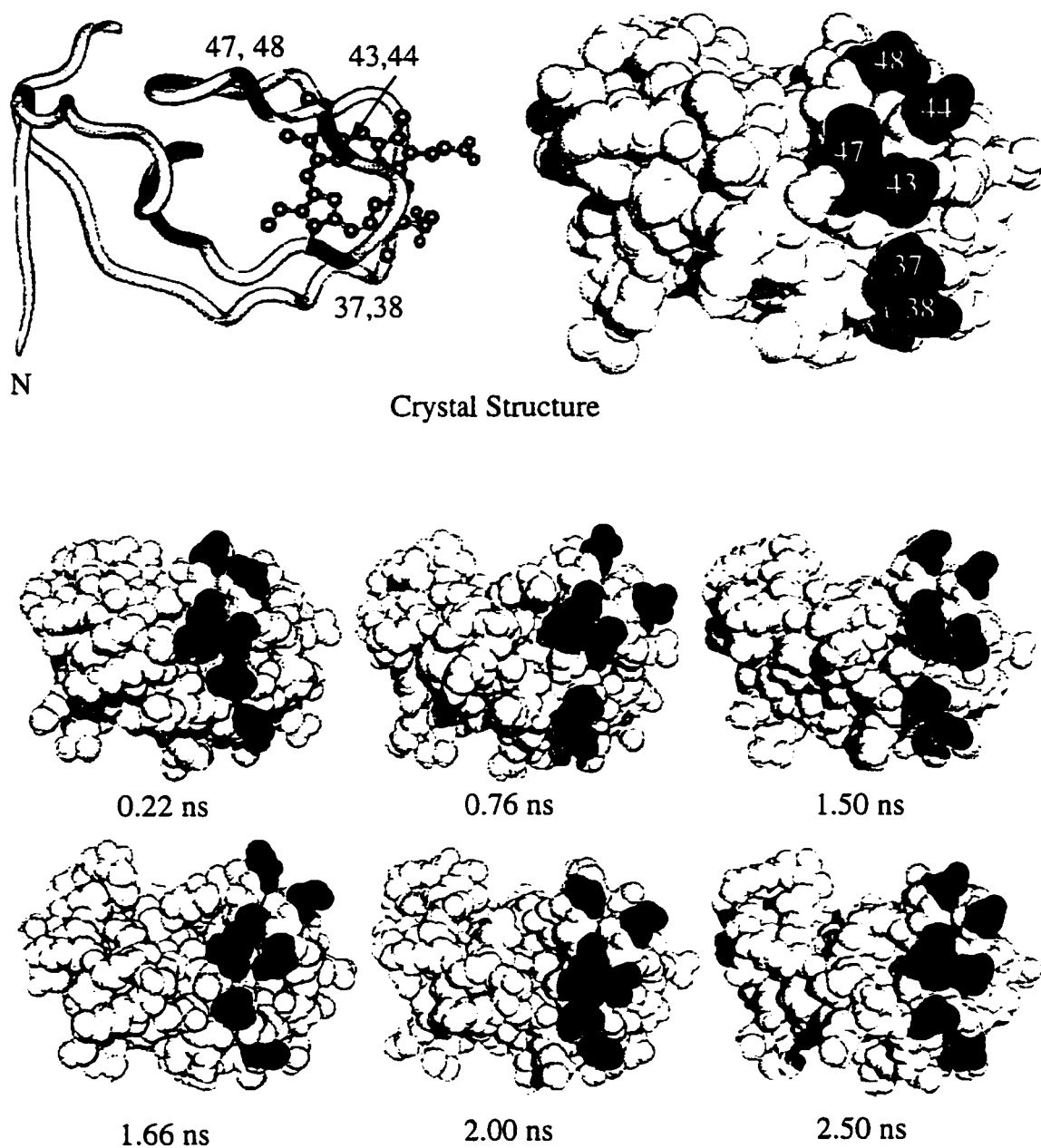
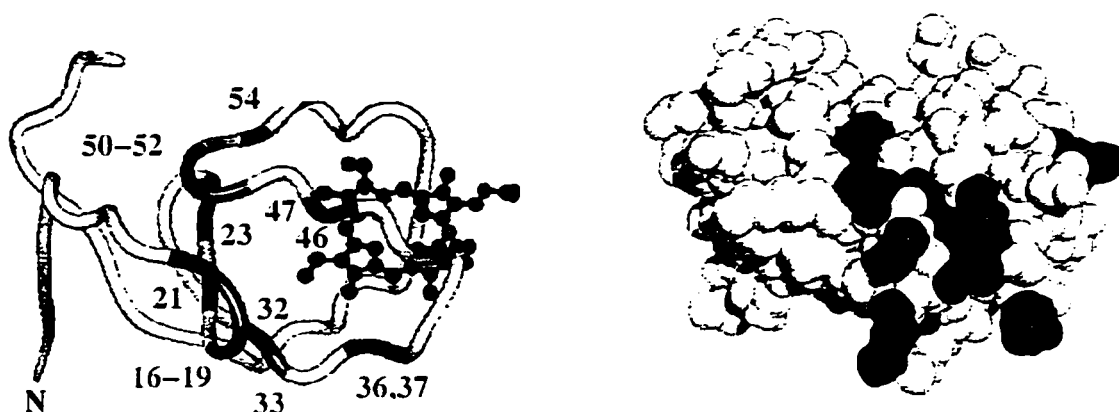


FIGURE 2.5: Mainchain trace and space-filling representations of the crystal structure and snapshots from the simulation of cytochrome b₅. Residues Glu 37, Glu 38, Glu 43, Glu 44, Arg 47, and Glu 48 are depicted in black. The different snapshots highlight the distinct surfaces that were displayed during the simulation.



Crystal Structure

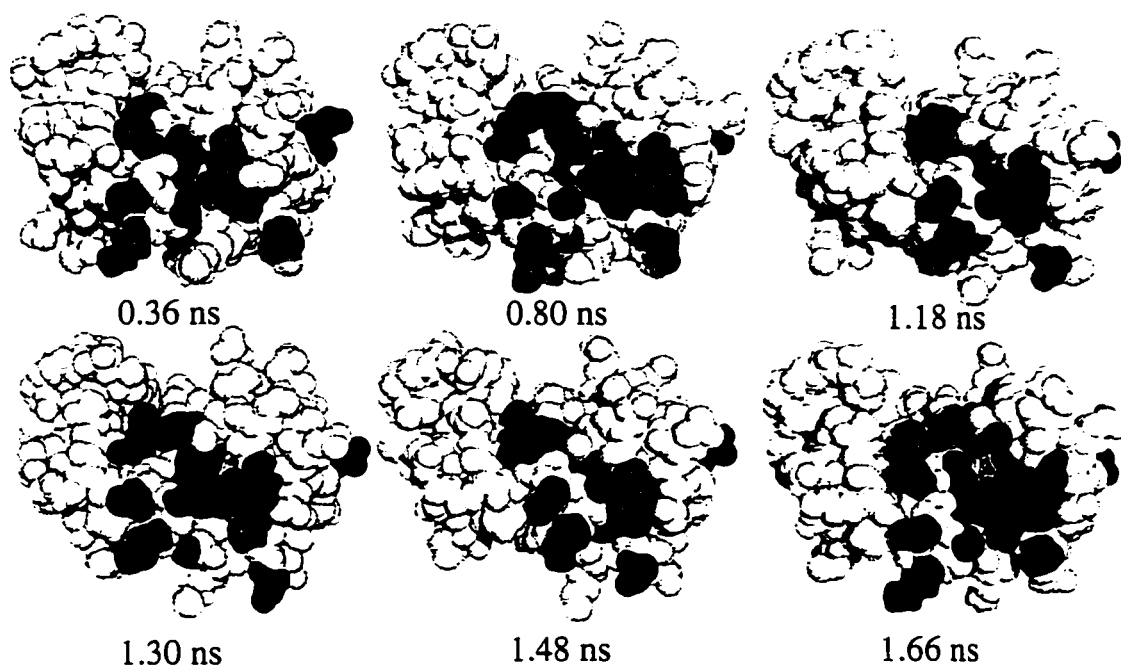


FIGURE 2.6: Mainchain trace and space-filling representations of cytochrome b5. The buried residues that intermittently became exposed upon cleft formation (Thr 21, Leu 23, Leu 32, Leu 46, and Ala 54) are colored red. The green residues (Asn 16, Asn 17, Ser 18, Lys 19, Ile 24, Thr 33, Leu 36, Glu 37, Arg 47, Ala 50, Gly 51, and Gly 52) depict surface residues along the rim of the cleft. The prosthetic heme group is colored blue.

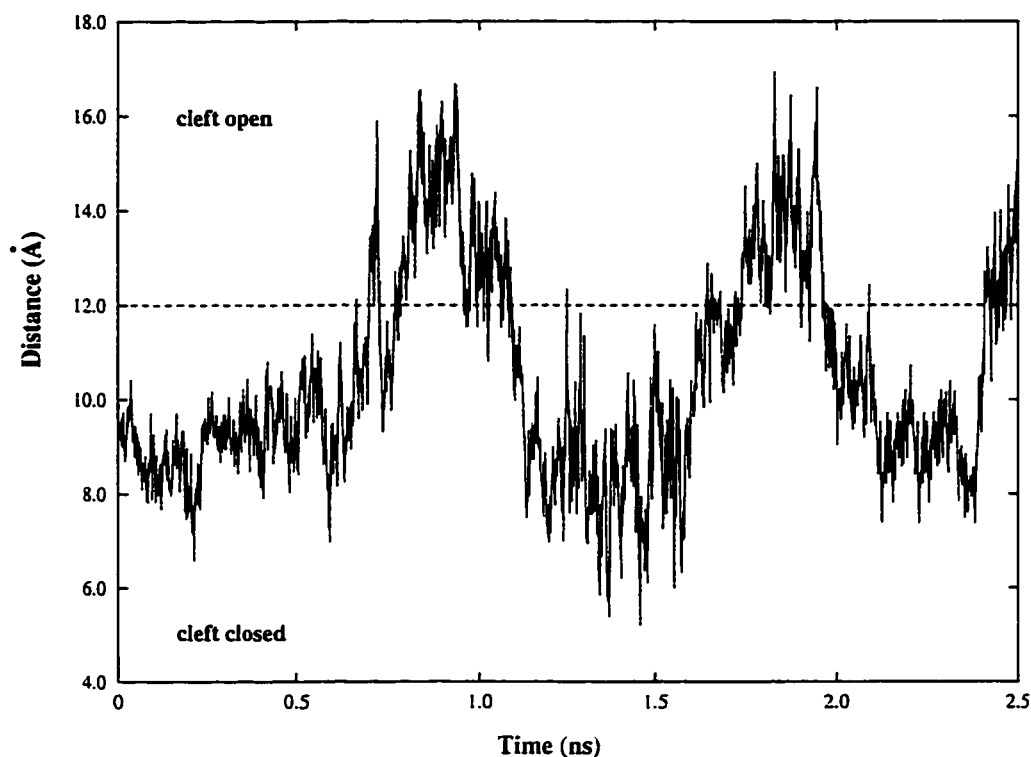


FIGURE 2.7: The distance between Ser 18 and Ala 50 as a function of time. Distances were measured from the hydroxyl hydrogen of Ser 18 to a methyl hydrogen of Ala 50. These two residues define partial boundaries of the cleft. The starting distance in the crystal structure was 9.4 Å. Distances below the dashed line indicate that the cleft was closed and above 12.0 Å the cleft was open.

The solvent accessible surface area of the residues in the cleft is given in Table 2.2. All of the residues are completely buried in the crystal structure and gain varying degrees of exposure during the simulation. Early on, all residues except for Ala 54 became accessible to solvent. Thr 21 became buried from 1.15–1.5 ns, which correlated with the opening of the cleft, as observed through the snapshots (0.80 and 1.48 ns) in Figure 2.6. Leu 23 remained buried from 0.45–1.6 ns and is located just behind Thr 21 in Figure 2.6. Leu 32 was alternately buried and exposed during the simulation. Leu 46, located on the other side of the cleft relative to the aforementioned residues (Figure 2.6), was exposed to solvent

early on but later became buried. At 1.6 ns all of the residues had large positive changes in their solvent accessible surface area that lasted for approximately 0.3 ns. This dramatic opening of the cleft is illustrated in the 1.66 ns snapshot (Figure 2.6). From this open position, it is evident that this cleft allows access to the heme group (note the blue atoms of the heme at the bottom of the cleft in the 0.80 and 1.66 ns structures of Figure 2.6). From 1.9 ns until the end of the simulation, all of the residues except Ala 54 became buried. Ala 54 is located away from the other residues and displayed a different pattern of exposure (Table 2.2).

The distance between Ser 18 and Ala 50, two residues that span the rim of the cleft, correlated with the opening and closing of the two regions (Figure 2.7). These distances reflect the solvent accessibility of the internal hydrophobic residues. Distances during the simulation ranged from 4.8 Å to 17.5 Å, as compared to the crystal structure value of 9.4 Å. The change of distance from low to high values parallels the opening and closing of the cleft as observed in the space-filling representations in Figure 2.6. At the end of the simulation, the distances between Ser 18 and Ala 50 began to rise again, suggesting the beginning of another cyclical opening of the cleft.

Table 2.2: Change in Solvent Exposed Surface Area of Residues Located in the Cleft ^a

Residue	Time (ns)							
	0.2–0.25	0.5–0.55	0.8–0.85	1.1–1.15	1.4–1.45	1.7–1.75	2.0–2.05	2.3–2.35
Thr 21	21	25	30	10	6	15	11	10
Leu 23	27	12	15	8	3	21	7	10
Leu 32	57	10	22	8	12	18	4	8
Leu 46	13	18	9	12	7	37	11	6
Ala 54	2	6	8	6	3	7	11	13

^a The values shown are in Å². The average change in solvent accessible surface area (Lee and Richards, 1971) is given over the averaging interval indicated. All of the changes are relative to the accessible surface area of residues in the crystal structure, which was 0 Å² for all residues.

2.4 Discussion

Molecular dynamic simulations are now frequently utilized to help elucidate the link between protein structure, mobility, and function. During the process of reaching this ultimate goal, several research objectives must be met. In this regard, our main objective was to perform a molecular dynamics simulation of cytochrome b_5 in a native environment and determine the stability of such a system over a long time period. Furthermore, we wanted to know what length of time would be needed in order for the structural implications from the simulation to be physically relevant. A great deal of predictive power still relies on the crystal structures of proteins. Therefore, we also set out to assess how our simulation compares to the crystal structure of cytochrome b_5 and also whether the simulation accurately models the solution structure and behavior of cytochrome b_5 . In the course of investigating these issues, interesting surface properties of the protein became apparent. Below we first discuss the stability of the simulation and then the possible biological relevance of the observed motion.

A gross overview of the simulation is provided by the C_α RMS deviation plot (Figure 2.2). The 2.5 ns length of the simulation allowed the molecule to explore different conformations that would not have been possible in a single shorter simulation. As a whole, the molecule adopted solution conformations that varied from the crystal structure, yet returned to a state that closely resembled the starting conformation. The secondary structure content (Table 2.1) and hydrogen-hydrogen distances corresponding to NOEs reflected the stability of the simulation, as well. Based on secondary structure content, the entire protein was well-behaved with minor exceptions involving $\alpha 1$, $\alpha 2$, $\alpha 6$, $\beta 2$, and $\beta 5$. $\alpha 1$ and $\alpha 2$ however, did maintain proper α -helical hydrogen bond distances, while $\beta 2$ participated in all of the experimentally observed interactions with $\beta 1$ and $\beta 3$. Moore and Lecomte (Moore and Lecomte, 1993) found that the β -sheet and the carboxy- and amino-

termini of cytochrome b_5 form an independent structural unit that can be monitored via NOE contacts. Even though $\alpha 6$ showed a dramatic decrease in α -helical content during the simulation, it remained docked to the carboxy-terminus of this structural unit (Moore and Lecomte, 1990). $\beta 5$ showed very low secondary structure content as well as a loss of interstrand contacts with $\beta 4$ during one portion of the simulation. However, the NOE connectivities predicted from the simulation indicated that the carboxy-end of $\beta 5$ was at all times docked onto the loop between $\beta 3$ and $\beta 4$. The secondary structure content based on dihedral angles was particularly stringent and could give the misleading idea that some of the secondary structure was unstable, which was not borne out by the hydrogen bond and NOE analysis. Because of its sensitivity, however, this definition is useful for highlighting the dynamic behavior of the secondary structure. Overall, the simulation was in very good agreement with the data describing the solution structure of cytochrome b_5 .

Although large average deviations from the crystal structure were observed during the simulation, the system was stable based on structural grounds and was at all times consistent with the solution NMR data. Such a long and stable trajectory was certainly encouraging in spite of, or maybe because of, the fact that large deviations are observed but drop with increasing simulation time. Thus, movement away from the crystal structure does not necessarily indicate that the protein is drifting in conformational space never to return. Optimistically, we may be sampling the relevant dynamical and structural properties of the equilibrium native state. But, as always, longer simulations are necessary to test this idea.

Nevertheless, whenever there are large movements away from the crystal structure in a simulation, the results must be carefully scrutinized. Generally, such deviations are taken as *prima facie* evidence that a simulation is unstable and it is then terminated. While this may be the case, several indirect pieces of evidence suggest that the motion exhibited by cytochrome b_5 may be real: (1) Even when the deviation from the crystalline

conformation was large, the structures were consistent with the solution NMR data. (2) The motion was localized to three specific regions of the protein (residues 10–20, 40–52, and 65–75). Two of these regions (regions 1 and 2) exhibit increased motion in the crystal structure, although region 2 shows less motion than observed in the simulation. However, this region and region 3 appear to be involved in crystal contacts (Mathews et al., 1972), which may impair their motion. (3) Various NMR studies (Guiles et al., 1990; Guiles et al., 1992; Mauk et al., 1986; McLachlan et al., 1988; Meyer et al., 1993; Reid et al., 1987; Veitch et al., 1988) indicate that the protein is more dynamic in solution than in the crystalline state. Furthermore, Veitch and co-workers (Veitch et al., 1990) found that residues 39–42 (region 2) are particularly mobile. (4) After deviating from the crystal structure, the crystalline conformation was restored, and reached a C_{α} RMS deviation that was better than has been obtained in many shorter simulations (<200 ps, see review by Daggett and Levitt, 1993). Furthermore, the deviations from the crystal structure and regions of high mobility may be biologically relevant.

As mentioned above, three specific regions of the protein contributed when a large C_{α} RMS deviation from the crystal structure was observed. The first two regions were at the interface of core 1 and core 2 (Figure 2.1). The second region incorporated most of the acidic residues implicated in protein-protein interactions. Even though both regions were highly mobile, this motion was not correlated (data not presented). That is, as one increased the other did not necessarily increase or decrease systematically. However, these backbone deviations translated into conformational changes on the surface of the protein. For example, the surface pattern displayed by the acidic residues in region 2 changed with time (Figure 2.5). In addition, a large cleft formed as a result of the mainchain motion, exposing several hydrophobic residues of core 1 (Figure 2.6). The solvent exposure of these residues was a function of the cleft rim movement. Furthermore, the periodic exposure of the core residues suggested a breathing motion of the protein.

A vast amount of experimental work has been performed attempting to reveal the mechanism of cytochrome b_5 protein-protein complex formation. Cytochrome b_5 interacts with a variety of proteins, including cytochrome b_5 reductase, cytochrome c , hemoglobin and the cytochrome P450s. Thus, this protein must discern and interact with a structurally varied set of proteins. Studies utilizing computer modeling, chemical modification and mutagenesis have implicated some of the acidic residues as mediators of cytochrome b_5 complex formation.

Based on the pioneering work of Salemme (Salemme, 1976), a cytochrome b_5 -cytochrome c complementary charge-paired complex is proposed and tested further (Wendoloski et al., 1987). In accord with these models, site-directed mutagenesis experiments coupled with high pressure techniques suggest that Glu 44, Glu 48, Asp 60 and the heme propionate group are important in maintaining and/or forming this complex (Rodgers et al., 1988). On the other hand, other nearby residues (Gln 13, Glu 37, Glu 43, Glu 56 and Asp 66) are not involved (Rodgers and Sligar, 1991). In agreement with the findings of Rodgers and co-workers (Rodgers et al., 1988), Whitford (Whitford, 1992) used 1- and 2-D NMR to show that Glu 44 and Glu 48 are involved in complex formation, in addition to Glu 37, Glu 38 and Glu 43. That Glu 37 and Glu 43 are implicated is in contrast to the findings of Rodgers and Sligar (Rodgers and Sligar, 1991). Strittmatter and co-workers (Strittmatter et al., 1990) characterized the cross-linking of a cytochrome b_5 -cytochrome b_5 reductase complex and suggest that Glu 43, Glu 44, Glu 48, Glu 56, Asp 60, and the heme propionate are important in interfacial interactions. Although Glu 43 forms a salt bridge with Arg 47, constraining the mobility of these two residues, the other residues within this region are known to be quite mobile (Veitch et al., 1990).

The acidic residues mentioned above are conserved across all cytochrome b_5 forms to date with the exception of one conservative change, Glu 37 \rightarrow Asp in chicken (Ozols, 1989). These residues belong to a region (residues 37–60) that is located along the

periphery of the heme cavity. It has been proposed that the conformational flexibility of these residues could either provide long-range steering for initial complex formation (Matthew et al., 1983) or fine tune the complex orientation for maximal electron transfer activity (Salemme, 1976). In any case, it is still unclear as to exactly which conformational displays of the acidic residues of cytochrome b_5 are responsible for interacting with other proteins. Furthermore, removal of Glu 44, Glu 48, Asp 60, and modification of the heme propionate yields only a 14% decrease in free energy of association to cytochrome c (Rodgers and Sligar, 1991); this finding suggests that the electrostatic interactions implicated thus far only play a minor role in complex recognition/formation. However, specificity is not always linked to stability and these interactions could still be important in obtaining favorable electron transfer geometries. In any case, a hydrophobic patch, as revealed through the simulation, could provide an additional mode of interaction regulated by intermittent exposure to the solvent.

Most of the docking studies to date propose that the partially exposed heme groups of the interacting species in the complex are nearly co-planar with minimal separation between the heme edges, an arrangement that may be favorable for electron transfer (Poulos and Mauk, 1983; Salemme, 1976). Stayton and co-workers (Stayton et al., 1989), however, have suggested that the heme groups may be perpendicular in a cytochrome b_5 -cytochrome P-450_{cam} complex. In each case, acidic groups flanking both sides of the heme crevice appear to contribute to the complex interface (Figure 2.8). However, an alternative mode of interaction between cytochrome b_5 and cytochrome c has also been proposed. Hartshorn and co-workers (Hartshorn et al., 1987) found that a paramagnetic relaxation probe interacts with the exposed heme propionate of a complexed cytochrome b_5 . This suggests that the propionate group is exposed and the alignment of the proteins has changed and does not involve the entire putative binding surface depicted in Figure 2.8. In addition, Whitford (1992) found that cytochrome c shields only one

anionic patch of cytochrome b₅, involving Glu residues 37, 38, 43, 44, and 48, which fall on one side of the heme crevice (right hand side of the protein, Figure 2.8). These findings suggest that although an electrostatic interaction does take place, it need not necessarily lead to a co-planar arrangement of the heme groups, as is suggested by the original Salemme (Salemme, 1976) model. In addition, the heme groups are not coplanar in the crystal structure of a cytochrome c-cytochrome c peroxidase complex, instead they make an angle of ~60° to each other (Pelletier and Kraut, 1992).

The cleft identified in the simulation was near the main patch of acidic residues implicated in protein-protein contacts by all investigators (Figure 2.8). Because of the close proximity of the cleft to these acidic residues, it seems likely that it could contribute to recognition and binding, even assuming the binding mode suggested by Salemme (see Figure 2.8). Alternatively, in another shifted binding mode, the position and depth of this cleft could allow the partner in the complex access to the heme group (Figure 2.8). Thus, our results suggested that another portion of the molecule, in addition to, or in lieu of, the binding surface indicated in Figure 2.8, may be important in recognition. And, as discussed by Cherfils and others (Cherfils et al., 1991), there can be several distinct solutions to the macromolecular recognition problem. In any case, if the heme portion of cytochrome b₅'s partner were to bind within the cleft, one would not obtain a co-planar arrangement of heme groups. Docking of our 1.66 ns snapshot of cytochrome b₅ with the cytochrome c crystal structure revealed that it was possible to construct a complex whereby a hydrophobic patch near the heme group of cytochrome c fits into the cleft on cytochrome b₅ (data not shown). Furthermore, the acidic residues above the cleft (right hand side of the protein, Figure 2.8) have salt bridging partners on cytochrome c even in this orientation. We are currently refining this complex and constructing others utilizing different conformations adopted during the simulation in an attempt to more directly correlate the observed surface properties with the different interfacial interactions

cytochrome b_5 must be involved in with different proteins. In addition, we are testing our hypothesis by making mutations aimed at perturbing cleft dynamics, utilizing both simulation and experimental techniques (Storch et al. (a) and (b), *In preparation*).

The ability to display different surfaces utilizing solely native thermal motion may represent a low-energy mechanism for controlling recognition processes. Over a decade ago, Tainer and co-workers (Tainer et al., 1984) demonstrated that mobility is a major factor in recognition of native proteins by antipeptide antibodies and they speculated that it may be generally valid in protein-protein recognition. They suggested that proteins adopt a range of conformations and only bind to antibodies when a particular conformation recognized by the antibody is displayed. Furthermore, they note that the many conformations adopted in solution and displayed to the antibodies can differ from the average structure seen by X-ray crystallography. Based on our findings, we suggest that this may also be the case with cytochrome b_5 . Thus, we could envision different conformations interacting with different proteins and binding occurs when a favorable surface is displayed or the cleft, if involved, is accessible. Along these lines, many investigators have discussed the importance of flexibility in fine tuning interfacial interactions of electron-transfer protein complexes involving cytochrome b_5 (Burch et al., 1990; Mauk et al., 1986; Meyer et al., 1993; Wendoloski et al., 1987). Our findings would just take this a step further and suggest that flexibility may also be important in recognition prior to actual complex formation.

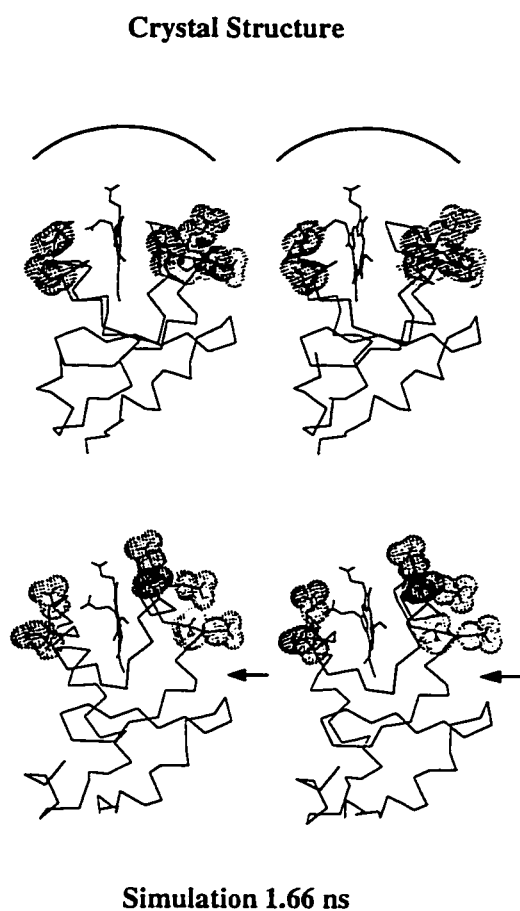


FIGURE 2.8: Stereo diagram of the C_α backbone of cytochrome b_5 : crystal structure and 1.66 ns snapshot from the simulation. The acidic residues implicated in protein-protein recognition are shown with van der Waal's surfaces displayed. Site I on the left contains Glu 56 and Asp 60 and site II on the right consists of Glu 37, 38, 43, 44, and 48. Most studies of cytochrome b_5 complexes assume that the protein-protein interface spans both sites and the heme group as shown with the curved line. The arrow near the structure from the simulation (1.66 ns) indicates the position of the cleft.

CHAPTER 3

STRUCTURAL CONSEQUENCES OF HEME REMOVAL: MOLECULAR DYNAMICS SIMULATIONS OF RAT AND BOVINE APOCYTOCHROME b₅

3.1 Introduction

An understanding of protein folding hinges upon elucidation of the progression of events occurring along the folding/unfolding pathway. Many experimental techniques have been applied to this problem; however, the cooperative nature of folding generally results in only minute amounts of partially folded intermediates at equilibrium. Exceptions to this behavior have been found in so-called molten globules, but these are generally found under denaturing conditions. Investigation of the nature of partially unfolded protein conformations under physiological or native conditions has been possible for a few hemoproteins destabilized through removal of their heme groups: apomyoglobin (Breslow et al., 1965; Brooks, 1992; Fink, 1995; Harrison and Blout, 1965; Hughson et al., 1991; Hughson et al., 1990; Lecomte and Cocco, 1990), apocytochrome b₅₆₂ (Feng et al., 1994; Feng and Sligar, 1991; Feng et al., 1991; Laidig and Daggett, 1996), and apocytochrome b₅ (Falzone et al., 1996; Huntley and Strittmatter, 1972; Moore et al., 1991; Moore and Lecomte, 1993; Moore and Lecomte, 1990; Tajima et al., 1976).

In addition to being a possible protein folding intermediate under native, *in vitro* conditions, apocytochrome b₅ appears to be populated *in vivo*. Apocytochrome b₅ is synthesized on the endoplasmic reticulum (Gonzalez and Kasper, 1980; Krieter and Shires,

1980) and an excess of the protein exists in microsomes (Hara and Minakami, 1970; Hara et al., 1970; Negishi and Omura, 1970; Shawver et al., 1984). Later, insertion of the iron and porphyrin moiety into the protein occurs in the mitochondria (Jones and Jones, 1969). Therefore, it may be necessary for apocytochrome b_5 to maintain a quasi-stable conformation following synthesis and intracellular transport prior to heme insertion.

Cytochrome b_5 consists of six α -helices, five strands making up a β -sheet and various β -turns. There are two hydrophobic cores in the molecule, one of which binds the heme group (core 1, Figure 3.1), while the other is important in maintaining the structural integrity of the protein (core 2, Figure 3.1). When the heme group is extracted under native conditions, the protein expands and is less stable than the holoprotein (Huntley and Strittmatter, 1972; Pfeil, 1993; Tajima et al., 1976). Circular dichroism (CD) studies suggest that there is an increase in disorder and less repetitive secondary structure in the apo form (Huntley and Strittmatter, 1972).

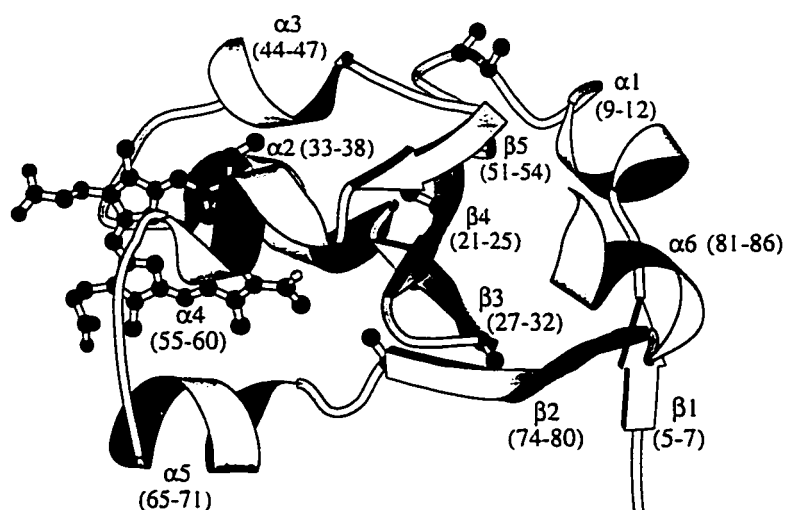


FIGURE 3.1: A ribbon diagram of the crystal structure of bovine cytochrome b_5 including the prosthetic heme group (Mathews et al., 1972). The heme group was not included in the apoprotein simulations. The two cores and the residue numbers comprising secondary structure elements are indicated. The C_β atoms for the six variant residues are displayed. This figure was made using MOLSCRIPT (Kraulis, 1991).

Using one- and two-dimensional NMR spectroscopy, Moore and Lecomte (Moore and Lecomte, 1990) found that there is a stable hydrophobic cluster in apocytochrome b_5 , in which Trp 22 figures prominently. This cluster is a key element of the second core. In addition, four of the five β -strands and at least two of the six α -helices are present in the apo form (Moore and Lecomte, 1993). The rest of the structure appears to fluctuate between different conformations (Moore et al., 1991). In fact, even structured portions of the protein are fluctuating more than in the holo form as measured by hydrogen exchange and NMR (Lecomte and Moore, 1991; Moore and Lecomte, 1993; Moore and Lecomte, 1990). More recent NMR studies utilizing ^{15}N -labeled protein support these earlier findings and provide further structural information (Falzone et al., 1996). This intermediate displays many of the hallmarks of the molten globule state except that there are well-populated tertiary interactions. Moore and Lecomte (Moore and Lecomte, 1993) have proposed a model in light of these results in which one of the cores folds rapidly (core 2), while core 1 requires the heme to fold properly.

Although structural data for apocytochrome b_5 exist, precise characterization of all portions of the molecule has been difficult because of its dynamic nature. Computer simulations provide an avenue for elucidating the atomic details of structural transitions and the detailed dynamic behavior of proteins. However, the information obtained from a simulation must be compared to experiment to ensure relevancy.

Cytochrome b_5 is a good choice for molecular dynamics (MD) simulation studies. It is small, containing 93 amino acid residues. The partially folded state occurs under native conditions, so we do not have to include denaturant or use high temperature to destabilize the native state. Most importantly, there is a wealth of structural information for both holo- and apocytochrome b_5 , and the necessary control simulation of holocytochrome b_5 is well-behaved (Storch and Daggett, 1995). Even though these structural data exist, there is still much to be learned from the simulations. For example, what do the

unstructured portions of the molecule look like? How much conformational sampling does the secondary structure experience, since it is present but fluctuating more than in the holo form? Are nonnative interactions important in stabilizing the folding intermediate? We can address these questions with simulations and provide a detailed dynamic, molecular model of apocytochrome b_5 that goes beyond, but is complementary to, what can be garnered using experimental methods.

To perform MD simulation studies of apocytochrome b_5 , one needs a starting structure. The only available crystal structure of cytochrome b_5 is of the bovine form, while the structural experimental work described above was performed on the rat protein. The sequence homology of the water-soluble fragment (residues 3–87) is 93% in the rat and bovine forms (Ozols et al., 1976), thus, structural differences between the two should be minor. This does indeed appear to be true for holocytochrome b_5 , as the six variant residues seem to have little to no effect based on the fact that our MD simulation of bovine holoprotein is in good agreement with both bovine and rat experimental results (Storch and Daggett, 1995). However, the MD simulation of bovine apocytochrome b_5 presented here exhibited slight structural deviations from the experimental data for the rat apoprotein. The discrepancy was localized to three regions of the protein and four of the six species variant residues are located within these regions. This led us to further investigate the structural and dynamical consequences of "mutating" these six residues. When the starting structure was modified to the rat sequence, the agreement between experiment and the MD results improved significantly, allowing us to propose a detailed model for the rat apocytochrome b_5 folding intermediate. In addition, these simulations demonstrate how mutations can lead to structural and dynamical changes in partially unfolded conformations while having no apparent effect on the folded state.

3.2 *Methods*

The starting conformation of apocytochrome b_5 was the crystal structure of bovine cytochrome b_5 with the prosthetic heme group removed (Brookhaven Protein Data Bank, 3b5c; (Mathews et al., 1972). The crystal structure contains residues 3–87; residues 1–2 and 88–93 were not visible in the electron density maps and were therefore omitted in the simulation. For the rat protein simulation, six modifications were made to the bovine crystal structure coordinates by placing the new sidechains in approximately the same orientation. The following mutations were made : Ala 3 \rightarrow Asp, Asn 16 \rightarrow Lys, Asn 17 \rightarrow Asp, Leu 23 \rightarrow Val, Tyr 27 \rightarrow His, and Phe 74 \rightarrow Tyr (bovine \rightarrow rat) (Ozols, 1989). The positions of these variant residues are indicated in Figure 3.1.

The potential energy function (Laidig and Daggett, 1996; Levitt, 1989; Levitt et al., 1995; Levitt et al., 1997; Levitt and Meirovitch, 1983) and associated protocols (Daggett and Levitt, 1992) are described in detail elsewhere. Energy minimization and the MD simulations were performed using the program ENCAD (Levitt, 1990). The simulations were performed at pH 2 for 200 ps and continued at pH 6.9 for 1400 ps. This procedure was followed because heme removal occurs experimentally by lowering the pH to 2 (Teale, 1959), which protonates the coordinating histidine residues (His 39 and 63) and subsequently releases the heme. Experiments are then resumed at a physiologically relevant pH of 6.9. The water density was set to the experimental value (0.997 g/ml) at 298 K (Kell, 1967) by adjusting the volume of the box prior to beginning the simulation. The MD simulation of rat protein contained 2901 water molecules at pH 2 and 3084 water molecules at pH 6.9. The bovine protein simulation contained 2771 water molecules at pH 2 and 3096 water molecules at pH 6.9.

Beginning with the low pH conditions (Glu, Asp, and His protonated), the systems were subjected to a variety of preparatory steps as described elsewhere (Storch and

Daggett, 1995). MD was then performed for 1×10^5 steps utilizing a 2 fs time step, resulting in the first 200 ps of the trajectory at 298 K. The starting structure for this portion of the simulation was used as the starting point for the simulation at pH 6.9. All Glu and Asp residues and His 26, His 27 (in the case of the rat simulation, the bovine form contained Tyr at this position) and His 80, were deprotonated. His 15, His 39, and His 63 and all Lys and Arg residues were protonated and positively charged. The experimentally determined pK_a values for the His residues were used to determine the ionization states (Altman et al., 1989; Moore et al., 1991). Again, the proteins were solvated and prepared for MD. The MD trajectory was then continued for 1400 ps at 298 K and structures were saved every 0.2 ps for analysis (7000 structures).

3.3 Results

3.3.1 Rat Apocytochrome b_5 : Tertiary Structure

The starting structure for the simulation of rat apocytochrome b_5 was the modified crystal structure of bovine cytochrome b_5 (Mathews et al., 1972); the six variant residues which involved “mutating” are shown in Figure 3.1. Cytochrome b_5 contains two distinct regions: core 1 (residues 33–73) and core 2 (residues 3–32 and 74–87) (Figure 3.1). The C_α root-mean-square (RMS) deviation from the crystal structure of each core was monitored separately (Figure 3.2) and a drastic difference between the cores was evident. Within the first 300 ps of the simulation, the deviation from the crystal conformation of core 1 climbed to 3.7 Å. These residues fluctuated greatly with time and reached values greater than 5.5 Å. Conversely, core 2 deviated much less from the crystal structure (~2 Å) and experienced only minor fluctuations.

In order to localize the motion to more distinct areas of the protein, the C_{α} RMS deviation was plotted as a function of residue number and time (Figure 3.3). The deviation was greatest in core 1, primarily for residues 33–76 and the C-terminus. The highest deviations, shown in black, occurred predominantly between residues 39–52 and 65–72. These residues incorporate the secondary structure elements $\alpha 3$ and the preceding loop, $\alpha 5$, and the loop prior to $\beta 2$ (Figure 3.1). In the latter part of the simulation, residues 52–60 ($\beta 5$, $\alpha 4$, and preceding loop) also showed large deviations. $\alpha 6$ accounted for the large degree of deviation in core 2, as it had few tethers to the rest of the protein. Throughout the simulation, more dramatic deviation was observed in core 1 (helices $\alpha 2$ – $\alpha 5$) than core 2.

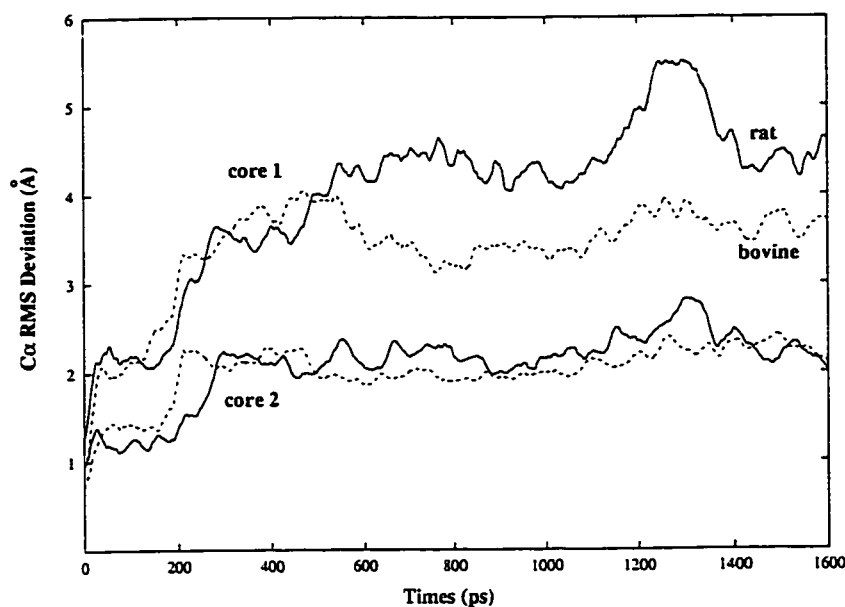


FIGURE 3.2: The C_{α} RMS deviation from the crystal structure as a function of time. The rat simulation is depicted in black and the bovine simulation in a stippled line. The two upper lines represent the deviation of core 1 residues (33–73) and the two lower lines represent core 2 residues (3–32 and 74–83). For simplicity, we defined the cores as being inclusive in sequence, instead of marking each individual hydrophobic group pointing into each core. The last three residues (84–87) were not monitored. The proteins were modeled at pH 2 for the initial 200 ps and pH 6.9 thereafter.

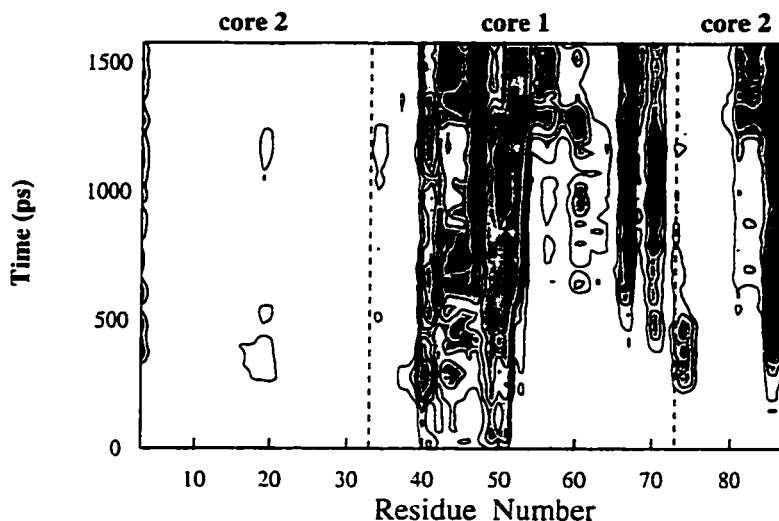


FIGURE 3.3: Contour plots of the C_{α} RMS deviation from the crystal structure per residue number as a function of time. Deviations are colored as follows: black, $\text{RMS} > 5$ Å; gray, $4 \text{ Å} < \text{RMS} < 5 \text{ Å}$; light gray, $3 \text{ Å} < \text{RMS} < 4 \text{ Å}$; white, $\text{RMS} < 3 \text{ Å}$. The core boundaries are denoted by dashed lines.

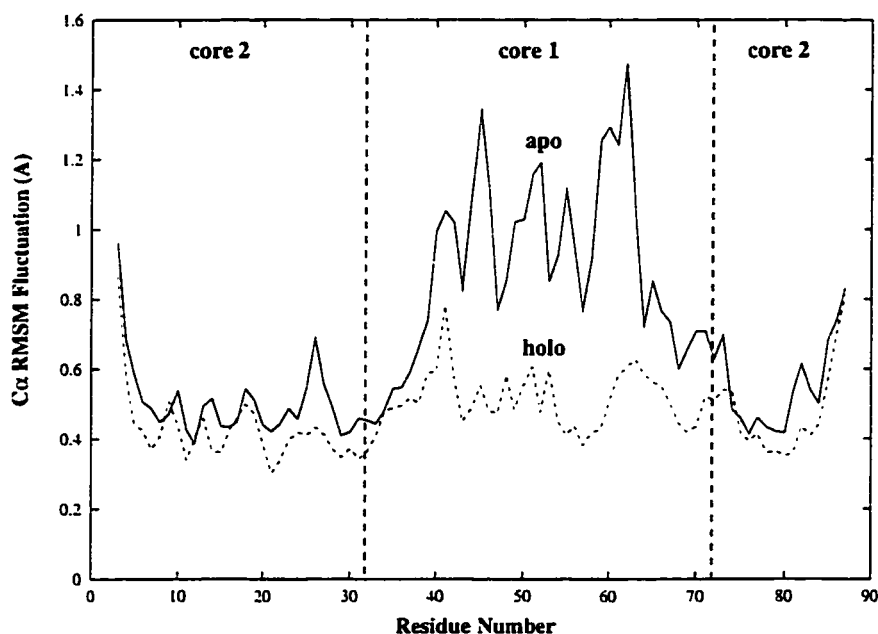


FIGURE 3.4: Plots of the C_{α} RMS fluctuation per residue number. The values were averaged over the last 200 ps of the simulations. The rat simulation is shown in black and the bovine run is shown in a stippled line.

Even though core 1 deviated considerably from the crystal structure, the deviation did not necessarily reflect heightened mobility. For example, a conformation may have been adopted that was different from the crystal structure, but could be quite immobile once it had stabilized in the new orientation. A more direct way to determine the mobility of a state was by calculating the C_{α} RMS fluctuation about the mean structure as in Figure 3.4. There was a dramatic increase in the mobility of core 1 in the apo form compared to its heme-bound state, although at certain time points the mobility of residues 40–50 was high in the control simulation as well. Thus, not only did the placement of core 1 in apo b₅ change compared to the crystal structure, but after doing so it remained very mobile.

A series of snapshots at various time points illustrate the areas of high mobility (Figure 3.5). The backbone displacement was highest in core 1 (residues 33–73). The helices in this core ($\alpha 2$ – $\alpha 5$) moved out and away from the center of the heme-binding pocket and became conformationally heterogeneous. $\beta 5$, which borders the heme pocket, became displaced from the β -sheet and disrupted the connectivity between cores 1 and 2 (this strand moved ~ 12 Å from its starting position). This was particularly evident when considering the solvent accessibility of $\beta 4$ residues (residues 21–25), all of which were sequestered in the holoprotein. The solvent accessibility of these residues increased 7–54 Å², with an average increase of 26 Å². In contrast to core 1, the backbone placement was strikingly similar to the crystal structure for most of core 2 with the possible exception of the N- and C-termini which fluctuated a great deal, and at times making even closer contacts with the protein core than in the crystal structure.

Additional tertiary contacts were monitored throughout the simulation and compared to the experimental NMR data. Potential nuclear-Overhauser effects (NOEs) were evaluated by calculating an average-weighted-distance ($\langle r^{-6} \rangle^{-1/6}$) between interacting hydrogens during the simulation. All of the hydrogen-hydrogen distances corresponding to the experimentally-observed NOEs (Moore and Lecomte, 1993) in hydrophobic core 2

(see Figure 4 of (Moore and Lecomte, 1990)) remained below 5 Å, which is considered a reasonable cutoff for an NOE (Wüthrich, 1986). These interactions are experimentally observed for both rat apo- and holocytochrome b_5 (Moore and Lecomte, 1990). Falzone and co-workers (Falzone et al., 1996) have found that the amide hydrogens of core 1 exchange with solvent, while many of the residues in core 2 are protected. In the simulation, the protected residues in core 2 participated in hydrogen bonds and would therefore be unlikely to exchange with solvent.

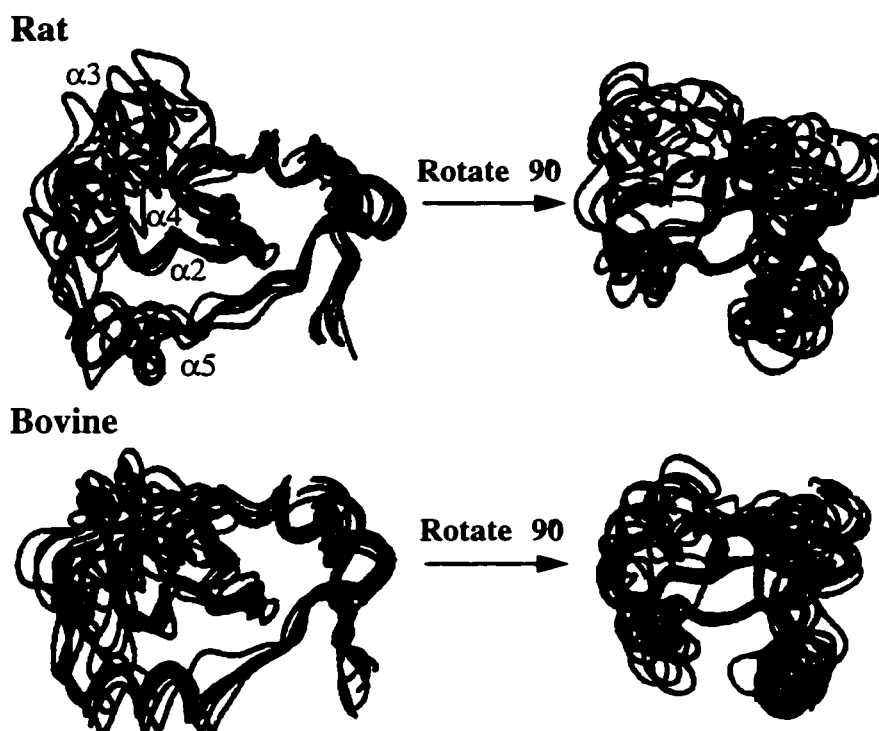


FIGURE 3.5: Mainchain traces from various time points throughout the rat and bovine simulations (350, 550, 750, 950, 1150, and 1350 ps). The crystal structure is shown in cyan. The figures on the left are in the same orientation as in Figure 3.1. The figures on the right provide a view into the heme binding pocket.

Pfeil (Pfeil, 1993) has reported second derivative heat capacity spectra of apo- and holocytochrome b_5 , indicating that the Trp and Tyr residues are in similar environments in the two forms of the protein, while the environment of the Phe residues changes upon heme removal. However, in comparison to our MD simulation, it must be noted that Pfeil's work focuses on the rabbit protein. The Phe, Tyr, and Trp residues were identical in the rat and rabbit sequences with the exception of Phe 74, which was a Tyr in rat and Phe in the bovine form (Ozols, 1989). In the MD simulations of apo- and holocytochrome b_5 , the solvent accessibility of the Tyr and Trp residues was low (the apoprotein showed an increase of 4–13 Å², where the residues are not exposed in holo), with the exception of Tyr 74 (with a 35 Å² increase from holo). The solvent exposure of the Phe residues increased in the apoprotein MD simulation (20–44 Å²), as suggested by experiment. Phe 35, 58, and Tyr 74 interact with the heme and are sequestered from solvent in the holoprotein.

3.3.2 *Secondary Structure*

The boundaries of the secondary structure were determined via (ϕ, ψ) dihedral angles using a previously described method (Daggett et al., 1991; Daggett and Levitt, 1992) that required at least 3 residues in succession to fit the dihedral angle criterion. The overall amounts of α -helical and β -sheet structure in apocytochrome b_5 were in good agreement with the CD results of Huntley and Strittmatter (Huntley and Strittmatter, 1972) (Table 3.1); however, it must be noted that CD is not reliable for definitive quantitative determination of secondary structure, as evidenced by the disparity in the results from two different research groups (Table 3.1).

When compared with the crystal structure, the helical content for α_2 increased (Table 3.1); this phenomenon is also observed in the control simulation of holocytochrome

b₅ (Storch and Daggett, 1995). α 3 showed low helix content throughout the simulation. After the first 500 ps, the helix content of α 5 dropped considerably and it was structurally labile for the remainder of the simulation. α 6 decreased significantly in helical content compared to the crystal structure. In contrast, α 1 and α 4 retained high helix contents, even though α 4 was extremely mobile (residues 55–60, Figures 3.4 and 3.5). α 2 was the most stable of the helices in core 1, in terms of internal structure and its dynamic behavior (Figure 3.5).

Two of the five strands in the β -sheet (β 2 and β 5) were structurally heterogeneous in the simulation. β 2 (residues 74–80) and β 5 (residues 51–54) are defined as irregular in the Brookhaven PDB file (Mathews et al., 1972). This irregularity was reflected in the low β -content of these segments in the crystal structure (Table 3.1). β 2 further decreased almost immediately in the simulation and remained low for the duration of the simulation. β 5, on the other hand, never adopted β -structure according to the dihedral angle definition used. The remainder of the β -strands (β 1, β 3 and β 4) were well-maintained during the simulation. Even though the β -content of β 3 was low, it was comparable to that of the crystal structure.

Table 3.1: Overall Percentage of Secondary Structure for Segments of Apocytochrome b_5 in the Holo Crystal Structure and During Molecular Dynamics^a

Secondary Structure ^b	Crystal Structure	MD Rat Apo b_5	Experiment Rat Apo b_5	MD Bovine Apo b_5
$\alpha 1$ (9–12)	100	99 (1)		97 (14)
$\alpha 2$ (33–38)	33	94 (10)		78 (32)
$\alpha 3$ (44–47)	100	75 (9)		94 (15)
$\alpha 4$ (55–60)	100	98 (1)		97 (10)
$\alpha 5$ (65–71)	100	62 (18)		97 (8)
$\alpha 6$ (81–86)	83	16 (16)		26 (38)
Overall α^c	33	28	25–30 ^d , 21 ^e	31
$\beta 1$ (5–7)	100	92 (8)		25 (44)
$\beta 2$ (74–80)	57	8 (6)		11 (19)
$\beta 3$ (27–32)	67	66 (2)		65 (6)
$\beta 4$ (21–25)	100	98 (2)		90 (19)
$\beta 5$ (51–54)	0	0		0
Overall β	19	14	10–15 ^d , 44 ^e	12

^a α -helical or β -structure was defined as having at least three consecutive residues with the appropriate (ϕ, ψ) dihedral angles (Daggett and Levitt, 1992). Secondary structure contents are given in percentage units, with the standard deviation in parentheses. The values are averages over the entire simulations (200–1600 ps).

^b The elements of secondary structure (residue numbers in parentheses) are shown in Figure 3.1.

^c The overall fraction secondary structure is for the entire protein over time divided by the total number of residues.

^d These data were obtained from CD experiments (Huntley and Strittmatter, 1972).

^e These data were obtained from CD experiments (Pfeil, 1993).

The intramolecular mainchain hydrogen bonds were monitored as another probe of secondary structure content. A hydrogen bond was defined as having a distance of ≤ 2.6 Å between carbonyl oxygen and amide hydrogen atoms and a hydrogen bonding angle (N–H \cdots O=C) within 45° of linearity. The values for the $i \rightarrow i + 4$ hydrogen bonds diagnostic of helical structure within the helices of the crystal structure (with added hydrogen atoms) were all ≤ 2.6 Å, with the exception of two hydrogen bonds within $\alpha 2$ (between residues 33–37 and 34–38) and $\alpha 6$ (residues 81–85 and 82–86). During the simulation, $\alpha 2$ formed the two helical hydrogen bonds not observed in the crystal structure. $\alpha 6$ also formed one of the missing hydrogen bonds (residues 81–85) in the first part of the simulation (0–750 ps), but lost it after 750 ps, reaching distances of ~ 3.7 Å. The $i \rightarrow i + 4$ distances of $\alpha 2$ (residues 34–38) exceeded ~ 3 Å intermittently throughout the simulation (900–1200 ps) as did those of $\alpha 3$ (residues 44–48, 500–1300 ps). One of the internal $i \rightarrow i + 4$ distances of $\alpha 5$ (residues 66–70) began increasing at 550 ps and the hydrogen bond was lost for the duration of the simulation. All other helical mainchain hydrogen bonds remained intact.

Interresidue hydrogen-hydrogen distances were also monitored and compared with the available NOEs. Moore and Lecomte (Moore and Lecomte, 1993) found that $\alpha 1$ contains many of the NOEs diagnostic of helical structure. There is some evidence for helical NOEs in $\alpha 2$ and $\alpha 3$, but the intensities are lower than in the holo form. There is one probable helical NOE in $\alpha 4$. Residues in $\alpha 5$ could not be assigned. There is some evidence for helical NOEs in $\alpha 6$ but a lack of resolution prevented full assignment.

In the simulation, all of the $i \rightarrow i + 3$ connectivities expected for α -helices remained below 4 Å in $\alpha 1$ – $\alpha 4$ throughout the simulation. The $i \rightarrow i + 3$ NOEs for $\alpha 5$ and $\alpha 6$, however, fluctuated greatly. In the C-terminal region of $\alpha 5$ (residues 66–69, 67–70, and 68–71), the distances were between 5 and 6 Å. The corresponding distances in the crystal structure were ≤ 3.9 Å. $\alpha 6$ had three $i \rightarrow i + 3$ NOEs within the defined region, residues

81–86. For the first 500 ps, all of these remained mostly below 4 Å. For the remainder of the simulation, the NOEs between residues 82–85 and 83–86 were ~4.8 Å. Overall, $\alpha 5$ experienced the most loss of structure of the α -helices as determined by calculated NOEs.

A network of experimentally-observed NOEs exist in the β -sheet of holocytochrome b_5 (Guiles et al., 1990; see Figure 6 Moore and Lecomte, 1993) and are retained in apocytochrome b_5 with the exception of the interactions between $\beta 4/\beta 5$ (Moore and Lecomte, 1993). All of these β -sheet NOEs were observed throughout the entire MD simulation, except for two NOEs between $\beta 2/\beta 3$ and the three between $\beta 4/\beta 5$ (Guiles et al., 1990). As mentioned previously, $\beta 2$ (residues 74–80) is irregular in the crystal structure. Furthermore, crystallographic studies indicate that there is a bend or kink in $\beta 2$ and that Ile 75, which is located in the middle of the strand, does not participate in the β -structure (Mathews et al., 1979). In addition, the hydrogen bond between the amide hydrogen of residue 77 and the carbonyl oxygen of residue 29 is long in the crystal structure at 3.8 Å. The NOEs corresponding to this region exceeded 5 Å in the simulation for the first 300–500 ps; the mean values for the hydrogen-hydrogen interactions between $C_\alpha H_{30}-NH_{76}$ and $C_\alpha H_{30}-C_\alpha H_{75}$ were 5 Å and 5.6 Å, respectively. After 500 ps, however, the distances dropped to well below 5 Å. The loss of the contacts between $\beta 4/\beta 5$ occurred first at the N-terminus of $\beta 5$ with residue 51. Eventually, distances for the $\beta 4/\beta 5$ region reached ~15 Å.

3.3.3 Bovine Apocytochrome b_5 : Tertiary Structure

The starting conformation for the simulation of bovine apocytochrome b_5 was the bovine crystal structure without the heme group. The C_α RMS deviation of the bovine apo simulation from the crystal structure is depicted in Figure 3.2. A difference of

approximately 1.5 Å was observed between cores 1 and 2, relative to the crystal structure. Interestingly, the rat form had a higher C_{α} RMS deviation for core 1.

Residues 31–80 (not shown) displayed C_{α} RMS deviations of ≥ 3 Å. This region includes the C-terminal portion of core 1, extending into $\beta 2$. In the latter part of the simulation (1200–1600 ps), residues 16–18 exhibited increased deviations, as well. This behavior differed from that of the rat form, where deviations were localized almost entirely to core 1 (Figure 3.3). As in the rat simulation, core 2 deviated much less from the crystal structure than core 1 (Figure 3.5). Core 1, however, was much less mobile than that of rat b5. In addition, the $\beta 4/\beta 5$ connection was never completely lost, as was observed for rat b5 (Moore and Lecomte, 1993). Moreover, the connectivities between $\beta 1/\beta 2$ ($C_{\alpha}H6-NH78$, $NH7-NH78$) and $\beta 2/\beta 3$ ($C_{\alpha}H30-C_{\alpha}H75$, $C_{\alpha}H30-NH76$) were disrupted, unlike the rat b5 simulation. The regions that differ between the two simulations contained four of the six variant residues (Figure 3.1).

3.3.4 Secondary Structure

The secondary structure elements of the bovine protein were analyzed via the methodology described above. All helices maintained high helical contents throughout the simulation, with the exception of $\alpha 2$ and $\alpha 6$ (Table 3.1). For the first 500 ps, the helical content of $\alpha 2$ remained below 42%, after which it rose to $\geq 88\%$ and remained high for the duration of the simulation. Large fluctuations were observed for $\alpha 6$, as was seen in the rat simulation. In contrast to the rat simulation, however, the overall α -helical content remained somewhat higher at 31%.

The β -structure, which comprises much of core 2, experienced much greater fluctuations. The β -content of $\beta 1$, dropped to 0% by 900 ps, where it remained for the duration of the simulation. $\beta 2$ and $\beta 5$ had very low β -content throughout the simulation.

$\beta 3$ and $\beta 4$, the central strands in the β -sheet, maintained relatively high β -contents. Note that although $\beta 3$ had only 65% β -structure, it was the same as that observed in the crystal structure. $\beta 4$ maintained high β -content ($\geq 94\%$) until 1100 ps when it dropped to 70–76%.

In addition, $i \rightarrow i + 3$ α -helical hydrogen-hydrogen NOE distances were measured. Almost all of the $i \rightarrow i + 3$ of the six helices remained in the detectable range (≤ 5 Å) throughout the simulation. The distances of $\alpha 2$ became slightly extended (≥ 4 Å) from 200–1100 ps and those of $\alpha 6$ reached higher values (≥ 4 Å) between 200–400 ps and 800–1600 ps. In contrast to the rat simulation, none of the contacts corresponding to NOEs in the helices exceeded 5 Å.

Many of the experimentally-observed β -sheet NOE connectivities for core 2 of rat apocytochrome b_5 were lost for the bovine apoprotein (Guiles et al., 1990). The corresponding values for the $\beta 1/\beta 2$ contacts, $C_\alpha H6-NH78$ and $NH7-NH78$, were 5.4 Å and 6.9 Å, respectively. The $\beta 2/\beta 3$ NOEs for $C_\alpha H75-C_\alpha H30$ and $C_\alpha H76-C_\alpha H30$ were 6.2 Å and 5.2 Å. The $\beta 4/\beta 5$ contacts $C_\alpha H23-NH51$, $C_\alpha H23-NH52$, and $NH24-C_\alpha H53$, that were lost in both the rat simulation and experiments were 5.8, 4.2, and 3.8 Å, respectively, in the bovine simulation. Additionally, the NOE contacts between residues 22 and 76 of the hydrophobic core were lost after 500 ps. Interestingly, all of these NOEs were retained in the MD simulation of bovine holocytochrome b_5 (Storch and Daggett, 1995).

3.3.5 Structural Effects of Variant Residues

The local structural effects of the variant residues were investigated in order to elucidate the observed global differences between the MD simulations of rat and bovine apo b_5 . The variant residues are given as changes from the bovine to the rat sequence. Two of

the six residues, Tyr 27 → His and Phe 74 → Tyr, showed no obvious stabilizing or destabilizing interactions in the two simulations.

One of the local effects of the Ala 3 → Asp substitution was a salt bridge that formed between Asp 3 and Lys 5 in the rat simulation. This interaction is not present in the crystal structure and formed during the first 50 ps of the rat simulation at pH 6.9 and was maintained for the rest of the simulation. The corresponding residues in the bovine simulation, Ala 3 and Lys 5, were unable to interact in such a way, which resulted in increased conformational sampling in $\beta 1$.

The Asn 16 → Lys and Asn 17 → Asp substitutions are illustrated in Figure 3.6. Residue 16 is located in the loop between $\alpha 1$ and $\beta 4$. In the rat simulation, the charged amine of Lys 16 burrowed between the two hydrophobic cores by 420 ps and remained in this position for the remainder of the simulation. Although Asn 16 showed some inclination toward such displacement in the bovine simulation, the structural effects were not as dramatic. Thus, Lys 16 contributed to the disruption of interactions between $\beta 4$ and $\beta 5$, while the neutral Asn 16 did not. Furthermore, Asn 16 formed a stabilizing hydrogen bond with the carbonyl of Gly 51 in the bovine simulation. In both proteins, residue 17 remained on the surface completely solvent accessible and did not participate in obvious stabilizing or destabilizing interactions.

The structural effects of the Leu 23 → Val substitution resulted in sustained van der Waals contacts between Leu 23, Ala 50, and Ala 54 in the bovine simulation, which constituted the prominent stabilizing interactions between $\beta 4$ and $\beta 5$. This effect was not seen in the rat simulation and the $\beta 4/\beta 5$ sheet became disrupted.

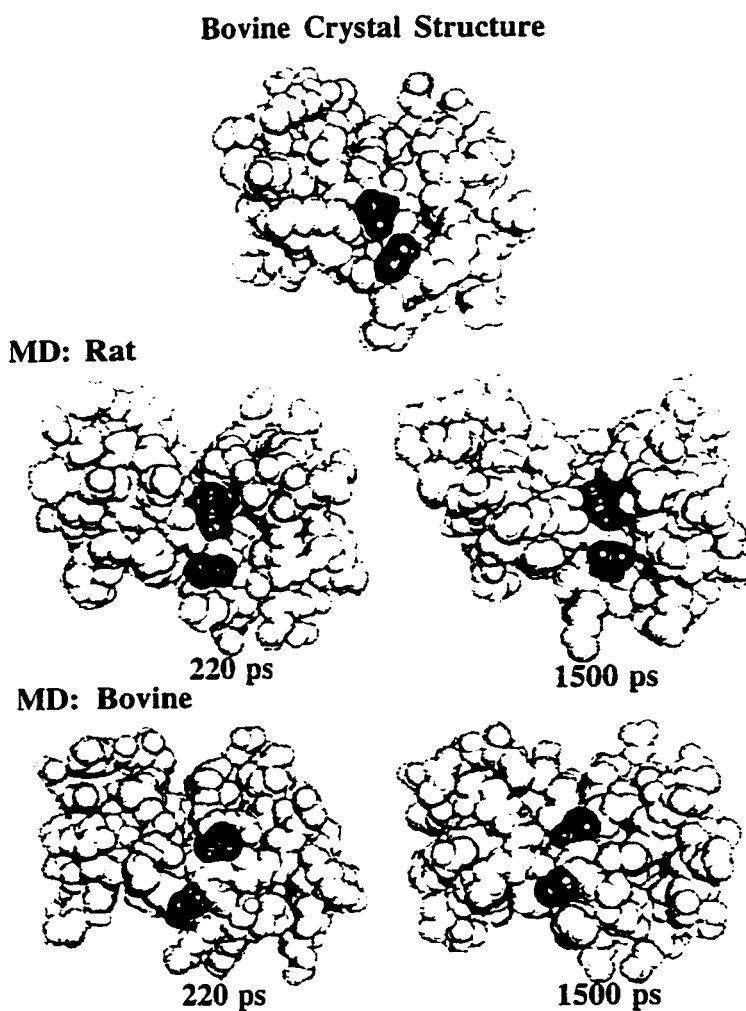


FIGURE 3.6: Space-filling representations of rat and bovine apocytochrome b_5 . The variant residues in the rat (Lys 16 and Asp 17) and bovine (Asn 16 and 17) proteins are shown in gray. The crystal structure is shown for reference.

3.4 Discussion

Initially, we intended to simulate the bovine form of apocytochrome b_5 and compare to the experimental data on rat apocytochrome b_5 , as the available crystal structure is of the

bovine form. The sequence identity between the rat and bovine sequences (for the water-soluble fragment of the protein used for simulation and experiment) is 93%, which corresponds to six amino acid substitutions. The high degree of homology suggested that the two forms should be structurally similar, if not identical. Furthermore, a control simulation of bovine holocytochrome b_5 (Storch and Daggett, 1995) is well-behaved as determined by comparison to structural experimental data (Guiles et al., 1990; Moore et al., 1991; Moore and Lecomte, 1990; Veitch et al., 1988). However, during the simulation of bovine apocytochrome b_5 presented here, we observed progressively more deviations from what is expected on the basis of experiments on the rat protein. The disagreement was localized to specific areas of the protein located near four of the variant residues.

Based on this observation, six residue substitutions were made to the bovine protein and we subsequently simulated "rat apocytochrome b_5 ." The rat simulation was in closer agreement to experiment. In this discussion, we first compare our results with the data on the rat protein and then present findings that illustrate the subtle differences in structure and dynamics between the rat and bovine simulations.

3.4.1 *Rat Apocytochrome b_5*

Previous studies indicate that apocytochrome b_5 retains limited native-like structure upon removal of the prosthetic heme group. The structure of the apoprotein is less compact, experiences an increase in disorder, and changes in secondary structure elements (Huntley and Strittmatter, 1972; Tajima et al., 1976). A variety of NOEs remain upon removal of the heme, and four of the five β -strands ($\beta 1$ – $\beta 4$) are configured as in the holoprotein by 2-D NMR studies (Moore and Lecomte, 1993). Lack of resolution and weak NOE patterns have hindered the assignment of all helical NOEs, and Moore and Lecomte concluded that the two terminal helices ($\alpha 1$ and $\alpha 6$) are present, as in the

holoprotein, with conformational multiplicity occurring in the others. Furthermore, characterization of core 2 provides details regarding a stable unit in the partially unfolded form (Moore and Lecomte, 1993; Moore and Lecomte, 1990).

As indicated in Figures 3.2, 3.3, and 3.4, the MD simulations of rat apocytochrome b_5 was in agreement with the general observation of core stability. That is, the residues of core 1 both deviated substantially from the crystal structure and experienced a conformational flexibility not observed in core 2. Numerous sidechain interactions led to the damping of mobility in core 2 (Figure 3.4), as observed by Moore and Lecomte (Moore and Lecomte, 1990).

Our studies indicated that loss of structure was localized to particular regions of the protein. Of the heme-binding helices, $\alpha 3$ and $\alpha 5$ experienced the greatest internal fluctuations in structure and both of these, in addition to $\alpha 4$, became displaced from their orientations in the crystal structure (Figures 3.2 and 3.5). $\alpha 5$ also became quite disrupted at its N-terminus as the simulation progressed. Characteristic α -helical NOEs were lost for $\alpha 5$ and it displayed a marked movement away from the $\beta 3/\beta 4$ loop. It should be reiterated that although experiment detects fluctuations in core 1 of the protein (Moore and Lecomte, 1993), the ability to resolve the exact magnitude and precise placement of the motion and structural disruptions is limited. Our simulations provided a structural model in which secondary structure disruption to the α -helices was limited, with $\alpha 3$, $\alpha 4$, and $\alpha 5$ being most affected in accord with experiment (Falzone et al., 1996), although all of the core 1 α -helices were highly mobile (Figures 3.2, 3.4, and 3.5).

Core 2 contains primarily the β -sheet and α -helices 1 and 6. The simulation revealed that the majority of the structural stability in this unit resided within $\beta 1$, $\beta 3$, and $\beta 4$. The C-terminal tail of $\alpha 6$ exhibited multiple conformations. Structure was progressively lost in this helix; however, the retention of the experimental NOE connectivities between NH7 and both NH78 and NH80 ($\beta 1$ and $\alpha 6$, respectively) (Moore

and Lecomte, 1993) throughout the simulation reflected the fact that tertiary structure in this region remained intact.

In contrast to the stability of the majority of core 2, conformational multiplicity of $\beta 5$ and the nearby α -helical regions ($\alpha 3$ and $\alpha 4$) of core 1 was observed. The NOEs lost between $\beta 4$ and $\beta 5$ led to disruptions in the interface between cores 1 and 2, thus allowed core 1 to become less ordered. The attachment of $\beta 5$ to the β -sheet is non-identifiable in the apoprotein 2-D NMR experiments (Moore and Lecomte, 1993). Comparison of solvent accessibility of the residues in apocytochrome b_5 and holocytochrome b_5 revealed that residues in $\beta 4$ (21–25) gained varying amounts of exposure, as has also been seen experimentally (Moore and Lecomte, 1993).

3.4.2 Bovine Apocytochrome b_5 and Structural Effects of the Variant Residues

The amount of experimental information for bovine apocytochrome b_5 is practically nonexistent (Huntley and Strittmatter, 1972). Therefore, we compared MD simulations of bovine and rat apocytochrome b_5 to explore their structural differences and similarities. Core 1 of the bovine form possessed a greater deal of conformational flexibility relative to core 2, as was also observed in the rat apo simulation (Figures 3.2 and 3.5). The increased mainchain mobility, resulting from heme removal, extended through residue 80, located in core 2. In contrast, the mobility present in the rat simulation was confined to core 1 (excluding the C-terminus), ending at residue 75 (Figure 3.3).

Although a “loosening” of core 1 occurred relative to the starting conformation, the overall secondary structure content of the helices was higher than in the rat form, with $\alpha 2$ being the most disrupted. Experimentally, a structural disruption at the interface between cores 1 and 2 is observed for the rat protein (Moore and Lecomte, 1993). Two of the three variant residues located in this region are near the interface of cores 1 and 2; Asn 16 →

Lys, Asn 17 → Asp, and Leu 23 → Val (bovine → rat). In both proteins, residue 16 moved in toward the interface (Figure 3.6). Lys 16 contributed to the disruption of the hydrophobic interactions between core 1 and 2 in the rat simulation, while Asn 16 in the bovine simulation did not achieve the same effects and instead formed some stabilizing hydrogen bonds with the loop between $\alpha 3$ and $\beta 5$. In both cases, residue 17 was not critical to the structure, and was completely accessible to solvent. An important stabilizing interaction at the interface of the two cores in the bovine simulation was a localized hydrophobic cluster involving Leu 23, Ala 50, and Ala 54. In the rat protein Val 23 interacted intermittently with Ala 54 but not Ala 50. This interaction, and the lack of disruption by Lys 16, as seen in the rat simulation, were the prominent factors leading to a more stable core 1 for bovine apo b5.

The secondary structure content of core 2 was lower overall in the bovine simulation. In contrast to the rat form, $\beta 1$ had low β -content and $\beta 4$ displayed high deviations. Furthermore, the conformational deviations of $\beta 1$ and $\beta 2$ had an effect on tertiary contacts and the overall stability of the sheet. These two regions contain three variant residues: Ala 3 → Asp, Tyr 27 → His, and Phe 74 → Tyr (bovine → rat). The Ala 3 → Asp variant in the rat simulation showed drastic improvements in connectivity between $\beta 1/\beta 2$ sheet. In addition, a salt bridge formed between Asp 3 and Lys 5, which stabilized the N-terminus of $\beta 1$, forming a more rigid “appendage” that remained in contact with the main portion of the protein. The lack of the rigidity in this region of the bovine protein allowed for more conformational sampling of the N-terminus. The added constraint in the rat simulation was also reflected in the secondary structure content of $\beta 1$, which was 92% in the rat form versus 25% in bovine (Table 3.1). Although the last two variant residues (27 and 74) are located in the region where the rat simulation showed greater agreement with experiment, there were no obvious local stabilizing interactions that occurred as a

consequence of the substitutions. It was more likely that the subsequent stabilization between $\beta 2$ and $\beta 3$ was due to the indirect effects of other substitutions.

3.5 *Conclusions*

Experimental studies suggest that core 1 of rat apocytochrome b_5 is well-maintained during the beginning stages of the unfolding process, while core 2 is conformationally heterogeneous and highly dynamic (Falzone et al., 1996; Moore et al., 1991; Moore and Lecomte, 1993; Moore and Lecomte, 1990). Our simulations revealed a similar pattern of structural and dynamic variation between the two cores. Core 2 remained compact and intact while core 1 experienced some loss of tertiary and secondary structure. A decrease in β -structure was observed at the interface of the cores, and portions of the α -helical structure in core 1 were disrupted as the entire core became dynamic and conformationally heterogeneous. We would suggest that α -helices in core 1 were basically intact, with the possible exception of $\alpha 5$, which became quite disrupted. These structural characteristics were consistent with NMR experiments of rat apo b_5 (Falzone et al., 1996), although we may have over predicted α -helical content for $\alpha 4$. Even though the helical content of helices in core 1 was high in the simulation, they became highly dynamic and may confound experiments designed to monitor their structural properties. For example, the difficulty in resolving the NMR crosspeaks in core 1 (Moore and Lecomte, 1993) may be due to the dynamic behavior of the apoprotein as opposed to extensive loss of helical structure, as is been observed for apocytochrome b_{562} (Feng et al., 1994; Laidig and Daggett, 1996).

Initially our studies were performed on bovine apocytochrome b_5 . Unfortunately, while displaying the same general properties as the rat simulation, many of the NOEs predicted from the MD-generated model did not accurately reproduce some of the more

precise structural NMR information available. Namely, the bovine simulation showed too much structure in some areas of the protein and too little in others. Therefore, we constructed and proceeded with a model of the rat form. Although the sequence changes appeared to be innocuous when viewed in the crystal structure, they have a marked effect on the structure and dynamics of the apoprotein. Interestingly, this structural variance only occurred once the heme group is removed, since the MD simulation of bovine holocytochrome b_5 correlated very well with the rat holocytochrome b_5 experimental data (Storch and Daggett, 1995).

CHAPTER 4

ENGINEERING OUT MOTION: INTRODUCTION OF A *DE NOVO* DISULFIDE BOND AND A SALT BRIDGE DESIGNED TO CLOSE A PUTATIVE DYNAMIC CLEFT ON THE SURFACE OF CYTOCHROME b_5

4.1 *Introduction*

It is generally expected that the stability of a protein should be balanced with dynamics that are essential for function. The goal of the following experiments was to study localized conformational fluctuations in the heme-containing electron transfer protein cytochrome b_5 , and their possible roles in equilibrium stability.

Here, we have chosen to focus on how conformational stability in cytochrome b_5 relates to protein dynamics at physiological temperatures. Previous molecular dynamics (MD) simulation studies suggest that tryptic-solubilized ferricytochrome b_5 has persistent areas of localized motion (Storch and Daggett, 1995). The MD results reveal pronounced motion in one region of the protein backbone resulting in the intermittent formation of a large cleft, exposing portions of the hydrophobic interior. The location of the cleft is at the interface of the two defined cores in cytochrome b_5 (Figures 4.1 and 4.2). Because previous experimental studies have shown the two cores to be structurally independent (Falzone et al., 1996; Lecomte and Moore, 1991; Moore et al., 1991; Moore and Lecomte, 1993; Moore and Lecomte, 1990; Storch and Daggett, 1996), the observed fluctuations in the cleft region may be important regarding stability and possibly function.

Previous experimental results predict the heme to be solvent accessible from only one face of the protein. Therefore, models of protein-protein interactions with redox partners have focused on a single anionic surface patch on cytochrome b_5 (Livingston et al., 1985; Mauk et al., 1986; Poulos and Mauk, 1983; Salemme, 1976; Stayton et al., 1989; Wendoloski et al., 1987). However, the cleft formation predicted by MD allows an additional route of access to the functional heme group -- not predicted in crystallographic models (Salemme, 1976). In addition, the cleft is in close proximity to many of the acidic residues which experiment shows to be important in protein-protein complex formation (Mauk and Mauk, 1989; Ng et al., 1977; Rodgers et al., 1988; Rodgers and Sligar, 1991; Tamburini et al., 1985). Together these results suggest that this region of the protein may be of functional importance in biological redox processes.

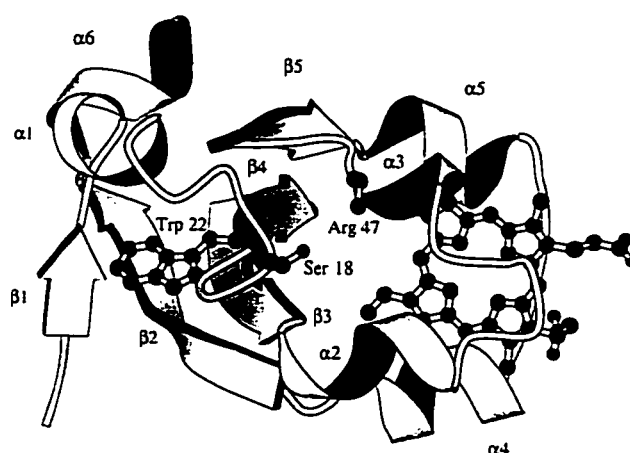


FIGURE 4.1: Ribbon diagram of the crystal structure of cytochrome b_5 (Mathews et al., 1972). The prosthetic heme group, Ser 18, Trp 22, and Arg 47 positions are shown in color. The proposed cleft region lies between the yellow residues 18 and 47. The residues involved in secondary structure are: $\alpha 1$ (9-12), $\alpha 2$ (33-38), $\alpha 3$ (44-47), $\alpha 4$ (55-60), $\alpha 5$ (65-71), $\alpha 6$ (81-86), $\beta 1$ (5-7), $\beta 2$ (74-80), $\beta 3$ (27-32), $\beta 4$ (21-25), and $\beta 5$ (51-54). The numbering scheme for bovine cytochrome b_5 is used. This figure was constructed using the Molscript program (Kraulis, 1991).

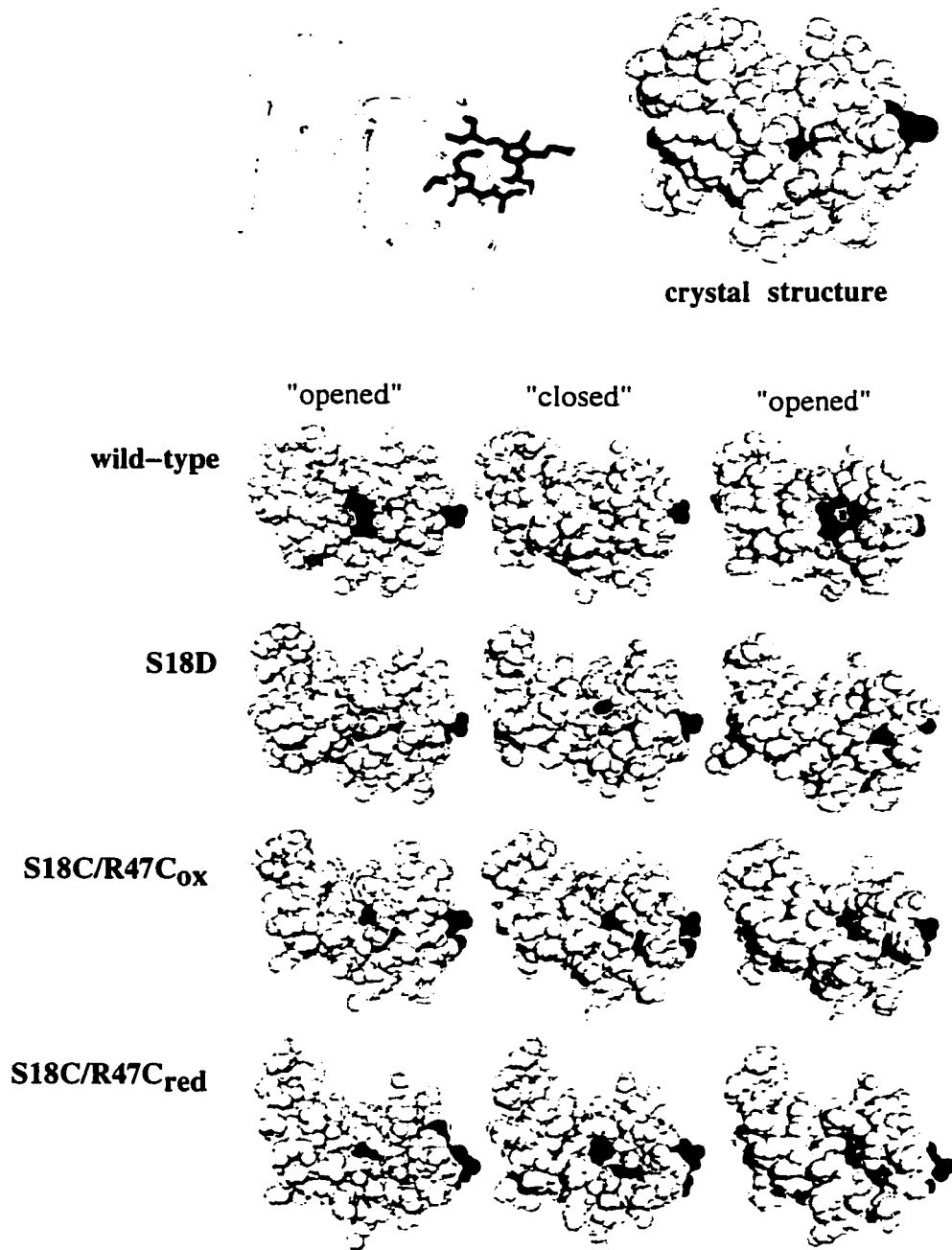


FIGURE 4.2: Space-filling representations of cytochrome b_5 , depicting control of the "opened" and "closed" conformations of cleft in the wild-type (Storch and Daggett, 1995), S18D, S18C/R47C_{ox}, and S18C/R47C_{red} MD simulations. The buried hydrophobic residues that intermittently became exposed upon cleft formation are colored blue, and include the backbone of Trp 22. The residues in yellow (Ser 18 and Arg 47) were mutated in our experiments. The prosthetic heme group is colored red.

On the basis of MD observations, we have studied the equilibrium stability of tryptic-solubilized cytochrome b_5 by introducing mutations in this area of putative mobility. Using computer modeling and mutagenesis, we designed two cytochrome b_5 mutants that could restrict or perturb the cleft fluctuations: an S18D mutant (proposed to form a salt bridge with Arg 47), and a disulfide mutant (designed to covalently close the cleft), which was expected to exhibit different dynamics in the oxidized and reduced states (S18C/R47C_{ox} and S18C/R47C_{red}). We have performed MD simulations of the wild-type and mutant proteins at 25 °C and 50 °C. Simulations under these conditions provided detailed information about the structural and dynamic consequences of the mutants prior to heme loss. The effects of the mutations on equilibrium stability were investigated experimentally using urea and thermal denaturation. In contrast to previous denaturation studies of cytochrome b_5 , however, we exploited two spectroscopic probes sensitive to structural perturbations: heme absorbance (core 1) and fluorescence of tryptophan 22 (core 2) shown in Figure 4.1. Both probes flanked the putative cleft region.

The mutations had only modest effects on heme binding, as determined by absorbance spectroscopy; however, they had pronounced effects on the conformational dynamics prior to heme release, as reported by the steady-state fluorescence of Trp 22. Taken together, the two probes suggested a complex, three-state denaturation pathway characterized by structural changes prior to heme expulsion, including conformational changes that may have corresponded to surface fluctuations. This was in contrast to the currently proposed two-state model of denaturation. The results were considered in light of a three-state model involving the native holoprotein (N), intermediate (I), and denatured apoprotein (D):



In the following sections we present and discuss results from the MD simulations and experiments as related to determinants of thermal stability in ferricytochrome b_5 . In addition, the results demonstrated that conformational stability of proteins can be rationally controlled.

4.2 *Materials and Methods*

Molecular Dynamics Simulations. The starting conformation for the computer simulations was the tryptic-solubilized bovine ferricytochrome b_5 crystal structure obtained from the Brookhaven Protein Data Bank (PDB Accession Number 3b5c). The structure was determined by Mathews and others (Mathews et al., 1972) to 1.5 Å resolution. The crystal structure contains residues 3–87; residues 1–2 and 88–93 are not visible in the electron density maps and were therefore omitted in the starting structure for the simulations. For the following mutant cytochrome b_5 simulations, modifications were made to the bovine crystal structure coordinates by placing the new sidechains in approximately the same orientation: S18D, S18C/R47C_{ox}, and S18C/R47C_{red}.

Energy minimizations and MD simulations were performed using the program ENCAD (Levitt, 1990). The potential energy function (Laidig and Daggett, 1996; Levitt, 1989; Levitt et al., 1995; Levitt et al., 1997; Levitt and Meirovitch, 1983) and associated protocols (Daggett and Levitt, 1992) are described in detail elsewhere. The heme parameters of Henry and co-workers were used (Henry et al., 1985). The system consisted of the protein in a rectangular box of water molecules with walls at least 8 Å from any protein atom (approximately 3000 water molecules per simulation). The water density was set to the experimental value of 0.997 g/mL at 298 K or 0.988 g/mL at 323 K by adjusting the volume of the box (Kell, 1967). The systems were subjected to a variety of preparatory steps as described elsewhere (Storch and Daggett, 1995). Each simulation was

carried out for 2 ns, except the wild-type simulation at 298K which was performed for 2.5 ns. An 8 Å nonbonded cutoff was used, and the nonbonded list was updated every five steps. Structures were saved every 0.2 ps and the last nanosecond of each simulation was analyzed.

Materials. Enzymes used in mutagenesis were purchased from New England Biolabs (Beverly, MA). Custom oligonucleotides were purchased non-phosphorylated from National Biosciences, Inc. (NBI, Plymouth, MN) or Life Technologies, Inc. (Gibco BRL, Rockville, MD). P-10 and P-30 gel filtration resins were obtained from Biorad (Hercules, CA). DEAE Sepharose anionic exchange resins were obtained from Pharmacia Biotech (Piscataway, NJ). All other chemicals were reagent grade.

Site-Directed Mutagenesis. A synthetic rat cytochrome b₅ gene (99 residues - corresponding to the tryptic-solubilized form) harbored in a pUC13 plasmid was kindly provided by Dr. S. Sligar and is described elsewhere (Beck von Bodman et al., 1986). Cassette mutagenesis was used to construct the S18D mutant, utilizing the Pst I and Sal I restriction sites in the synthetic gene. Because of the large distance between these sites, a cassette made of five individual oligonucleotides was used: three wild-type and two mutant complementary oligonucleotides containing the GAC codon (Ser → Asp) and a silent mutation encoding a Sty I restriction site to facilitate mutant identification. The oligonucleotides were annealed and ligated into the double-digested plasmid following the protocol previously described (Stayton et al., 1988). The S18C/R47C mutant was constructed using the commercially available ClonTech® kit (Palo Alto, CA). Two oligonucleotide primers were used: one contained a TGT codon (Ser → Cys) and a silent mutation deleting a native Sal I restriction site and the second primer contained a TGC codon and a silent mutation deleting the native Nae I restriction site. The protocols for standard mutagenesis procedures, such as plasmid isolations and transformations, as well

as SDS-PAGE analysis of proteins are published elsewhere (Sambrook et al., 1989). Dideoxy sequencing was used to confirm successful mutations.

Protein Expression, Purification, and Characterization. *E. coli* DH5 α cells containing pUC13 plasmids harboring the wild-type or mutant cytochrome b_5 genes were expressed following the method of Stayton and others (Stayton et al., 1988). A buffer system of 50 mM K_2HPO_4 , 1 mM EDTA, and 0.1 mM dithiothreitol (DTT) (omitted for S18C/R47C) at pH 7 was used. When DTT was included in the S18C/R47C purification, significant heme loss occurred due to decreased stability of heme ligation in the reduced dicysteine protein (data not shown). Red fractions with an absorbance ratios of 280 nm/412 nm of ≤ 0.18 were pooled and concentrated. Protein purity was determined by SDS-PAGE analysis and mass spectrometry. Mass spectrometry experiments were performed on a Perceptive Systems Voyager Elite MALDI-TOF instrument. The mass range scanned was m/z 1000 to 45000 at 337 nm. The matrix consisted of a 50% acetonitrile solution saturated with 95% dihydroxybenzoic acid/5% methoxy salicylic acid. Approximately 5 pmol of protein per sample was analyzed in triplicate. Internal standards were ubiquitin and myoglobin (8565.81 Da and 16952.5 Da, respectively). MALDI-TOF indicated that the averaged molecular weights of the proteins were: 11212.4 Da (WT), 11240.3 Da (S18D), and 11173.8 Da (S18C/R47C). These weights are in excellent agreement with values calculated from the amino acid composition of apocytochrome b_5 lacking the N-terminal methionine residue: 11210.31 Da (WT), 11238.32 Da (S18D), and 11173.33 Da (S18C/R47C). Protein concentrations were determined from the absorbance at 412 nm using an extinction coefficient of 117 mM $^{-1}$ cm $^{-1}$ (Visser et al., 1975).

S18C/R47C Oxidized and Reduced Disulfide Determination. The S18C/R47C protein was subjected to iodoacetic acid modification in the presence and absence of DTT as published elsewhere (Coligan et al., 1996) to yield oxidized (S18C/R47C $_{ox}$) and reduced-carboxymethylated (S18C/R47C $_{red}$) proteins. All reactions contained 0.1 M Tris at pH 8.6

purged with argon. Typically 200 μ M protein in 500 μ L total volume was used. DTT was added in ten-fold molar excess over protein thiol concentration, while the control contained no DTT, and incubated for 3 hours at 37 °C. Iodoacetic acid was added in a five-fold excess over total thiol concentration and the mixture was incubated in the dark for 1 hour at 37 °C. To this reaction was added β -mercaptoethanol (β -ME) in ten-fold excess over iodoacetic acid concentration and the mixture was immediately desalted on a P-30 gel filtration column. Modification was determined by MALDI-TOF and non-reducing SDS-PAGE analysis.

Urea Denaturation. All stock solutions for denaturation studies were prepared in 5 mM K_2HPO_4 at pH 7 and filtered. A final protein concentration of 10 μ M was used in all denaturation experiments. A known amount of 10 M stock urea solution, buffer, and stock protein solution were added to a cuvette and incubated for 15 minutes for each desired urea concentration. The absorption spectra were measured on a Varian Cary 3E UV-VIS spectrophotometer using matched 1 cm quartz cuvettes at a temperature of 25 °C. Absorption denaturation curves were constructed by plotting the absorption at 412 nm versus the molar concentration of urea. The fluorescence spectra were measured on a SLM-8100 fluorimeter using 1 cm quartz cuvettes at a temperature of 25 °C. The excitation wavelength was 295 nm using a detection cutoff filter of 305 nm. The slit widths were 4-8 nm. Fluorescence denaturation curves were constructed by plotting the spectral center of mass in nm ($\lambda_{mass} = 1 / \sum v_i F_i / \sum F_i$, where F_i is the fluorescence intensity at wavenumber v_i) or intensity of the intrinsic fluorescence of proteins versus the molar concentration of urea. The data were analyzed as described by Pace (Pace, 1986), and curves were fit to the following equations taking sloping baselines into account. Assuming a two-state denaturation mechanism, the equilibrium constant, K_{eq} , was estimated by the equation:

$$K_{eq} = (A_n(U) - A(U)) / (A(U) - A_d(U))$$

Values $A_n(U)$ and $A_d(U)$ were absorbance or fluorescence values of the native and denatured proteins at urea concentration U , respectively, and $A(U)$ is the measured absorbance or fluorescence at a specific urea concentration. The free energy difference between the native and denatured conformations was calculated by :

$$\Delta G_{app} = -RT \ln(K_{eq})$$

A linear dependence of ΔG_{app} on denaturant concentration was assumed:

$$\Delta G_{app} = \Delta G_{app}(\text{H}_2\text{O}) - m[U]$$

where $\Delta G_{app}(\text{H}_2\text{O})$ is the free energy difference between native and denatured forms of cytochrome b_5 in the absence of urea and m reflects the sensitivity of the transition region to denaturant concentration.

Temperature Denaturation. The buffer conditions, instrumentation and setup were the same as described for the urea denaturation experiments. High temperature 1 cm quartz cuvettes with teflon stoppers and stir bars were used to prevent evaporation. Samples were heated in increments of 2.5 °C from approximately 20 to 95 °C and equilibrated for 10 minutes at each temperature before collecting spectral data. Thermal denaturation curves were fit to an equation that accounts for baselines with non-zero slopes (Agashe and Udgaonkar, 1995).

4.3 Results

4.3.1 Molecular Dynamics Characterization of Wild-type and Mutant Proteins

In order to design mutants in which the state of the putative cleft could be controlled and provide a structural basis for the experimental denaturation studies, MD simulations were performed (Figure 4.2). Each simulation was performed for 2 ns in water and yielded similar overall C_{α} RMS (root-mean-squared) deviations from the crystal structure at 25 °C of ~ 2.4 Å, with the exception of S18D which was ~ 3 Å. The motion, however, was distributed differently along the backbone in each of the proteins. At 50 °C, the wild-type protein yielded the largest C_{α} RMS deviation (~ 3.8 Å) from the crystal structure, while the mutant deviations were ~ 3 Å. Tertiary contacts were monitored throughout the simulation and compared to experimental NMR data. Potential nuclear Overhauser effect crosspeaks (NOEs) were evaluated by calculating an average-weighted distance ($\langle r^{-6} \rangle^{-1/6}$) between interacting hydrogens during the simulation. The validity of the simulations were determined by how well experimentally determined NOEs were retained (Moore and Lecomte, 1993; Moore and Lecomte, 1990). All of the hydrogen-hydrogen distances corresponding to the core 2 NOEs (see Figure 4 of Moore and Lecomte, 1990) remained below 5 Å, which is considered a reasonable cutoff for an NOE (Wüthrich, 1986). These NOEs are present even in the more structurally dynamic apoprotein (Moore and Lecomte, 1990; Storch and Daggett, 1996) and they were therefore expected to be present in mutant forms of the holoprotein as well.

As a measure of internal motion, the C_{α} RMS fluctuations describing the motion about the mean structure were used to determine the distribution of mobility along the sequence. The average fluctuations for the last 1 ns of each simulation were calculated and are shown superimposed on the calculated mean structures in Figure 4.3. At 25 °C, the

wild-type simulation had the highest mobility in the putative cleft region (Storch and Daggett, 1995): a loop (residues 14–18), α -helices 2 and 3 (residues 35–49), and the C-terminus (residues 83–85). The mutant simulations, however, showed much lower fluctuations in this area. The S18D simulation showed much less backbone mobility where the highest fluctuations were in the termini and β 5 (residue 51–52). In the S18C/R47C_{ox} simulation, mobility was restricted to β 5 (residues 51–52) and the C-terminus (residues 85–87). Surprisingly, the S18C/R47C_{red} simulation also showed decreased mobility in α 3 (42–52) and the C-terminus (residues 85–87) relative to the wild-type. In comparison, the mean structures of the mutants have RMS deviations of 1.89 Å (S18D), 1.42 Å (S18C/R47C_{ox}), and 1.38 Å (S18C/R47C_{red}) from the mean wild-type structure, where much of this difference was caused by fluctuations in the cleft area.

The C _{α} RMS fluctuations at 50 °C are shown in Figure 4.3B. The wild-type simulation increased in mobility in the same areas as seen at 25 °C, extending further along the mainchain backbone. The S18D simulation fluctuations paralleled the wild-type simulation with additional mobility in α 5. The S18C/R47C_{red} simulation also increased, but to a much lesser degree. Increased fluctuation was seen only in α 1 and the adjacent loop (residues 9–21) and β 2 (residues 72–75). In comparison, S18C/R47C_{ox} still showed low mobility, even at this higher temperature. Both the oxidized and reduced disulfide proteins were ~2.6 Å from the mean wild-type structure, while the S18D was only 1.9 Å from the wild-type.

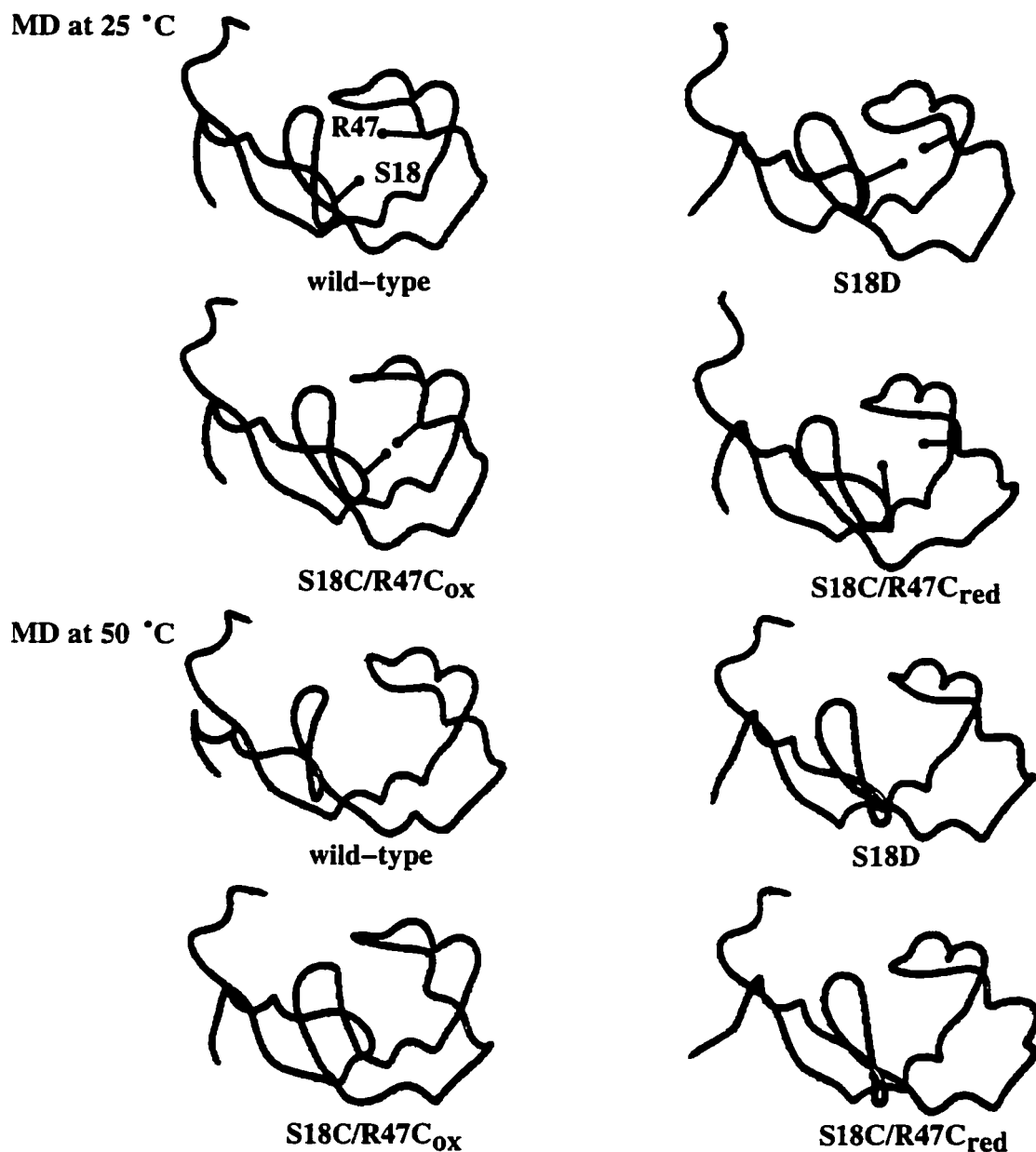


FIGURE 4.3: Mainchain C α traces of cytochrome b₅ depicting relative mobility as determined from the C α RMS fluctuation from the last 1 ns of the simulations. Orientation is the same as in Figure 4.1, but the heme is not displayed. Structures are colored according to relative motion from blue (low mobility) to red (high mobility). (A) Mean structures from MD simulations at 25 °C. (B) Mean structures from MD simulations at 50 °C.

4.3.2 *Experimental Characterization of Oxidized and Reduced Forms of the Disulfide Mutant*

To confirm the oxidation state of the S18C/R47C mutant, the protein was subjected to thiol alkylation with iodoacetic acid in the presence or absence of DTT, and major protein products were detected by MALDI-TOF. The spectrum of S18C/R47C exposed to iodoacetic acid in the presence of DTT (S18C/R47C_{red}) is shown in Figure 4.4A. The major product at 11232.9 Da was determined to be the mono-adducted acetate-containing protein. The second largest product at 11292.6 Da was calculated to be a dicarboxymethylated protein. The minor peak at 11378 Da may have corresponded to the incorporation of one acetate and one DTT molecule yielding a di-adduct (expected weight is 11384.33). The other peak at 11173.8 Da was due to unmodified S18C/R47C_{red} protein. The spectrum of S18C/R47C exposed to iodoacetic acid in the absence of DTT (S18C/R47C_{ox}) is shown in Figure 4.4B. The major species produced from the reaction was the unmodified S18C/R47C_{ox} at 11173.8 Da. Two minor products at 11205.5 and 11307.8 Da may have corresponded to the addition of a potassium ion, and an acetate/ β -ME di-adduct (expected weights are 11212.8 and 11309.8 Da, respectively). The mass spectra indicated that in the absence of DTT, very little carboxymethylation occurred, as expected for an intramolecular disulfide bond predominantly in the oxidized state.

In addition to the mass spectrometry data, SDS-PAGE analysis was performed on the purified protein products from the above reactions (data not shown). Under non-reducing conditions, the oxidized disulfide bonded protein (S18C/R47C_{ox}) migrated distinctly faster than both reduced (S18C/R47C_{red}) and wild-type proteins. When β -ME was added, the S18C/R47C_{ox} protein migration was similar to that of S18C/R47C_{red} and wild-type. These results were consistent with disulfide bond formation effects on electrophoretic mobility, where the oxidized disulfide protein has a smaller radius of

gyration relative to its reduced counterpart and hence faster migration through the gel matrix.

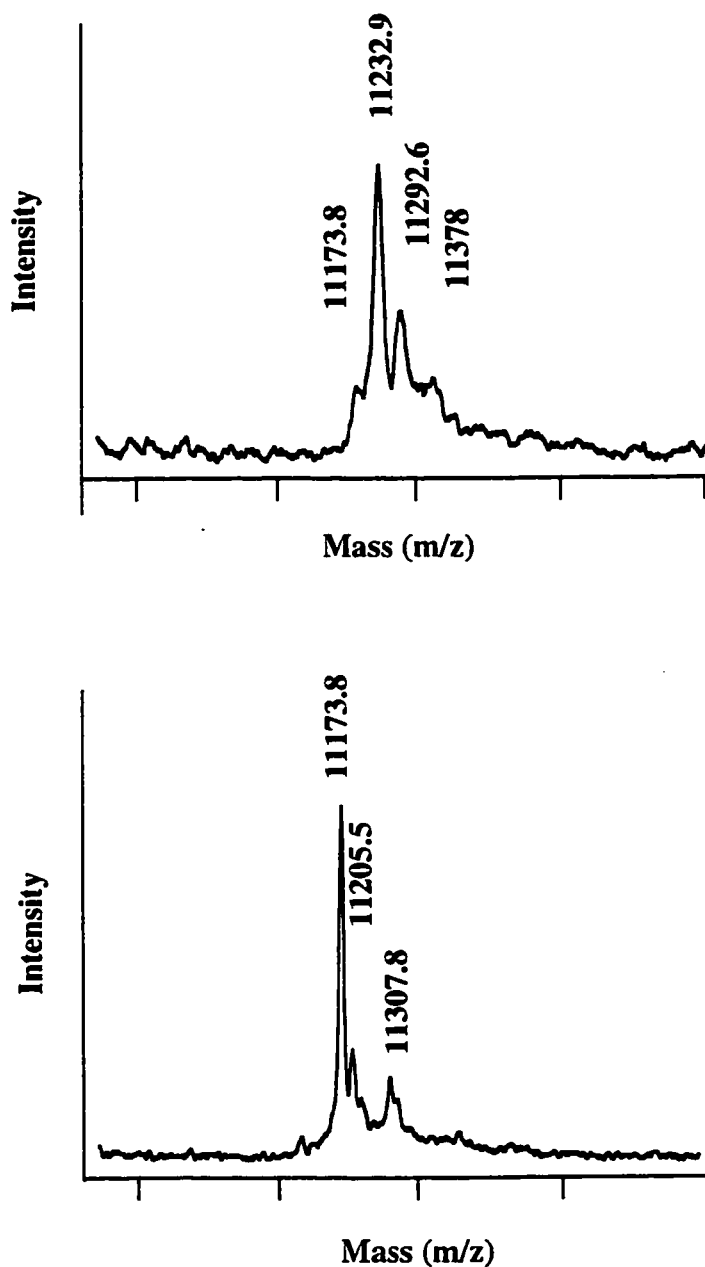


FIGURE 4.4: Positive-ion MALDI mass spectra of S18C/R47C cytochrome b_5 . Matrix 95% dihydroxybenzoic acid/5% methoxy salicylic acid; wavelength, 337 nm. S18C/R47C with iodoacetic acid and DTT (top). S18C/R47C with iodoacetic acid only (bottom).

4.3.3 Urea and Thermal Denaturation Detected by Heme Absorbance

Stability, as determined by heme dissociation, was measured by absorbance spectroscopy. Typical urea and thermal denaturation profiles are shown in Figure 4.5. In all cases, denaturation was followed by measuring optical absorbance of the heme at the Soret maximum of 412 nm. Increasing the temperature or urea concentration led to a denaturant-dependent decrease in intensity and a blue-shift in the absorbance maximum. The native spectra of the wild-type and mutant proteins were indistinguishable, while the spectra for the denatured states of the proteins at 92.5 °C or 8 M were slightly different (data not shown).

Each urea denaturation profile of wild-type or mutant cytochrome b_5 followed cooperative sigmoidal behavior. The urea-induced denaturation was characterized by an isosbestic point at 400 nm. The results from the thermodynamic analysis of the denaturation curves are given in Table 4.1. The midpoints of urea denaturation for the wild-type, S18D, and S18C/R47C proteins varied over a 0.54 M urea range and $\Delta G_{app}(H_2O)$ values varied by 3.55 kcal/mol. Wild-type exhibited the greatest stability, and S18C/R47C_{ox} the lowest. Similarly, the reported m values were highest for wild-type and lowest for S18C/R47C_{ox}.

The thermal denaturation profiles of cytochrome b_5 approximated a two-state transition, as previously reported for cytochrome b_5 tryptic fragments of varying lengths (Hewson et al., 1993; Kitagawa et al., 1982; Newbold et al., 1992). Thermal unfolding changes for the tryptic fragment of cytochrome b_5 were partially reversible, being dependent on the exposure time at temperatures up to T_m . Isosbestic points for wild-type, S18D, and S18C/R47C_{ox} were observed at 395 nm, as previously reported for the wild-type protein (Kitagawa et al., 1982; Newbold et al., 1992), which further supports a two-state denaturation reaction. The thermally induced transitions were similar for the wild-type

and mutants and only subtle differences in the thermodynamic parameters were observed (Table 4.1). The T_m values were similar for wild-type and mutants at ~ 75 °C. This was close to the previously reported T_m of ~ 73 °C for a similar tryptic bovine cytochrome b_5 fragment (residues 1–90).

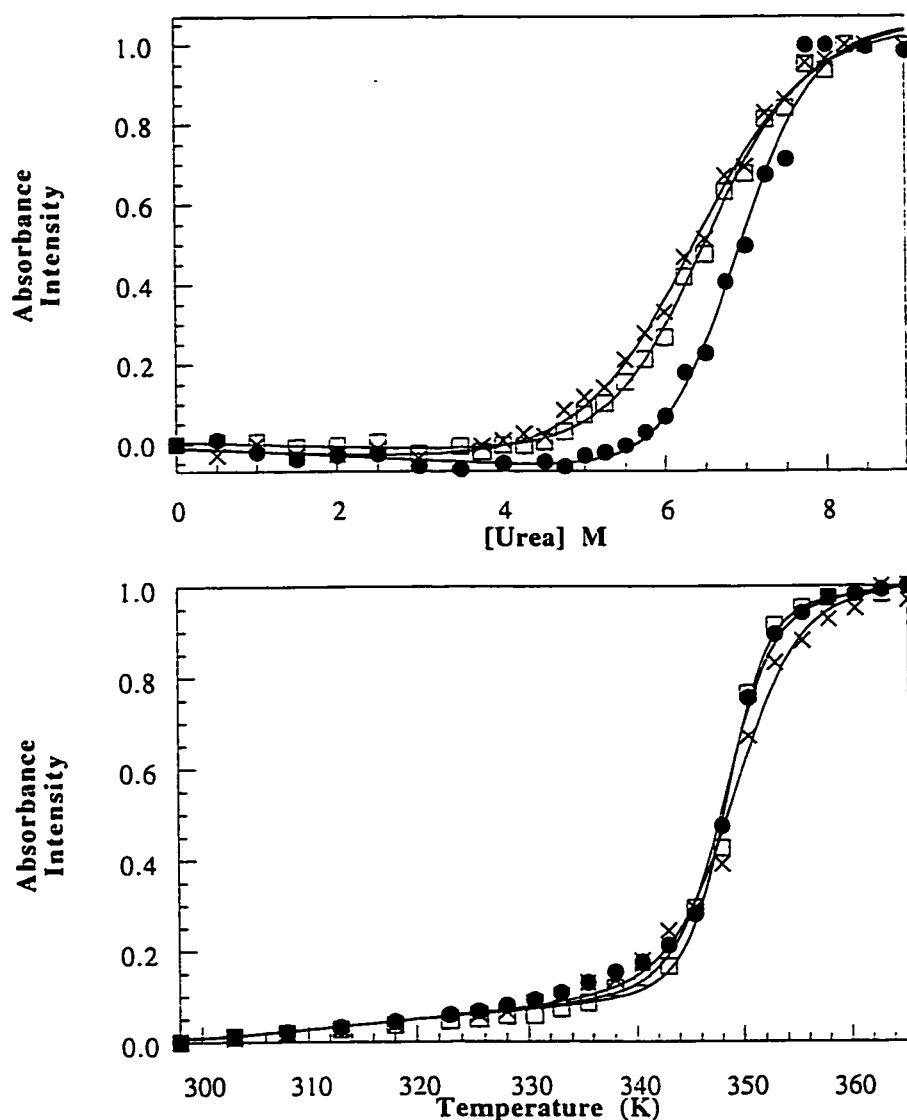


FIGURE 4.5: Changes in absorbance of wild-type (●), S18D (□), and S18C/R47C_{ox} (x) cytochrome b_5 with (A) increasing urea and (B) increasing temperature. The data sets were analyzed assuming a two-state denaturation process and fit to the equations given in the Materials and Methods section.

Table 4.1: Thermodynamic Parameters for Urea and Thermal Denaturation Determined by Absorbance Spectroscopy

Urea Denaturation ^a			
protein	$U_{1/2}$ (M)	$\Delta G_{app}(\text{H}_2\text{O})$ (kcal/mol)	m (kcal/mol/M)
wild-type	6.92 (0.05)	8.72	1.26 (0.12)
S18D	6.50 (0.04)	6.31	0.97 (0.05)
S18C/R47C _{ox}	6.38 (0.06)	5.17	0.81 (0.06)
Thermal Denaturation ^b			
protein	T_m (°C)	ΔT_m (K)	
wild-type	75.21 (0.16)	–	
S18D	75.45 (0.12)	0.24	
S18C/R47C _{ox}	76.00 (0.21)	0.79	
^a The parameters are derived as described in the text from the plots in Figure 4.5A. Standard deviations are shown in parentheses. The protein concentration was 10 μM for each experiment in 5 mM K_2PO_4 at pH 7 and 25 °C.			
^b The parameters are derived as described in the text from the plots in Figure 4.5B. Standard deviations are shown in parentheses. The protein concentration was 10 μM for each experiment in 5 mM K_2PO_4 at pH 7.			

4.3.4 Urea and Thermal Denaturation Detected by Tryptophan Fluorescence

Equilibrium stability was also determined by fluorescence spectroscopy, wherein environmental changes of Trp 22 were measured. The steady-state fluorescence spectra of wild-type and mutant forms of cytochrome b_5 are given in Figure 4.6. Denaturation was followed by measuring the intrinsic fluorescence of Trp 22 at the spectral center of mass (λ_{mass}) between 310 nm–370 nm, and by monitoring maximum fluorescence intensity. Under native conditions (25 °C and 0 M urea) the spectra showed subtle, reproducible differences. Notably, the wild-type emission center of mass was always red-shifted (λ_{mass} ~340 nm) relative to the mutants (λ_{mass} ~338–339 nm).

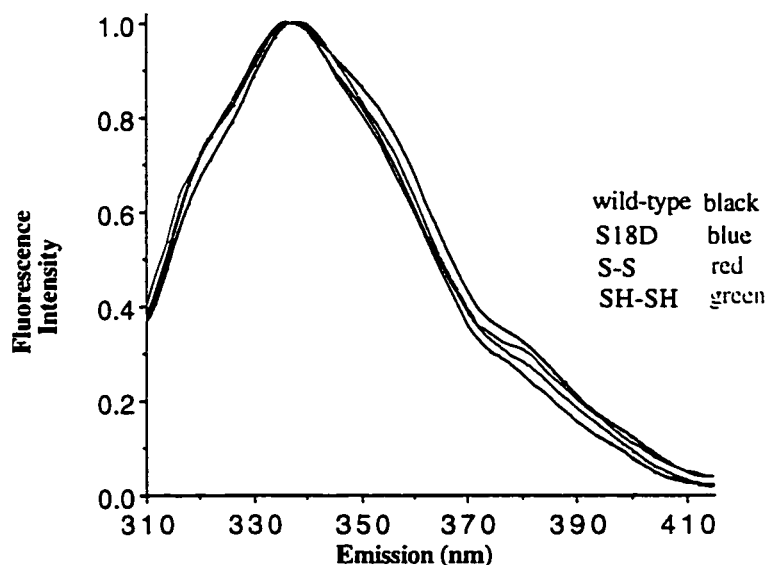


FIGURE 4.6: Steady-state fluorescence emission spectra of wild-type (black), S18D (blue), S18C/R47C_{ox} (red), and S18C/R47C_{red} (green) cytochrome b_5 (excitation wavelength 295 nm). The spectra were recorded at 25 °C.

The urea denaturation curves for wild-type and mutant forms of cytochrome b_5 , determined by emission center of mass are shown in Figure 4.7A. The thermodynamic parameters are shown in Table 4.2. Unlike the urea denaturation followed by absorbance spectroscopy, a large difference between the wild-type and mutant proteins was observed. It should be noted that while the native structures yielded different fluorescence spectra, the denatured states under these conditions were essentially identical. The native and denatured S18C/R47C_{ox} fluorescence spectra were slightly blue-shifted relative to the corresponding spectra of the other proteins (Figure 4.6; denatured spectra not shown). Based on this spectroscopic probe, the S18C/R47C_{ox} protein was ~ 1.77 kcal/mol more stable to urea denaturing conditions than the other proteins and the midpoint of denaturation occurred at much lower urea concentrations than for heme dissociation. The fluorescence intensity versus urea concentration is shown in Figure 4.7B. As expected, a rise in intensity was observed as the protein denatured, the tryptophan became more solvent accessible, and energy transfer between the heme and tryptophan became less effective. All of the proteins showed similar behavior. Initially very little rise in intensity occurred as urea denatured the protein and the tryptophan became more solvent accessible. Once the heme was no longer hexa-coordinated to the protein (Kitagawa et al., 1982), a dramatic rise in intensity was observed. This rise occurred at ~ 5 M urea which correlated with heme release as observed by absorbance (Figure 4.5A). The wild-type and S18D proteins showed slight plateaus at low urea concentrations. Unlike the aforementioned case using absorbance spectroscopy, the m values for the disulfide mutant were larger than wild-type and S18D.

Thermal denaturation was also monitored by fluorescence, and the data are shown in Figure 4.8A. As seen for urea denaturation, the T_m values occurred much sooner than observed by absorbance. Additionally, the transition region of each protein as observed by fluorescence varied with respect to each other. The differences were reflected in the thermodynamic analyses derived from theoretical fits to a two-state process (Table 4.2). T_m

values were similar only for the wild-type and S18D proteins (~51 °C). The double cysteine mutant showed the greatest disparity with a T_m of ~60 °C when oxidized and ~45 °C when reduced. At extreme temperatures, a long-wavelength shoulder became more prominent relative to native spectra (data not shown).

In addition to the spectral center of mass, peak fluorescence intensities were followed as a function of temperature (Figure 4.8B). In all cases, the intensity values ultimately rose with an increase in temperature. All proteins exhibited a decrease in intensity after a maximum was reached. Interestingly, the wild-type protein experienced first a slight rise, a plateau between 55–65 °C, and then a sharp increase. The S18D intensity paralleled this trend. Conversely, S18C/R47C_{ox} showed a steady decline in intensity, before rising sharply at ~65 °C. The intensity of S18C/R47C_{red} increased at ~50 °C. There was a direct correlation between the sharp rise in fluorescence intensity and the loss of heme (compare Figures 4.8B and 4.5B). Therefore, it was likely that other local fluctuations contributed to the changes in intensity and emission λ_{mass} at temperatures prior to heme release.

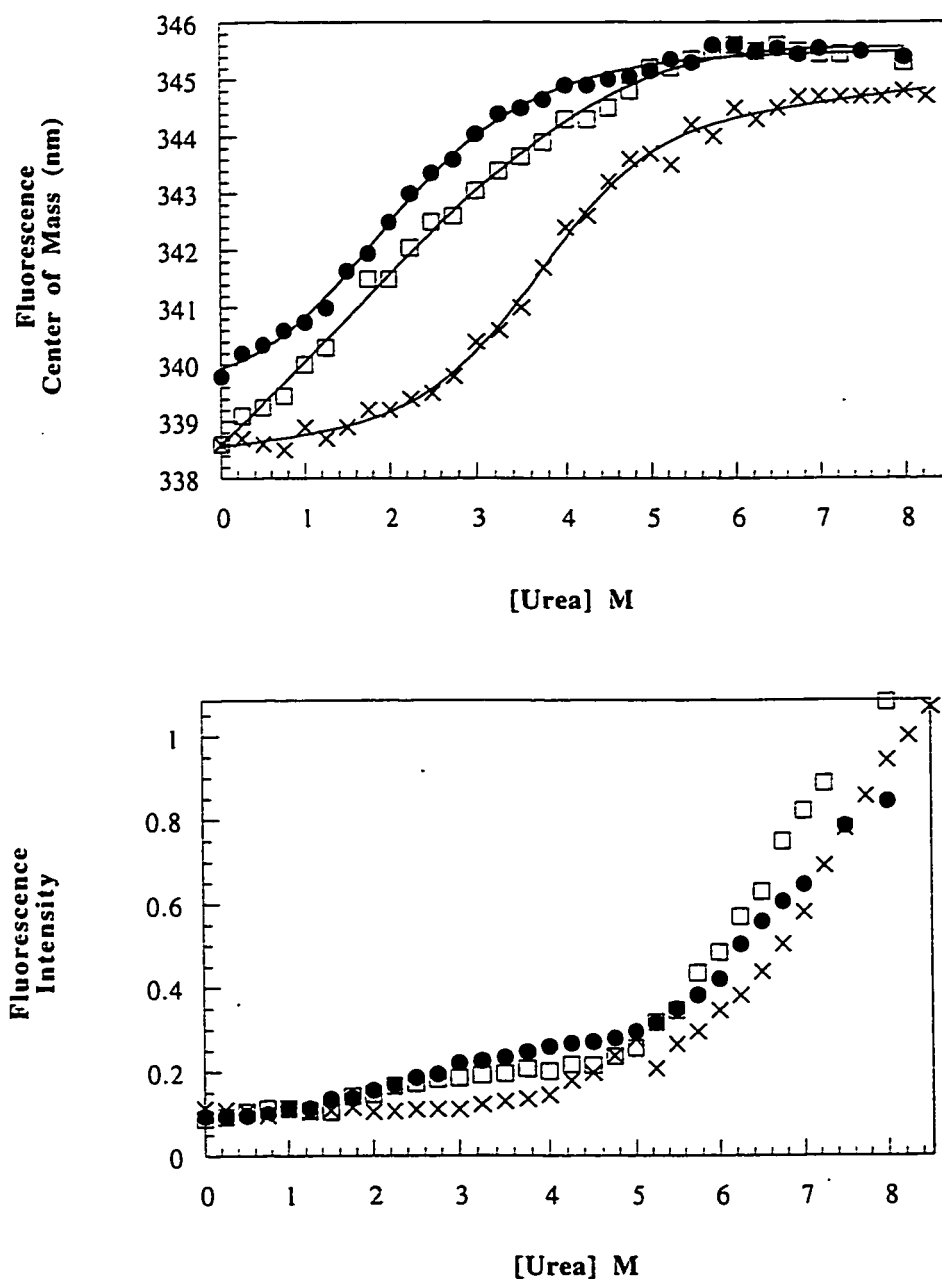


FIGURE 4.7: Changes in fluorescence of wild-type (●), S18D (□), and S18C/R47C_{ox} (x) cytochrome b_5 (excitation wavelength 295 nm). (A) Fluorescence emission as a function of increasing urea. (B) Fluorescence intensity as a function of increasing urea. The data sets were analyzed assuming a two-state denaturation process and fit to the equations given in the Materials and Methods section.

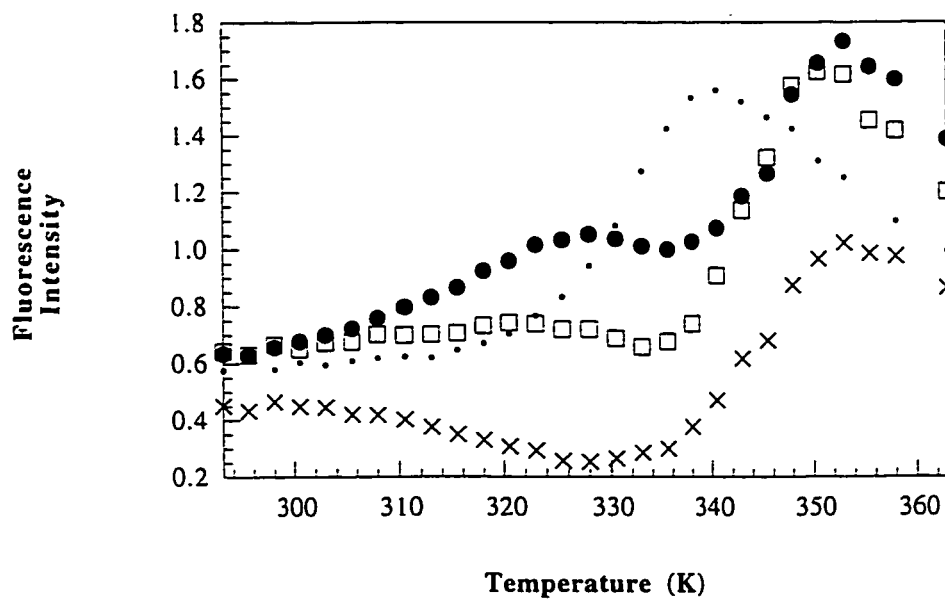
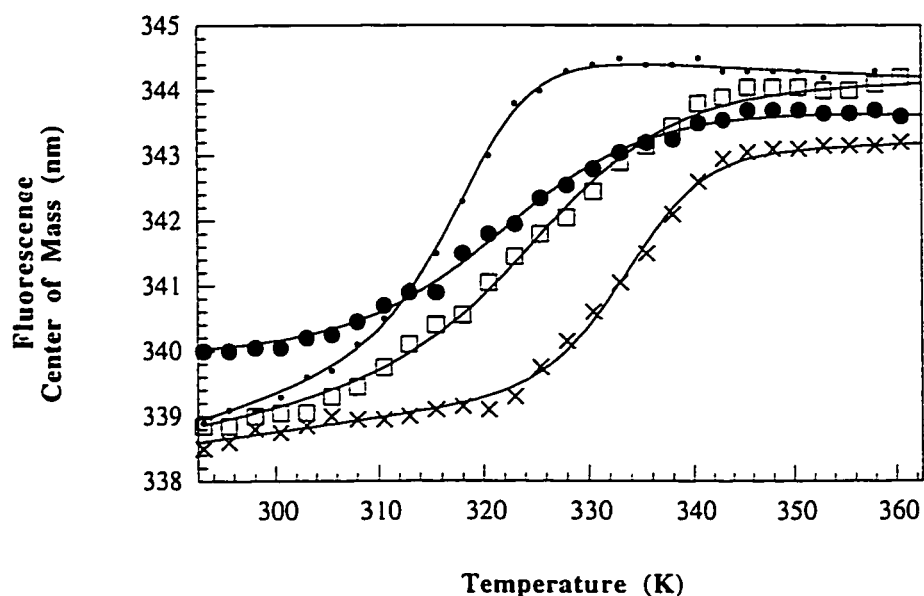


FIGURE 4.8: Changes in fluorescence of wild-type (●), S18D (□), S18C/R47C_{ox} (x), and S18C/R47C_{red} (●) cytochrome *b*₅ (excitation wavelength 295 nm). (A) Fluorescence emission center of mass as a function of increasing temperature. The data sets were analyzed assuming a two-state denaturation process and fit to the equations given in the Materials and Methods section. (B) Fluorescence intensity as a function of increasing temperature.

Table 4.2: Thermodynamic Parameters for Urea and Thermal Denaturation Determined by Fluorescence Spectroscopy

Urea Denaturation ^a			
protein	$U_{1/2}$ (M)	$\Delta G_{app}(\text{H}_2\text{O})$ (kcal/mol)	m (kcal/mol/M)
wild-type	2.27 (0.25)	1.66	0.73 (0.03)
S18D	2.97 (0.50)	1.72	0.58 (0.05)
S18C/R47C _{ox}	3.69 (0.10)	3.43	0.93 (0.11)
Thermal Denaturation ^b			
protein	T_m (°C)	ΔT_m (K)	
wild-type	50.11 (0.29)	—	
S18D	52.72 (0.34)	2.61	
S18C/R47C _{red}	44.78 (0.16)	-5.33	
S18C/R47C _{ox}	60.83 (0.23)	10.72	

^a The parameters are derived as described in the text from the plots in Figure 4.7A. Standard deviations are shown in parentheses. The protein concentration was 10 μM for each experiment in 5 mM K_2PO_4 at pH 7 and 25 °C.

^b The parameters are derived as described in the text from the plots in Figure 4.8A. Standard deviations are shown in parentheses. The protein concentration was 10 μM for each experiment in 5 mM K_2PO_4 at pH 7.

4.4 Discussion

The goal of the studies presented here was to investigate the stability of cytochrome b_5 through MD simulations, mutagenesis, and denaturation studies. The experimental studies were motivated by the predictions from a previous MD simulation in which native ferricytochrome b_5 was studied (Storch and Daggett, 1995). The protein structure is divided into two cores: core 1 contains the heme group and is thereby a critical functional domain, whereas core 2 is considered as part of the structural scaffold that retains native-like structure even when the heme is removed (Moore and Lecomte, 1990). In the simulations, we observed large-scale fluctuations on the surface of the protein, that resulted in the formation of a cleft that transiently exposed the heme group and the hydrophobic interior (Figure 4.2) (Storch and Daggett, 1995). The cleft region lies between the two cores and may be structurally important, play a role along the folding pathway, or be involved in electron transfer functions. Cytochrome b_5 contains spectroscopic probes in each of its cores: a heme (core 1) and tryptophan 22 (core 2) (Figure 4.1). Therefore, in the studies presented here we have used absorbance and fluorescence spectroscopy to monitor the effects of the mutations in cores 1 and 2, respectively. In addition, we have used modeling and mutagenesis to construct two mutants designed to impair cleft dynamics. One mutant introduced a salt bridge across the cleft, and the other introduced a covalent bond (S-S) spanning the cleft. The introduction of non-native disulfide bonds can both stabilize (Clarke et al., 1995; Kanaya et al., 1991; Mansfeld et al., 1997; Matsumura et al., 1989; Takagi et al., 1990; Wakarchuk et al., 1994) and destabilize proteins (Betz et al., 1996; Mitchinson and Wells, 1989; Van den Burg et al., 1993; Villafranca et al., 1987; Wells and Powers, 1986). In many cases, introduction of disulfide bonds leads to unexpected or uninterpretable changes in protein stability. The introduction of a *de novo* disulfide bond in cytochrome b_5 revealed interesting results regarding equilibrium stability

in this protein. First, we discuss the MD simulations and the structural information they provide relating to conformational stability. Then, we present the characterization of the mutants through denaturation studies and discuss the identification of a newly proposed denaturation intermediate.

4.4.1 MD Simulations

We performed MD simulations at 25 °C and 50 °C in order to compare protein structure and dynamics in the native state and at a point along the thermal denaturation pathway before loss of heme. Specifically, we were interested in the structural implications of the mutations on the putative cleft region and other areas of the protein. In the wild-type simulation, we saw an area of localized motion that encompassed the cleft region. This motion became even more dramatic as the temperature was increased to 50 °C and the protein began to denature. The flexibility in the region between α -helices 2 and 3 was important for progression to the more dynamic structures seen at 50 °C. At 25 °C the S18D structure fluctuated very little except at the termini, due to the constraint imposed by the S18D-R47 interactions. At 50 °C, the S18D-R47 salt bridge was broken, and the dynamic behavior was similar to that of wild-type. In the S18C/R47C_{ox} simulation, the fluctuations in the cleft region were damped and remained so even at 50 °C. The S18C/R47C_{red} simulation, however, revealed the most unexpected results. In this simulation, the introduction of the R47C mutation introduced a kink in the segment between α -helices 2 and 3, preventing fluctuations in the cleft region as observed in the wild-type protein. Even at 50 °C, the motion in this area increased very little. However, increased dynamics in α -helix 1 and the adjacent loop were observed as in the wild-type simulation. These structural perturbations would most likely affect the denaturation pathway of S18C/R47C_{red}. The experimental results showed that the thermal transition

occurred earlier than for the other proteins, indicating a destabilized native state for S18C/R47C_{red}. In summary, the MD simulations provided a picture of the localized dynamics and their susceptibility to mutations which helped to guide structural interpretation of the experimental results.

4.4.2 *Experimental Mutational Effects on Heme Binding*

Through monitoring changes in heme absorbance, we measured mutational effects on protein stability, specifically between the native and denatured states, $N \rightleftharpoons D$. In all cases, the results showed a single cooperative transition between the compact folded state and the more disordered, denatured state. The thermal denaturation results showed very little variation upon introduction of the mutations. However, urea effects on heme-dissociation were more pronounced. Wild-type cytochrome b_5 was the most stable species under these conditions. On the basis of heme dissociation, the wild-type protein was 2.41–3.55 kcal/mol more stable than the variants. In addition transition midpoints were differentially sensitive to urea based on m values. This value usually or nearly always decreases as a protein is constrained by covalent cross-links due to a decreased solvent accessible surface area of the denatured state (Shortle, 1995). Both mutants showed smaller m values relative to the wild-type protein. Although these results were interesting in terms of mutant effects on stability as related to heme association, absorbance spectroscopy did not reveal structural changes around the heme at low denaturant concentrations.

Although the data were analyzed as a two-state model, as others have done in the past, we noticed that they were poorly fit by the theoretical curves, particular in areas of low concentrations of denaturant (Figures 4.4 and 4.5). The denaturation results obtained

by fluorescence, however, shed light on structural events that may have contributed to these poor fits.

4.4.3 *Experimental Mutational Effects at the Interface of Cores 1 and 2*

Fluorescence spectroscopy is very sensitive to changes in environment and solvent accessibility and, therefore, is an excellent probe of structural dynamics and changes in tertiary structure. The sidechain of tryptophan 22 is contained within core 2 while the mainchain is also in direct contact with core 1. Any solvent accessibility of the Trp 22 sidechain through core 2 fluctuations was expected to remain similar in the wild-type and mutants because of the structural rigidity of this domain. Even in the absence of heme, core 2 remains very structured, maintaining all of the native Trp 22 NOE contacts found in the holoprotein (Moore and Lecomte, 1993; Moore and Lecomte, 1990). We hypothesized that differences in solvent penetration through the core 1 / core 2 cleft region, however, would be affected by the mutations and evidenced by changes in fluorescence. As observed in the wild-type cytochrome b_5 MD simulation, the cyclical formation and closure of the cleft allows solvent accessibility of the Trp 22 mainchain through this route (Storch and Daggett, 1995). The S18D and S18C/R47C_{ox} mutants were designed to prevent cleft opening and hence affect overall solvent accessibility of Trp 22. In our steady-state fluorescence results of wild-type cytochrome b_5 and mutants we observed subtle, but reproducible differences in the intrinsic fluorescence (Figure 4.6). The λ_{mass} of the wild-type protein was red-shifted by up to 1.5 nm relative to the mutants. S18C/R47C_{ox} was the most blue-shifted. These differences reflected the environment of Trp 22 and were attributed to decreased solvent accessibility through the cleft region due to mutations designed to form the “cleft-closed” conformation (Figure 4.2).

Unlike the results obtained from absorbance spectroscopy, fluorescence revealed large alterations in conformational equilibria in the wild-type and mutant proteins prior to heme release (summarized in Table 4.2). By the time heme release occurred, all denaturant-related events monitored by fluorescence were completed. The thermodynamic parameters in Table 4.2, which significantly differ from Table 4.1, reflected the equilibrium between the native state (N) and a newly proposed intermediate (I) along b_5 denaturation pathway. The introduction of the disulfide cross-link into the protein affected the $N \rightleftharpoons I$ equilibrium, and increased the transition temperature by ~ 10 °C, as measured by fluorescence. Conversely, when the disulfide bond was broken, the protein was destabilized relative to wild-type by ~ 6 °C. Introduction of the salt bridge in the S18D mutant had modest effects on conformational equilibria, but the observed differences were consistent with an engineered salt bridge leading to decreased preference for the “cleft-open” conformation.

4.4.4 Differences Between Absorbance and Fluorescence Results Prior to Heme Release

Interestingly, for each protein, absorbance and fluorescence revealed different transition points. More denaturant was required to reach the T_m when heme absorbance was monitored, than when the tryptophan environment was monitored. This indicated that the most dramatic differences in fluorescence occurred and were completed at urea concentrations or temperatures prior to heme dissociation (Figures 4.7B and 4.8B). Presumably, several factors contributed to the fluorescence changes, such as quenching due to energy transfer to the heme, changes in solvent accessibility, and differences in polar residue interactions with the excited-state dipole of the fluorophore.

The fluorescence intensity profiles prior to heme release were complex. Our structural interpretations based on these results were aided by MD simulations at 25 and 50

°C. Urea had modest effects on fluorescence intensity prior to heme release. Both wild-type and S18D, however, showed slight plateaus at low urea concentrations. At temperatures prior to heme dissociation, the intensity profile of each protein was quite different. For the wild-type and S18D proteins a pronounced plateau was reached. We interpreted this as the formation of a denatured intermediate corresponding to a “cleft-open” conformation (Figure 4.2). The plateau was completely absent in the S18C/R47C_{ox}. It is reasonably proposed that the covalent “tether” in the disulfide bonded protein prevented formation of this proposed intermediate, and the protein remained in a “cleft-closed” conformation until heme release occurred.

Taken together, the temperature- and urea-dependence of fluorescence emission wavelength and intensity depicted a more complex denaturation scheme than just a simple release of heme concomitant with loss of structure. The differences in transition regions between the absorbance and fluorescence denaturation curves reflected structural changes that occurred at two different points along the denaturation pathway. The absorbance data strictly showed the effects of denaturant on heme release occurring at large concentrations of urea or high temperatures; the transition region of heme release began at 65 °C or 5 M urea. However, the fluorescence data showed that significant structural perturbations were occurring prior to heme release. At 65 °C, nearly all of the spectral perturbations detected by fluorescence were completed. In marked contrast to the wild-type, formation of this denatured state was insignificant in the S18C/R47C_{ox} mutant.

4.5 Conclusions

The results from the thermal and urea denaturation of wild-type and mutant forms of cytochrome b₅ can be described by a three-state model involving native holoprotein (*N*), intermediate (*I*), and denatured apoprotein (*D*) shown in Figure 4.9:

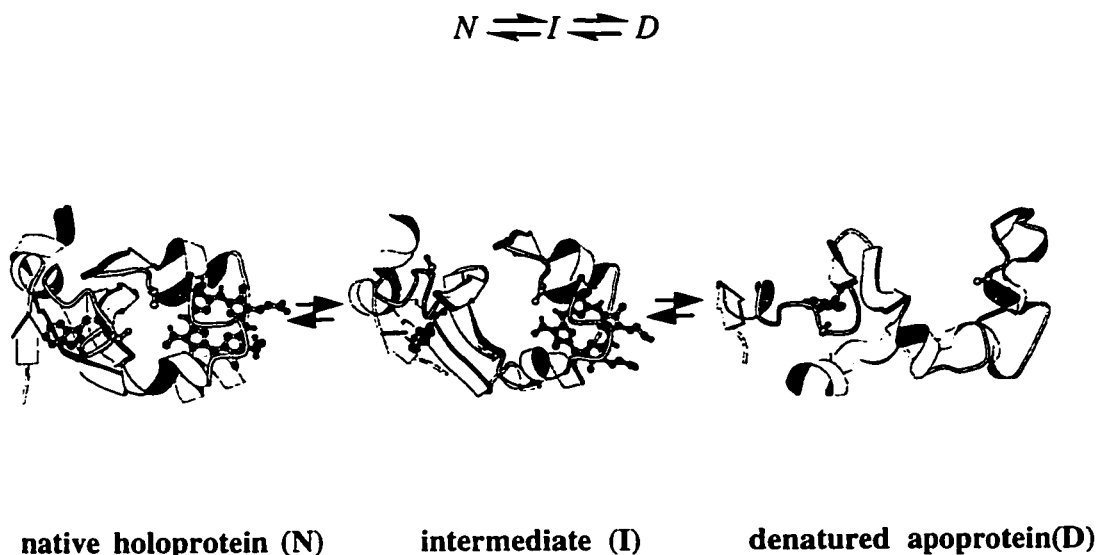


FIGURE 4.9: Mainchain C_{α} traces of wild-type cytochrome b_5 at different points along the denaturation pathway as described by the model presented in the text. Orientations are the same as in Figure 4.1. The native structure (N) was obtained from the holocytochrome b_5 simulation (Storch and Daggett, 1995). The intermediate structure (I) was generated from the 50 °C simulation presented in this paper and reflected the “open-conformation.” The denatured state was obtained from a 225 °C MD simulation performed without the heme present (unpublished data).

The denaturation results of this study suggested that some structural rearrangement occurs during the early stages of the denaturation process before heme was released and that a simple two-state model cannot fully describe cytochrome b_5 denaturation. The fluorescence intensity results suggested that the intermediate was structurally more similar to the native state (N) than the denatured state (D). The equilibrium between N and I was affected by a strategically placed *de novo* salt bridge or disulfide bond. Although our denaturation results did not allow the different conformational states to be directly determined, they were

consistent with our MD generated data which showed limited structural differences between the *N* and *I* states that were concentrated in one region -- the proposed cleft region. We have performed steady-state acrylamide quenching experiments at various temperatures along with time-resolved fluorescence studies that further support this hypothesis (Storch et al. (a), *In preparation*). Additionally, we are currently testing the importance of the critical cleft area and implications of the mutations in biological function.

CHAPTER 5

CONTROLLING DYNAMICS OF A CLEFT ON THE SURFACE OF CYTOCHROME b_5 THROUGH RATIONAL MUTAGENESIS: A STEADY-STATE AND TIME-RESOLVED FLUORESCENCE STUDY

5.1 *Introduction*

As pointed out in previous chapters, proteins in their native aqueous environments are not rigid molecules, but continually undergo structural fluctuations. Static X-ray crystal structures, however, have traditionally been used as structural models. While these models may certainly provide some dynamic information in the way of temperature factors, it is difficult to gain information regarding large-scale motion or affects that mutations may have on these motions. Additionally, crystallographic packing may affect dynamic areas. With the advent of more advanced technology, it is possible to explore proteins in aqueous environments with computer simulations that may reveal detailed atomic information about important fluctuations. Furthermore, this information may be compared to and helpful in elucidating experimental results.

Previous molecular dynamics (MD) simulation studies suggest that native cytochrome b_5 (Figure 5.1) has persistent areas of increased localized dynamics not previously noted by experimental techniques (Storch and Daggett, 1995). In particular, pronounced dynamics in one region of the protein backbone result in the formation of a large cleft, exposing portions of the hydrophobic interior (Figure 5.2). The location of the cleft is at the interface of the two defined cores in cytochrome b_5 . Because previous

experimental studies show the two cores to be structurally independent of one another (Moore and Lecomte, 1993), the observed dynamics in the cleft region may be important for interdomain communication. Furthermore, the cleft opening would allow an additional route of access to the functional heme group, which is not revealed in the crystallographic studies. Solvent accessibility of the heme is considered possible from one face of the protein; the only face predicted to interact with other functionally relevant proteins (Livingston et al., 1985; Mauk et al., 1986; Poulos and Mauk, 1983; Salemme, 1976; Stayton et al., 1989; Wendoloski et al., 1987). The cleft is also in close proximity to many of the acidic residues which experiment shows to be important in protein-protein complex formation, suggesting that this region of the protein may be functionally relevant (Mauk and Mauk, 1989; Ng et al., 1977; Rodgers et al., 1988; Rodgers and Sligar, 1991; Tamburini et al., 1985).

Tryptophan (Trp) residues are valuable probes of localized protein motion (Harris and Hudson, 1991; Lakowicz, 1989; Royer et al., 1990). The sensitivity of Trp fluorescence to various environmental influences is well recognized. The Trp indole can be completely surrounded by the protein matrix, or partially or fully exposed to solvent molecules. In turn the local environment can influence the excited-state dipole and hence the steady-state emission and lifetimes of the fluorophore. Steady-state fluorescence provides overall information or a weighted average about the emitting fluorophores. Time-resolved fluorescence in contrast provides detailed information on the population distribution of the excited-state components characterized by distinct lifetimes. The latter monitors events that occur during the lifetime of the excited-state which can range from a few picoseconds to hundreds of nanoseconds. Together, the two techniques can be used to obtain a complete picture of fluorophore accessibility to, and interactions with other molecules, providing insight into protein dynamics.

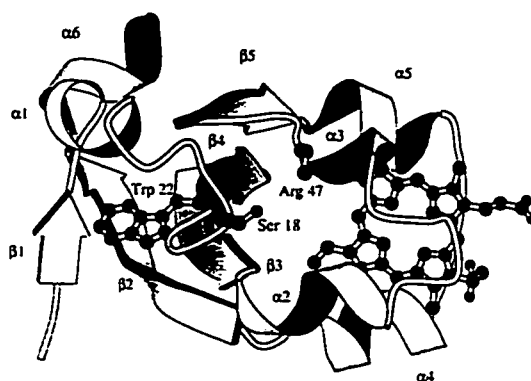
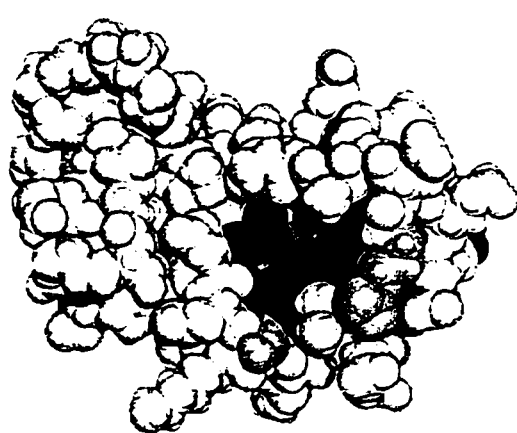
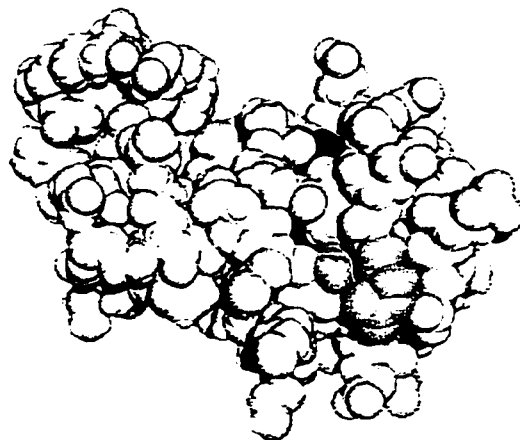


FIGURE 5.1: Ribbon diagram of the crystal structure of cytochrome b_5 (Mathews et al., 1972). The prosthetic heme group, Ser 18, Trp 22, and Arg 47 are shown in black with ball and stick. The proposed cleft region lies between Ser 18 and Arg 47. The residues involved in secondary structure are: $\alpha 1$ (9–12), $\alpha 2$ (33–38), $\alpha 3$ (44–47), $\alpha 4$ (55–60), $\alpha 5$ (65–71), $\alpha 6$ (81–86), $\beta 1$ (5–7), $\beta 2$ (74–80), $\beta 3$ (27–32), $\beta 4$ (21–25), and $\beta 5$ (51–54). The numbering scheme for bovine cytochrome b_5 is used. This figure was constructed using the Molscript program (Kraulis, 1991).



"opened" conformation



"closed" conformation

FIGURE 5.2: Space-filling representations of cytochrome b_5 depicting cleft conformations observed in the wild-type MD simulation (Storch and Daggett, 1995). The buried hydrophobic residues that intermittently became exposed upon cleft formation are colored blue, and include the backbone atoms of Trp 22. The residues in yellow (Ser 18 and Arg 47) were mutated in our experiments. The prosthetic heme group is colored red.

A variety of low molecular weight substances have been found to act as quenchers of indole fluorescence (Eftink and Ghiron, 1981). These molecules decrease fluorescence intensity through physical contact with the excited indole ring and the extent of quenching depends upon the molecules' accessibility to the fluorophore. Quenching can be measured as a decrease in the fluorescence intensity and/or emission lifetime, referred to as either static or dynamic (collisional) quenching. In the case of static quenching, the quencher and chromophore molecules are very close at the moment the fluorophore becomes excited and quenching occurs instantaneously (statically), without an effect on the excited-state lifetime. Collisional quenching, which effects both intensity and lifetime, is described by the diffusion-controlled physical encounter between the excited-state fluorophore and the quencher, where the penetration of the quencher can be facilitated by fluctuations in the conformation of the protein. Thus, solute quencher studies are excellent probes of protein dynamics. The two modes of quenching can be distinguished by fluorescence lifetime measurements. Acrylamide has been shown to be an effective, uncharged quencher that is very sensitive to probing the random exposure of buried Trp residues (Eftink and Ghiron, 1976). The utility of solute quenching was first appreciated by Lakowicz and Weber (Lakowicz and Weber, 1973), when they asserted that the bimolecular rate constants for quenching are larger than expected due to structural fluctuations in proteins.

Cytochrome b_5 is a single tryptophan-containing protein, which makes it well suited for fluorescence studies. Trp 22 is located at the interface of two cores and in the cleft region described above (Figure 5.1), making it a convenient probe of the proposed dynamic mode. Heme proteins typically incur energy transfer from the excited fluorophore to the heme (Warburg and Negelein, 1928). The energy transfer occurs to different extents depending on the distance between donor and acceptor and the relative orientation. Although the fluorescence intensity of cytochrome b_5 is low due to this energy transfer, the

detectable fluorescence is of great interest due to the location of Trp 22 -- an ideally located intrinsic probe of dynamics in the hydrophobic cleft.

In order to elucidate the effects of proposed protein fluctuations on Trp fluorescence, we introduced several mutations into cytochrome b_5 designed to alter the dynamics of the cleft region. We constructed a dicysteine mutant and studied the mutational effects in both the oxidized and reduced states (S18C/R47C_{ox} and S18C/R47C_{red}, respectively). We also constructed an S18D mutant that formed a putative salt bridge with the native Arg 47. The two are useful tools in analysis of long-range backbone motions (Villafranca et al., 1983; Matsumura and Matthews, 1989; Srinivasan et al, 1990). If the dynamics cause the two residues of interest to separate transiently, then the motion can be trapped by the bond formation; covalently in the case of S18C/R47C_{ox} (Careaga and Falke, 1992; Careaga and Falke, 1992; Falke and Koshland, 1987).

In this paper we present steady-state and time-resolved fluorescence data for the wild-type and mutant forms of cytochrome b_5 obtained under a variety of temperatures and acrylamide quenching conditions. These results are consistent with previous MD simulations that predict a dynamic area of the protein. The differences between the wild-type and mutant proteins supported the hypothesis that localized dynamics could be rationally controlled through the introduction of constraining mutations.

5.2 *Materials and Methods*

Site-Directed Mutagenesis and Protein Purification. Mutagenesis and protein purification protocols are described in detail in Chapter 4 *Materials and Methods*. Protein purity was determined by UV-VIS absorbance spectroscopy at a ratio of 280/412 nm of ≤ 0.18 . The purities were verified by SDS-PAGE analysis and MALDI-TOF mass spectrometry (data not shown). The oxidation states of the disulfide mutants,

S18C/R47C_{ox} and S18C/R47C_{red}, were determined by susceptibility to carboxymethylation by iodoacetate based on analysis by MALDI-TOF MS (data shown in Figure 4.4).

Steady-State Fluorescence. Steady-state fluorescence experiments were performed on an SLM-8100 fluorimeter using 1 cm quartz cuvettes with stir bars at a temperature of 25 °C, unless otherwise noted. The excitation was 295 nm using a detection cutoff filter of 305 nm. The slit widths were 4–8 nm. Samples contained 10 µM cytochrome b₅ in 5 mM K₂HPO₄ at pH 7. Acrylamide quenching experiments used a 7 M acrylamide stock in 5 mM K₂HPO₄ at pH 7 buffer. Blank spectra (buffer only and buffer plus acrylamide) were subtracted from all sample spectra. All spectra reported were the average of at least two emission spectra. The spectral center of mass, λ_{mass} , was determined by integrating the area under the curve from 310 nm - 370 nm: $\lambda_{\text{mass}} = 1 / \sum \nu_i F_i / \sum F_i$, where F_i is the fluorescence intensity at wavenumber ν_i . Stern-Volmer quenching constants were obtained from the relationship (Birks, 1970):

$$F/F_o = 1 + K_{SV} [Q] = 1 + k_q \tau_o [Q]$$

where F_o and F are the fluorescence intensities in the absence and presence of quencher, respectively, Q is the acrylamide concentration, and K_{SV} is the Stern-Volmer quenching constant. K_{SV} is equal to $k_q \tau_o$, where k_q is the apparent bimolecular rate constant and τ_o is the excited-state lifetime in the absence of quencher. The apparent rate constant for the quenching reaction, k_q , is equal to γk_d , where γ is the efficiency of the quenching process. Eftink and Ghiron have shown that the efficiency of acrylamide quenching of indole is unity (Eftink and Ghiron, 1976). Therefore k_q is equal to k_d , the diffusion limited rate constant for collisional quenching.

Fluorescence Lifetime Measurements. Time-resolved frequency-domain fluorescence measurements were carried out at the Center for Fluorescence Spectroscopy,

University of Maryland, Baltimore. Lifetimes were measured with a frequency-domain 10 GHz fluorometer equipped with a Hamamatsu microchannel plate detector (MCP-PMT), described in detail elsewhere (Laczko et al., 1990). Excitation was at 295 nm from a mode-locked Ar-ion laser source. Sample emission was filtered through an Oriel interference filter centered at 340 nm. For reference, we used the scatter of the sample solution filtered through an Oriel interference filter at 289 nm with neutral density filters.

Data Analysis. The frequency domain fluorescence phase and modulation data were subject to non-linear least squares analysis using the software developed at the Center for Fluorescence Spectroscopy (Lakowicz et al., 1987). Time-resolved intensity decays were described by the multiexponential equation: $I(t) = I_0 \sum_i \alpha_i e^{-t/\tau_i}$, where $I(t)$ is the emission intensity at time t , and I_0 is the initial emission intensity. The amplitude (pre-exponential factor), α_i , describes the fraction of molecules in each environment with lifetime τ_i . The measured quantities at each frequency ω , were phase shift, ϕ_ω , and demodulation factor, m_ω , of the emitted light versus the reference light.

5.3 Results

5.3.1 Steady-State Fluorescence and Acrylamide Quenching

The corrected steady-state emission spectra of wild-type and mutant cytochrome b_5 with an excitation wavelength of 295 nm are shown in Figure 5.3. The corresponding spectral center of mass, λ_{mass} , are shown in Table 5.1. The wild-type emission maximum and spectral center of mass were always red shifted (λ_{mass} 339.8 nm) relative to the mutants (λ_{mass} 338.5 – 338.9 nm).

Addition of acrylamide caused a decrease in steady-state fluorescence intensity in all the proteins. Stern-Volmer plots are shown in Figure 5.4. The plots were linear at all the

temperatures tested (5 °C, 35 °C, and 50 °C), indicating a collisional reaction for acrylamide quenching. The collisional quenching constant, K_{SV} , is equal to the slope of each line. The data corresponding to each protein and temperature are shown in Table 5.1. At each temperature, the wild-type had the largest K_{SV} values, suggesting increased exposure of Trp 22 relative to the mutants. At 5 °C the solvent accessibility of the Trp in all of the proteins was similar. At 35 °C, the solvent accessibility of Trp increased slightly in each protein. At 50 °C, the K_{SV} for S18C/R47C_{ox} was significantly lower than the other proteins, while the values for wild-type and S18D were the same. When the reduced disulfide mutant (S18C/R47C_{red}) was tested at 50 °C and the K_{SV} increased to nearly the same as the wild-type value. Because the differences between S18C/R47C_{ox} and other proteins were minimal at 5 °C and 35 °C, the reduced protein was only used in the 50 °C experiments. The λ_{mass} for each protein was determined after acrylamide addition and plotted against increasing acrylamide concentrations. As the acrylamide concentration increased, the spectral center of mass blue-shifted by ~1.5 nm (data not shown).

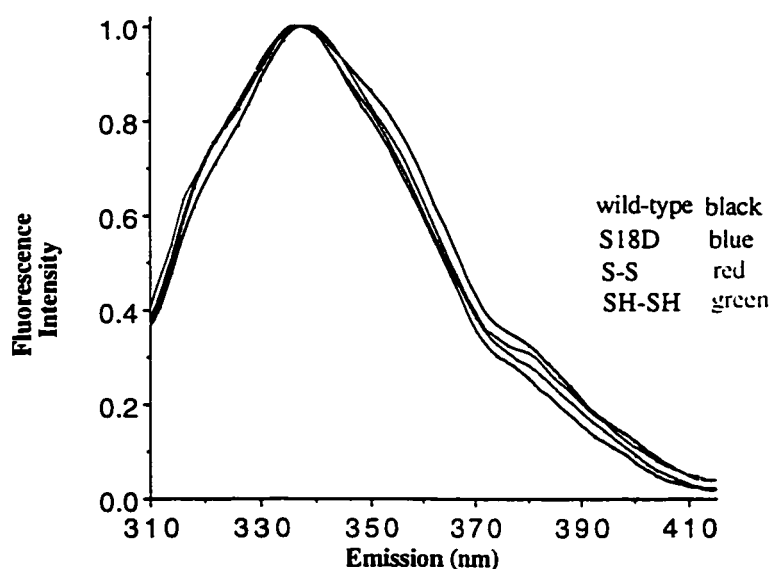


FIGURE 5.3: Normalized fluorescence emission spectra at 25 °C.

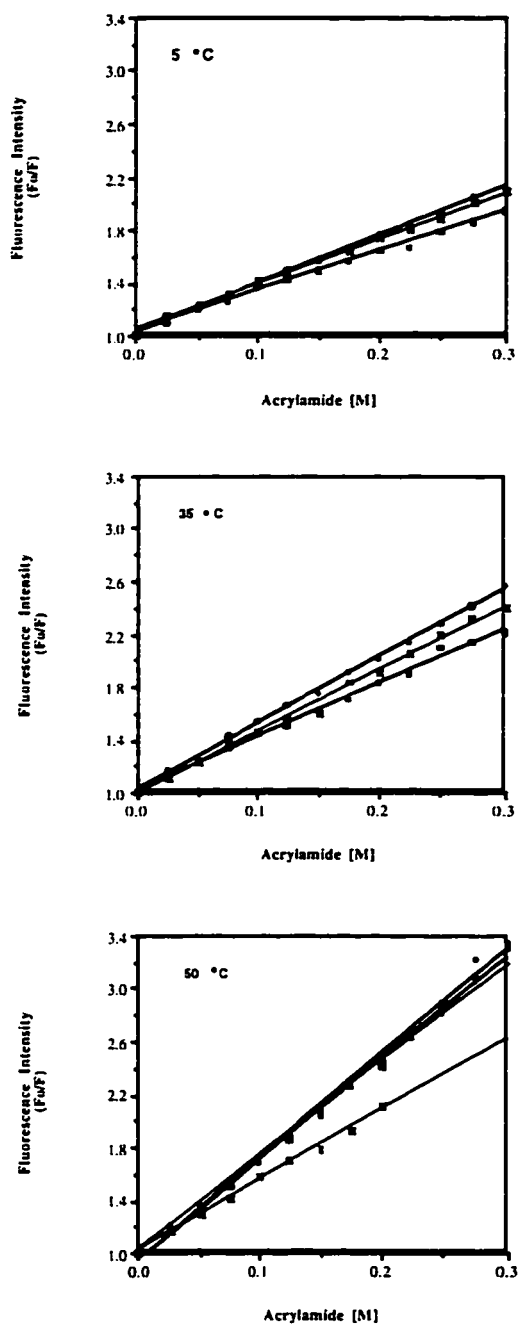


FIGURE 5.4: Stern-Volmer plots determined at 5 °C (top), 35 °C (middle), and 50 °C (bottom). Data for the proteins are depicted by: black (wild-type), blue (S18D), red (S18C/R47C_{ox}), and green (S18C/R47C_{red}). Each data set was fit to a linear equation.

Table 5.1: Acrylamide Quenching Parameters for Cytochrome b₅

	λ_{mass} (nm) ^a	K_{SV} 5 °C (M ⁻¹)	K_{SV} 35 °C (M ⁻¹)	K_{SV} 50 °C (M ⁻¹)
wild-type	339.8	3.69 (0.15) ^b	5.05 (0.08)	7.85 (0.37)
S18D	338.8	2.98 (0.14)	4.04 (0.03)	7.66 (0.06)
S18C/R47C _{ox}	338.5	3.46 (0.18)	4.71 (0.02)	5.32 (0.31)
S18C/R47C _{red}	338.9			7.22 (0.18)

^a Determined from integrating the area under the curve from 310 nm – 370 nm, and termed the spectral center of mass as defined in the Materials and Methods.

^b Standard deviations are shown in parentheses.

5.3.2 Fluorescence Lifetimes

The largest difference in steady-state results appeared in the wild-type and oxidized disulfide forms of cytochrome b₅ at 25 °C and 50 °C. In order to differentiate the fluorescence properties of these two proteins at these temperatures, fluorescence lifetimes were determined at 340 nm, near the λ_{max} of cytochrome b₅. Due to the low quantum yield of the protein, it was not possible to determine phase and modulation data at wavelengths with lower emission intensities. Examples of the phase and modulation data for wild-type and S18C/R47C at 50 °C are shown in Figure 5.5. Both proteins were best fit to a triple exponential decay scheme, based on χ^2 values and weighted residuals (Table 5.2). The mean-lifetimes and related parameters are also reported. The data have were not globally analyzed; the lifetimes and fractional intensities, and fractional amplitudes were determined as individual data sets. At 25 °C, both proteins had similar lifetime components of approximately 0.08 ns, 1.43 ns, and 4.96 ns. The population distribution as determined

by the amplitudes (α_i) of each component did not significantly differ, with the largest contribution (~81%) from the short-lifetime component. The S18C/R47C_{ox} protein had a slightly lower (by 14%) short-lifetime (α_1) and a slightly higher (by 8%) median-lifetime (α_2). At increased temperatures (50 °C), the median- and long-lifetimes of each protein decreased, while the shortest component remained the same as at lower temperatures. Quenching rate constants were not determined for the individual lifetime components and therefore the mean-lifetimes were used to calculate the bimolecular rate constants, k_q , for the steady-state quenching reaction (Table 5.2). At 25 °C, k_q was similar for each protein. At 50 °C, the k_q for S18C/R47C_{ox} was 2.2-fold lower than in wild-type.

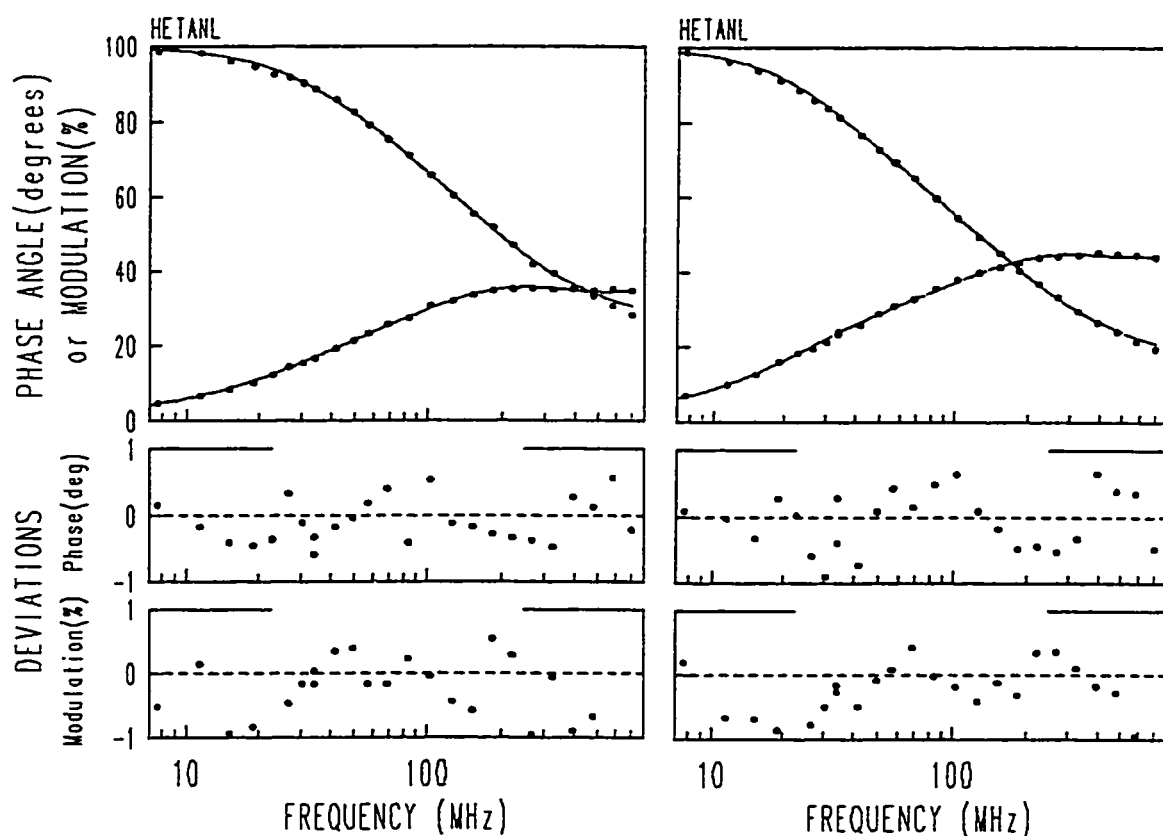


FIGURE 5.5: Phase and modulation data for wild-type (l) and S18C/R47C (r) at 50 °C.

Table 5.2: Fluorescence Lifetime Data Analysis

protein	temp	$\langle \tau \rangle$ (ns) ^a	f_1, f_2, f_3^b	τ_1, τ_2, τ_3 (ns)	$\alpha_1, \alpha_2, \alpha_3^c$	χ^2	k_q (x 10 ⁹ M ⁻¹ s ⁻¹)
wild-type	25 °C	3.01	0.177 0.301 0.522	0.082 1.498 4.878	0.875 0.082 0.043	1.18	1.67
S18C/R47C _{ox}		3.60	0.075 0.290 0.635	0.078 1.368 5.032	0.739 0.163 0.097	2.96	1.12
wild-type	50 °C	1.72	0.261 0.435 0.303	0.076 1.230 3.839	0.888 0.092 0.021	1.33	4.56
S18C/R47C _{ox}		2.57	0.157 0.358 0.485	0.093 1.189 4.402	0.804 0.143 0.052	1.52	2.07

^aMean-lifetime equals $\sum_i f_i \tau_i$.
^cNormalized fractional steady-state intensities.
^bNormalized fractional amplitudes.

5.4 Discussion

We began with the hypothesis that rationally designed mutations in cytochrome b_5 should perturb localized surface dynamics predicted by MD simulations to form a putative cleft region (Storch and Daggett, 1995). In order to challenge this hypothesis, the single Trp 22 located in the area of interest was exploited as a probe of dynamics (Storch and Daggett, 1995). The present results were consistent with this hypothesis. In the two mutants, S18D and S18C/R47C_{ox}, designed to perturb dynamics in the putative cleft region and restrict solvent accessibility to Trp 22, the steady-state fluorescence spectra were blue-shifted relative to the wild-type. Acrylamide quenching studies at different temperatures showed decreased solvent accessibility of Trp in the mutant proteins; particularly at elevated temperatures. Furthermore, from fluorescence lifetime measurements the bimolecular quenching rate constant was calculated to be lower in the disulfide mutant relative to the wild-type protein.

Cytochrome b_5 is ideal for the fluorescence studies presented here. It is a single Trp containing protein and the Trp is conveniently located near the dynamic cleft area of interest. MD simulations have shown that the backbone of Trp 22 is accessible to solvent through the proposed cleft region at the core 1/2 interface shown in Figure 5.1 (Storch and Daggett, 1995). The sidechain of Trp 22 has limited solvent accessibility through core 2. Because of the rigidity of this core even in the apoprotein (Moore et al., 1991; Moore and Lecomte, 1990), solvent accessibility through this route should not differ in the wild-type and mutant proteins, since the mutations should only affect cleft dynamics at the core 1/2 interface.

Steady-state fluorescence revealed the S18D and S18C/R47C_{ox} mutants to have slightly blue-shifted emission spectra relative to wild-type protein. The emission spectrum is a direct indicator of local environmental effects on the excited-state of the fluorophore.

In comparing two proteins, a blue-shifted spectrum may be due to decreased solvent relaxation effects with the excited-state dipole. Other factors may contribute to spectral shifts and it is therefore necessary to further probe the physical origins of spectral changes through techniques such as quenching and excited-state lifetime measurements.

The steady-state emission spectrum is an average emission resulting from the entire excited-state population. If the population distribution changes, the steady-state spectrum changes. Several techniques exist that allow the distribution of excited-states to be probed. Solute quenching is a technique that measures physical encounters of the quencher with the fluorophore excited-state. If the fluorophore is physically inaccessible to a quencher, as in the case of a buried tryptophan, quenching is decreased. If the fluorophore is in an environment that does not stabilize the excited-state, such as a solvent inaccessible environment, the excited-state lifetime is shorter and has a decreased probability of coming into physical contact with the quencher. Furthermore, quenchers may gain increased access to seemingly buried fluorophores through protein fluctuations. Therefore quenching reveals the extent of solvent accessibility of Trp residues and hence may reveal information regarding protein dynamics.

Acrylamide was chosen as a quencher because it is a small neutral molecule that gains access to protein cores and is useful for probing changes in accessibility of buried Trp residues. A Stern-Volmer analysis of the acrylamide quenching results presented here supported the hypothesis of decreased Trp solvent accessibility in the mutant proteins designed to perturb cleft dynamics. Thermal fluctuations are temperature dependent, and it was not inconsistent with the hypothesis that at low temperatures (5 °C), the solvent accessibility of Trp 22 was similar in the wild-type and mutant proteins. As the temperature increased, so did the thermal fluctuations, and differences in acrylamide accessibility for each protein became more apparent. At increased temperatures (50 °C), the data suggested that the salt bridge added little to constrain cleft dynamics, resulting in

similar Trp accessibility in S18D and wild-type proteins. Because of the covalent nature of the disulfide bond, however, the solvent accessibility of Trp 22 in S18C/R47C_{ox} was remarkably lower than the other proteins. As further evidence that the engineered disulfide bond impeded solvent accessibility of Trp 22, the results of the reduced form of the protein were similar to wild-type and S18D.

Because the steady-state emission spectrum is the result of a population of excited-states with different lifetimes and intensities, acrylamide apparently quenches the excited-states with the longer lifetimes preferentially. As the excited-state lifetime increases, there is an increased probability of a physical encounter with the quencher. In general, longer lifetime components have red-shifted emission spectra relative to their shorter counterparts, and therefore a predominantly blue-shifted spectrum should result after quencher is added if the longer lifetimes are being preferentially quenched. This is exactly what we observed in the quenching experiments (data not shown).

Excited-state lifetime measurements allowed for the determination of bimolecular rate constants (k_q) of steady-state quencher-fluorophore interactions. We expected to see a decreased k_q for S18C/R47C_{ox} relative to the wild-type due to decreased diffusion of the quencher through the proposed cleft region as a consequence of the disulfide bond. The lack of difference in the rate constants for the two proteins at 25 °C was not surprising, given that at 35 °C there was little difference in steady-state quenching results. At 50 °C, the expected difference was observed. Specifically, at 50 °C acrylamide has a 2.5-fold greater rate of diffusion in the wild-type relative to S18C/R47C_{ox}. The rate increase was small, but consistent with the hypothesis. The results further supported the interpretation that the increased K_{SV} in the steady-state quenching experiments was due to an increased diffusion rate, possibly through the putative cleft region, in the wild-type protein.

It was difficult to interpret the lifetime amplitudes (α_i) other than the overwhelming amplitude of the short-lifetime was expected because of the large degree of quenching due

to the prosthetic heme group. Assuming that the multiple excited-state lifetimes reflected ground-state heterogeneity, the preponderance of the short-lifetime component for each of the proteins presumably resulted from Trp 22 conformations that effectively transferred excitation energy to the heme co-factor, as observed for essentially all heme proteins. In light of the experimental data, we expected to see similar lifetimes (τ_i) when comparing the wild-type and mutants, but different amplitudes reflecting changes in population distributions due to the changed Trp microenvironment. In summary, the two proteins had similar lifetimes, and the observed differences in amplitudes were not significant.

5.5 Conclusions

As a whole, the fluorescence results indicated that the microenvironment of Trp 22 differed in the wild-type and mutant forms of cytochrome b_5 designed to alter cleft dynamics. The differences reflected in the results strongly suggested a decrease in Trp solvent accessibility for the mutant proteins, particularly in the case of S18C/R47C_{ox}.

The results were consistent with a model system, originally predicted by MD simulations (Storch and Daggett, 1995), described by an equilibrium between “opened” and “closed” cleft conformations in the wild-type protein as depicted in Figure 5.2. With increasing temperature, the large thermal fluctuations of the cleft region allowed increased solvent accessibility of the Trp backbone. The introduction of the constraining mutations, however, restricted the structurally labile cleft area and therefore solvent accessibility of the Trp was gained through other fluctuating areas considerably less dynamic in nature than the cleft region.

Based on the fluorescence studies alone, the definitive structural effects of the mutations on the cleft dynamics were not completely conclusive and therefore the results from these studies warrant further experimental investigations.

BIBLIOGRAPHY

- Agashe, V. R., and Udgaonkar, J. B. (1995) Thermodynamics of denaturation of barstar: Evidence for cold denaturation and evaluation of the interaction with guanidine hydrochloride. *Biochemistry* 34, 3286-3299.
- Altman, J., Lipka, J. J., Kuntz, I., and Waskell, L. (1989) Identification by proton nuclear magnetic resonance of the histidines in cytochrome b₅ modified by diethyl pyrocarbonate. *Biochemistry* 28, 7516-7523.
- Beck von Bodman, S., Schuler, M. A., Jollie, D. R., and Sligar, S. G. (1986) Synthesis, bacterial expression, and mutagenesis of the gene coding for mammalian cytochrome b₅. *Proc. Natl. Acad. Sci. USA* 83, 9443-9447.
- Bernardi, P., and Azzone, G. F. (1981) Cytochrome c as an electron shuttle between the outer and inner mitochondrial membranes. *J. Biol. Chem.* 256, 7187-7192.
- Betz, S. F., Marmorino, J. L., Saunders, A. J., Doyle, D. F., Young, G. B., and Pielak, G. J. (1996) Unusual effects of an engineered disulfide on global and local protein stability. *Biochemistry* 35, 7422-7428.
- Birch, D. J. S., and Imhof, R. E. (1991) Time-domain fluorescence spectroscopy using time-correlated single-photon counting. In *Topics in Fluorescence Spectroscopy*, J. R. Lakowicz, ed. (New York: Plenum), pp. 1-88.
- Birks, J. B. (1970) In *Photophysics of aromatic molecules* (New York: Wiley-Interscience), pp. 433-447.

- Braatz, J. A., Paulsen, M. D., and Ornstein, R. L. (1992) 3 Nsec molecular dynamics simulation of the protein ubiquitin and comparison with X-ray crystal and solution NMR structures. *J. Biomol. Struct. Dyn.* 9, 935-949.
- Brunne, R. M., Liepinsh, E., Otting, G., and Wüthrich, K. (1993) Hydration of proteins. A comparison of experimental residence times of water molecules solvating the bovine pancreatic trypsin inhibitor with theoretical model calculations. *J. Mol. Biol.* 231, 1040-1048.
- Burch, A. M., Rigby, S. E., Funk, W. D., and MacGillivray, R. T. (1990) NMR characterization of surface interactions in the cytochrome b₅-cytochrome c complex. *Science* 247, 831-833.
- Burstein, E. A., Vedenkina, N. S., and Ivkova, M. N. (1973) Fluorescence and the location of tryptophan residues in protein molecules. *Photochem. Photobiol.* 18, 263-279.
- Careaga, C. L., and Falke, J. J. (1992) Structure and dynamics of Escherichia coli chemosensory receptors. Engineered sulfhydryl studies. *Biophys. J.* 62, 209-219.
- Careaga, C. L., and Falke, J. J. (1992) Thermal motions of surface alpha-helices in the D-galactose chemosensory receptor. Detection by disulfide trapping. *J. Mol. Biol.* 226, 1219-1235.
- Chandrasekhar, I., Clore, G. M., Szabo, A., and Gronenborn, A. M. (1992) A 500 ps molecular dynamics simulation study of interleukin-1 beta in water. Correlation with nuclear magnetic resonance spectroscopy and crystallography. *J. Mol. Biol.* 226, 239-350.

- Cherfils, J., Duquerroy, S., and Janin, J. (1991) Protein-protein recognition analyzed by docking simulation. *Proteins 11*, 271-280.
- Clarke, J., Henrick, K., and Fersht, A. R. (1995) Disulfide mutants of barnase I: Changes in stability and structure assessed by biophysical methods and X-ray crystallography. *J. Mol. Biol.* 253, 493-504.
- Clore, G. M., Gronenborn, A. M., James, M. N., Kjaer, M., McPhalen, C. A., and Poulsen, F. M. (1987) Comparison of the solution and X-ray structures of barley serine proteinase inhibitor 2. *Protein Eng.* 1, 313-318.
- Coligan, J. E., Dunn, B. M., Ploegh, H. L., Speicher, D. W., and Wingfield, P. T. (1996). In *Current Protocols in Protein Science*, J. E. Coligan, Dunn, B.M., Ploegh, H.L., Speicher, D.W., and Wingfield, P.T., eds. (John Wiley and Sons, Inc.), pp. 15.1.3.
- Daggett, V., Kollman, P. A., and Kuntz, I. D. (1991) A molecular dynamics simulation of polyalanine: An analysis of equilibrium motions and helix-coil transitions. *Biopolymers* 31, 1115-1134.
- Daggett, V., and Levitt, M. (1992) A model of the molten globule state from molecular dynamics simulations. *Proc. Natl. Acad. Sci. USA* 89, 5142-5146.
- Daggett, V., and Levitt, M. (1992) Molecular dynamics simulations of helix denaturation. *J. Mol. Biol.* 223, 1121-1138.
- Dailey, H. A., and Strittmatter, P. (1979) Modification and identification of cytochrome b₅ carboxyl groups involved in protein-protein interaction with cytochrome b₅ reductase. *J. Biol. Chem.* 254, 5388-5396.

- Eftink, M. R., and Ghiron, C. A. (1976) Exposure of tryptophanyl residues in proteins. Quantitative determination by fluorescence quenching studies. *Biochemistry* 15, 672-680.
- Eftink, M. R., and Ghiron, C. A. (1976) Fluorescence quenching of indole and model micelle systems. *J. Phys. Chem.* 80, 486-493.
- Eftink, M. R., and Ghiron, C. A. (1981) Fluorescence quenching studies with proteins. *Analytical Biochemistry* 114, 199-227.
- Falke, J. J., and Koshland, J., D.E. (1987) Global flexibility in a sensory receptor: A site-directed cross-linking approach. *Science* 237, 1596-1600.
- Falzone, C. J., Mayer, M. R., Whiteman, E. L., Moore, C. D., and Lecomte, J. T. J. (1996) Design challenges for hemoproteins: The solution structure of apocytochrome b₅. *Biochemistry* 35, 6519-6526.
- Feng, Y., Sligar, S. G., and Wand, A. J. (1994) Solution structure of apocytochrome b₅₆₂. *Nat. Struct. Biol.* 1, 30-35.
- Feng, Y. Q., and Sligar, S. G. (1991) Effect of heme binding on the structure and stability of *Escherichia coli* apocytochrome b₅₆₂. *Biochemistry* 30, 10150-10155.
- Feng, Y. Q., Wand, A. J., and Sligar, S. G. (1991) ¹H and ¹⁵N NMR resonance assignments and preliminary structural characterization of *Escherichia coli* apocytochrome b₅₆₂. *Biochemistry* 30, 7711-7717.
- Gonzalez, F. J., and Kasper, C. B. (1980) Phenobarbital induction of NADPH-cytochrome c (P-450) oxidoreductase messenger ribonucleic acid. *Biochemistry* 19, 1790-1796.

- Guiles, R. D., Altman, J., Kuntz, I. D., and Waskell, L. (1990) Structural studies of cytochrome b_5 : Complete sequence-specific resonance assignments for the trypsin-solubilized microsomal ferrocycytochrome b_5 obtained from pig and calf. *Biochemistry* 29, 1276-1289.
- Guiles, R. D., Basus, V. J., Kuntz, I. D., and Waskell, L. (1992) Sequence-specific ^1H and ^{15}N resonance assignments for both equilibrium forms of the soluble heme binding domain of rat ferrocycytochrome b_5 . *Biochemistry* 31, 11365-11375.
- Hara, T., and Minakami, S. (1970) Presence of apocycytochrome b_5 in microsomes. Incorporation of radioactive heme to the cytochrome *in vitro*. *J. Biochem. Tokyo* 67, 741-743.
- Hara, T., Tanaka, S., and Minakami, S. (1970) Incorporation of radioactive iron into cytochrome b_5 and cytochrome P-450 of liver microsomes. *J. Biochem. Tokyo* 68, 805-810.
- Harris, D. L., and Hudson, B. S. (1991) Fluorescence and molecular dynamics study of the internal motion of the buried tryptophan in bacteriophage T4 lysozyme: Effects of temperature and alteration of nonbonded networks. *Chem. Physics* 158, 353-383.
- Hartshorn, R. T., Mauk, A. G., Mauk, M. R., and Moore, G. R. (1987) NMR study of the interaction between cytochrome b_5 and cytochrome c. *FEBS Letters* 213, 391-395.
- Hegesh, E., Hegesh, J., and Kaftory, A. (1986) Congenital methemoglobinemia with a deficiency of cytochrome b_5 . *N. Engl. J. Med.* 314, 757-761.

- Henry, E. R., Levitt, M., and Eaton, W. A. (1985) Molecular dynamics simulation of photodissociation of carbon monoxide from hemoglobin. *Proc. Natl. Acad. Sci. U.S.A.* 82, 2034-2038.
- Herskovits, T. T., and Sorensen, M. (1968) Studies of the location of tyrosyl and tryptophyl residues in proteins. I. Solvent perturbation data of model compounds. *Biochemistry* 7, 2523-2532.
- Hewson, R., Newbold, R. J., and Whitford, D. (1993) The expression of bovine microsomal cytochrome b₅ in *Escherichia coli* and a study of the solution structure and stability of variant proteins. *Protein Engineering* 6, 953-964.
- Hong, M. K., Braunstein, D., Cowen, B. R., Fraenfelder, H., Iben, I. E., Mourant, J. R., Ormos, P., Scholl, R., Schulte, A., Steinbach, P. J., Xie, A., and Young, R. D. (1990) Conformational substates and motions in myoglobin. External influences on structure and dynamics. *Biophys. J.* 58, 429-436.
- Housset, D., Kim, K. S., Fuchs, J., Woodward, C., and Wlodawer, A. (1991) Crystal structure of a Y35G mutant of bovine pancreatic trypsin inhibitor. *J. Mol. Biol.* 220, 757-770.
- Hua, Q., and Weiss, M. A. (1990) Toward the solution structure of human insulin: Sequential 2D-¹H NMR assignment of a des-pentapeptide analogue and comparison with crystal structure. *Biochemistry* 29, 10545-10555.
- Hultquist, D. E., Dean, R. T., and Douglas, R. H. (1974) Homogeneous cytochrome b₅ from human erythrocytes. *Biochem. Biophys. Res. Commun.* 60, 28-34.

- Hultquist, D. E., and Passon, P. G. (1971) Catalysis of methaemoglobin reduction by erythrocyte cytochrome b_5 and cytochrome b_5 reductase. *Nat. New Biol.* 229, 252-254.
- Huntley, T. E., and Strittmatter, P. (1972) The effect of heme binding on the tryptophan residue and the protein conformation of cytochrome b_5 . *Journal of Biological Chemistry* 247, 4641-4647.
- Jablonski, A. (1935) Über den Mechanismus des Photolumineszenz von Farbstoffphosphoren. *Z. Phys.* 94, 38-46.
- Jones, M. S., and Jones, O. T. (1969) The structural organization of haem synthesis in rat liver mitochondria. *Biochem. J.* 113, 507-514.
- Kabsch, W. (1976) A solution for the best rotation to relate two sets of vectors. *Acta Crystallogr. sect. A* 32, 922-923.
- Kanaya, S., Katsuda, C., Kimura, S., Nakai, T., Kitakuni, E., Nakamura, H., Katayanagi, K., Morikawa, K., and Ikehara, M. (1991) Stabilization of *Escherichia coli* ribonuclease H by introduction of an artificial disulfide bond. *J. Biol. Chem.* 266, 6038-6044.
- Kell, G. S. (1967) Precise representation of volume properties of water at one atmosphere. *J. Chem. Eng. Data* 12, 66-69.
- Kitagawa, T., Sugiyama, T., and Yamano, T. (1982) Differences in stability against thermal unfolding between trypsin- and detergent-solubilized cytochromes b_5 and structural changes in the heme vicinity upon the transition: Resonance raman and absorption study. *Biochemistry* 21, 1680-1686.

- Kline, A. D., Braun, W., and Wuthrich, K. (1988) Determination of the complete three-dimensional structure of the alpha-amylase inhibitor tendamistat in aqueous solution by nuclear magnetic resonance and distance geometry. *J. Mol. Biol.* 204, 675-724.
- Kraulis, P. (1991) MOLSCRIPT: A program to produce both detailed and schematic plots of proteins. *J. Appl. Crystallogr.* 24, 946-950.
- Krieter, P. A., and Shires, T. K. (1980) Cell-free translation of apocytochrome b₅ messenger RNA and analysis of the peptide product. *Biochem. Biophys. Res. Commun.* 94, 606-611.
- Laczko, G., Gryczynski, I., Gryczynski, Z., Wicz, W., Malak, H., and Lakowicz, J. R. (1990) A 10-GHz frequency-domain fluorometer. *Rev. Sci. Instrum.* 61, 2331-2337.
- Laidig, K. E., and Daggett, V. (1996) Molecular dynamics simulations of apocytochrome b₅₆₂: A "highly ordered" molten globule. *Folding and Design* 1, 353-364.
- Laidig, K. E., and Daggett, V. (1996) Testing the modified hydration-shell hydrogen-bond model of hydrophobic effects using molecular dynamics simulation. *J. Phys. Chem.* 100, 5616-5619.
- Lakowicz, J. R. (1989) Principles of frequency-domain fluorescence spectroscopy and applications to protein fluorescence. In *Cell Structure and Function by Microspectrofluorometry* (New York: Academic Press), pp. 163-183.
- Lakowicz, J. R. (1983) Quenching of Fluorescence. In *Principles in Fluorescence Spectroscopy* (New York: Plenum), pp. 258-297.

- Lakowicz, J. R., Cherek, H., Gryczynski, I., Joshi, N., and Johnson, M. L. (1987) Analysis of fluorescence decay kinetics measured in the frequency domain using distributions of decay times. *Biophys. Chem.* 28, 35-50.
- Lakowicz, J. R., and Gryczynski, I. (1991) Frequency-domain fluorescence spectroscopy. In *Topics in Fluorescence Spectroscopy*, J. R. Lakowicz, ed. (New York: Plenum), pp. 293-331.
- Lakowicz, J. R., and Weber, G. (1973) Quenching of protein fluorescence by oxygen. Detection of structural fluctuations in proteins on the nanosecond time scale. *Biochemistry* 12, 4171-4179.
- Lecomte, J. T. J., and Moore, C. D. (1991) Helix formation in apocytochrome b₅: The role of a neutral histidine at the N-cap position. *J. Am. Chem. Soc.* 113, 9663-9665.
- Lee, B., and Richards, F. M. (1971) The interpretation of protein structures: estimation of static accessibility. *J. Mol. Biol.* 55, 379-400.
- Lehrer, S. S. (1971) Solute perturbation of protein fluorescence. The quenching of the tryptophyl fluorescence of model compounds and of lysozyme by iodide ion. *Biochemistry* 10, 3254-3263.
- Levitt, M. (1990) *ENCAD-Energy Calculation and Dynamics* (Palo Alto, CA: Molecular Applications Group).
- Levitt, M. (1989) Molecular dynamics of macromolecules in water. *Chemica Scripta* 29A, 197-203.

- Levitt, M., Hirshberg, M., Sharon, R., and Daggett, V. (1995) Potential energy function and parameters for simulations of the molecular dynamics of proteins and nucleic acids in solution. *Computer Physics Communications* 91, 215-231.
- Levitt, M., Hirshberg, M., Sharon, R., Laidig, K. E., and Daggett, V. (1997) Calibration and testing of a water model for simulation of the molecular dynamics of proteins and nucleic acids in solution. *Journal of Physical Chemistry B* 101, 5051-5061.
- Levitt, M., and Meirovitch, H. (1983) Molecular dynamics of native proteins. I. Computer simulation of trajectories. *J. Mol. Biol.* 168, 595-620.
- Livingston, D. J., McLachlan, S. J., Mar, G. N. L., and Brown, W. (1985) Myoglobin: Cytochrome b₅ interactions and the kinetic mechanism of metmyoglobin reductase. *J. Biol. Chem.* 260, 15699-15707.
- Mansfeld, J., Vriend, G., Dijkstra, B. W., Veltman, O. R., Van den Berg, B., Venema, G., Ulbrich-Hofmann, R., and Eijssink, V. G. H. (1997) Extreme stabilization of a thermolysin-like protease by an engineered disulfide bond. *J. of Biological Chemistry* 272, 11152-11156.
- Mathews, F. S., Argos, P., and Levine, M. (1972) The structure of cytochrome b₅ at 2.0 Å resolution. *Cold Spring Harbor Symp.* 36, 387-395.
- Mathews, F. S., and Czerwinski, E. W. (1976) In *The Enzymes of Biological Membranes*, Volume 4, A. Martonosi, ed. (New York: Plenum).
- Mathews, F. S., Czerwinski, E. W., and Argos, P. (1979) In *The Porphyrins*, Volume VII, Part B, D. Dolphin, ed. (New York: Academic Press, Inc.).

- Matsumura, M., Signor, G., and Matthews, B. W. (1989) Substantial increase of protein stability by multiple disulfide bonds. *Nature* 342, 291-293.
- Matthew, J. B., Weber, P. C., Salemme, F. R., and Richards, F. M. (1983) Electrostatic orientation during electron transfer between flavodoxin and cytochrome c. *Nature* 301, 169-171.
- Mauk, M. R., and Mauk, A. G. (1989) Crosslinking of cytochrome c and cytochrome b₅ with a water-soluble carbodiimide. Reaction conditions, product analysis and critique of the technique. *Eur. J. Biochem.* 186, 473-486.
- Mauk, M. R., Mauk, A. G., Weber, P. C., and Matthew, J. B. (1986) Electrostatic analysis of the interaction of cytochrome c with native and dimethyl ester heme substituted cytochrome b₅. *Biochemistry* 25, 7085-7091.
- McLachlan, S. J., La Mar, G. N., and Lee, K. B. (1988) One- and two-dimensional nuclear Overhauser effect studies of the electronic/molecular structure of the heme cavity of ferricytochrome b₅. *Biochim. Biophys. Acta* 957, 430-445.
- Meyer, T. E., Rivera, M., Walker, F. A., Mauk, M. R., Mauk, A. G., Cusanovich, M. A., and Tollin, G. (1993) Laser flash photolysis studies of electron transfer to the cytochrome b₅-cytochrome c complex. *Biochemistry* 32, 622-627.
- Mitchinson, C., and Wells, J. A. (1989) Protein engineering of disulfide bonds in subtilisin BPN'. *Biochemistry* 28, 4807-4815.
- Moore, C. D., Al-Misky, O. N., and Lecomte, J. T. J. (1991) Similarities in structure between holocytochrome b₅ and apocytochrome b₅: NMR studies of the histidine residues. *Biochemistry* 30, 8357-8365.

- Moore, C. D., and Lecomte, J. T. J. (1993) Characterization of an independent structural unit in apocytochrome b_5 . *Biochemistry* 32, 199-207.
- Moore, C. D., and Lecomte, J. T. J. (1990) Structural properties of apocytochrome b_5 : Presence of a stable native core. *Biochemistry* 29, 1984-1989.
- Muskett, F. W., Kelly, G. P., and Whitford, D. (1996) The solution structure of bovine ferricytochrome b_5 determined using heteronuclear NMR methods. *J. Mol. Biol.* 258, 172-189.
- Negishi, M., and Omura, T. (1970) Presence of apocytochrome b_5 in microsomes from rat liver. *J. Biochem. Tokyo* 67, 745-747.
- Newbold, R. J., Hewson, R., and Whitford, D. (1992) The thermal stability of the tryptic fragment of bovine microsomal cytochrome b_5 and a variant containing six additional residues. *FEBS* 314, 419-424.
- Newbold, R. J., and Whitford, D. (1997) The thermal stability of cytochrome b_5 . *Biochem. Soc. Trans.* 25, 57S.
- Ng, S., Smith, M. B., Smith, H. T., and Millet, F. (1977) Effect of modification of individual cytochrome c lysines on the reaction with cytochrome b_5 . *Biochemistry* 16, 4975-4978.
- Okayasu, T., Ono, T., and Shinogima, K. (1977) Involvement of cytochrome b_5 in the oxidative desaturation of linoleic acid to gamma-linoleic acid in rat liver microsomes. *Lipids* 12, 267-271.
- Ozols, J. (1989) Structure of cytochrome b_5 and its topology in the microsomal membrane. *Biochimica et Biophysica Acta* 997, 121-130.

- Ozols, J., Gerard, C., and Nobrega, F. G. (1976) Proteolytic cleavage of horse liver cytochrome b₅. Primary structure of the heme-containing moiety. *J. Biol. Chem.* 251, 6767-6774.
- Pace, C. N. (1986) Determination and analysis of urea and guanidine hydrochloride denaturation curves. *Methods in Enzymology* 131, 266-280.
- Pelletier, H., and Kraut, J. (1992) Crystal structure of a complex between electron transfer partners, cytochrome c peroxidase and cytochrome c. *Science* 258, 1748-1755.
- Pfeil, W. (1993) Thermodynamics of apocytochrome b₅ unfolding. *Protein Science* 2, 1497-1501.
- Pfeil, W., and Bendzko, P. (1980) Thermodynamic investigations of cytochrome b₅ unfolding. I. Tryptic fragment of cytochrome b₅. *Biochim. Biophys. Acta* 626, 73-78.
- Pflugrath, J. W., Wiegand, G., Huber, R., and Vertesy, L. (1986) Crystal structure determination, refinement and the molecular model of the alpha-amylase inhibitor Hoe-467A. *J. Mol. Biol.* 189, 383-386.
- Poulos, T. L., and Mauk, A. G. (1983) Models for the complexes formed between cytochrome b₅ and the subunits of methemoglobin. *J. Biol. Chem.* 258, 7369-7373.
- Reid, L. S., Gray, H. B., Dalvit, C., Wright, P. E., and Saltman, P. (1987) Electron transfer from cytochrome b₅ to iron and copper complexes. *Biochemistry* 26, 7102-7107.
- Rodgers, K. K., Pochapsky, T. C., and Sligar, S. G. (1988) Probing the mechanisms of macromolecular recognition: The cytochrome b₅-cytochrome c complex. *Science* 240, 1657-1659.

- Rodgers, K. K., and Sligar, S. G. (1991) Mapping electrostatic interactions in macromolecular associations. *J. Mol. Biol.* 221, 1453-1460.
- Royer, C., Gardner, J., Beechem, J. M., Brochon, J. C., and Mathews, K. S. (1990) Resolution of the intrinsic fluorescence decay kinetics of the two tryptophan residues of *E. coli lac* repressor using genetically engineered single tryptophan mutants. *Biophys. J.* 58, 363-373.
- Salemme, F. R. (1976) An hypothetical structure for an intermolecular electron transfer complex of cytochromes c and b₅. *J. Mol. Biol.* 102, 563-568.
- Sambrook, J. E., Fritsch, E. F., and Maniatis, T. (1989) In *Molecular Cloning: A Laboratory Manual* (Cold Spring Harbor, NY: Cold Spring Harbor Laboratory Press).
- Schenkman, J. B., and Greim, H. (1993) In *Cytochrome P450*, J. B. Schenkman and H. Greim, eds. (Berlin: Springer-Verlag).
- Shawver, L. K., Seidel, S. L., Krieter, P. A., and Shires, T. K. (1984) An enzyme-linked immunoabsorbent assay for measuring cytochrome b₅ and NADPH-cytochrome P-450 reductase in rat liver microsomal fractions. Evidence for functionally inactive protein. *Biochem. J.* 217, 623-632.
- Shortle, D. (1995) Staphylococcal nuclease: A showcase of m-value effects. *Adv Protein Chem* 46, 217-247.
- Smith, J. L., Hendrickson, W. A., Honzatko, R. B., and Sheriff, S. (1986) Structural heterogeneity in protein crystals. *Biochemistry* 25, 5018-5027.
- Stayton, P. S., Fisher, M. T., and Sligar, S. G. (1988) Determination of cytochrome b₅ association reactions. *J. Biol. Chem.* 263, 13544-13548.

- Stayton, P. S., Poulos, T. L., and Sligar, S. G. (1989) Putidaredoxin competitively inhibits cytochrome b_5 -cytochrome P-450_{cam} association: A proposed molecular model for a cytochrome P-450_{cam} electron-transfer complex. *Biochemistry* 28, 8201-8205.
- Stokes, G. G. (1852) On the change of refrangibility of light. *Phil. Trans. R. Soc. London* 142, 463-562.
- Stonehuerner, J., Williams, J. B., and Millett, F. (1979) Interaction between cytochrome c and cytochrome b_5 . *Biochemistry* 18, 5422-5427.
- Storch, E. M., and Daggett, V. (1995) Molecular dynamics simulation of cytochrome b_5 : Implications for protein-protein recognition. *Biochemistry* 34, 9682-9693.
- Storch, E. M., and Daggett, V. (1996) Structural consequences of heme removal: Molecular dynamics simulations of rat and bovine apocytochrome b_5 . *Biochemistry* 35, 11596-11604.
- Storch, E. M., Daggett, V., and Atkins, W. M. (a) Controlling dynamics of a cleft on the surface of cytochrome b_5 through rational mutagenesis: A steady-state and time-resolved fluorescence study. *In preparation*.
- Storch, E. M., Daggett, V., Lim, K., and Atkins, W. M. (b) Engineering out motion: Introduction of a *de novo* disulfide and salt bridge designed to close a dynamic cleft on the surface of cytochrome b_5 . *In preparation*.
- Strittmatter, P. (1964) In *Rapid Mixing and Sampling Techniques in Biochemistry*, E. Chance, Gibson, Lundberg-Holmes, ed. (New York: Academic Press).

- Strittmatter, P., Hackett, C. S., Korza, G., and Ozols, J. (1990) Characterization of the covalent cross-links of the active sites of amidinated cytochrome b_5 and NADH:cytochrome b_5 reductase. *J. Biol. Chem.* 265, 21709-21713.
- Strittmatter, P., Spatz, L., Corcoran, D., Rogers, M. J., Setlow, B., and Redline, R. (1974) Purification and properties of rat liver microsomal stearyl coenzyme A desaturase. *Proc. Natl. Acad. Sci. U.S.A.* 71, 4565-4569.
- Tainer, J. A., Getzoff, E. D., Alexander, H., Houghten, R. A., Olson, A. J., Lerner, R. A., and Hendrickson, W. A. (1984) The reactivity of anti-peptide antibodies is a function of the atomic mobility of sites in a protein. *Nature* 312, 127-134.
- Tajima, S., Enomoto, K. I., and Soto, R. (1976) Denaturation of cytochrome b_5 by guanidine hydrochloride: Evidence for independent folding of the hydrophilic and hydrophobic moieties of the cytochrome molecule. *Arch. Biochem. Biophys.* 172, 90-97.
- Takagi, H., Takahashi, T., Momose, H., Inouye, M., Maeda, Y., Matsuzawa, H., and Ohta, T. (1990) Enhancement of the thermostability of subtilisin E by introduction of a disulfide bond engineered on the basis of structural comparison with a thermophilic serine protease. *J. Biol. Chem.* 265, 6874-6878.
- Tamburini, P. P., White, R. E., and Schenkman, J. B. (1985) Chemical characterization of protein-protein interactions between cytochrome P-450 and cytochrome b_5 . *J. Biol. Chem.* 260, 4007-4015.
- Teale, F. W. J. (1959) Cleavage of the haem-protein link by acid methylethylketone. *Biochem. J.* 35, 543.

- Urbanova, M., Dukor, R. K., Pancoska, P., Gupta, V. P., and Keiderling, T. A. (1991) Comparison of alpha-lactalbumin and lysozyme using vibrational circular dichroism. Evidence for a difference in crystal and solution structures. *Biochemistry* 30, 10479-10485.
- Van den Burg, B., Dijkstra, B. W., Van der Vinne, B., Stulp, B. K., Eijssink, V. G. H., and Venema, G. (1993) Introduction of disulfide bonds into *Bacillus subtilis* neutral protease. *Protein Engineering* 6, 521-527.
- Veitch, N. C., Concar, D. W., Williams, R. J. P., and Whitford, D. (1988) Investigation of the solution structures and mobility of oxidized and reduced cytochrome b_5 by 2-D NMR spectroscopy. *238 I*, 49-55.
- Veitch, N. C., Whitford, D., and Williams, R. J. (1990) An analysis of pseudocontact shifts and their relationship to structural features of the redox states of cytochrome b_5 . *FEBS Letters* 269, 297-304.
- Villafranca, J. E., Howell, E. E., Oatley, S. J., Xuong, N. H., and Kraut, J. (1987) An engineered disulfide bond in dihydrofolate reductase. *Biochemistry* 26, 2182-2189.
- Visser, L., Robinson, N. C., and Tanford, C. (1975) The two-domain structure of cytochrome b_5 in deoxycholate solution. *Biochemistry* 14, 1194-1199.
- Wakarchuk, W. W., Sung, W. L., Campbell, R. L., Cunningham, A., Watson, D. C., and Yaguchi, M. (1994) Thermostabilization of the *Bacillus circulans* xylanase by the introduction of disulfide bonds. *Protein Engineering* 7, 1379-1386.
- Warburg, O., and Negelein, E. (1928) *Biochem. Z.* 193, 339-346.

- Weiss, M. A., Nguyen, D. T., Khait, I., Inouye, K., Frank, B. H., Beckage, M., O'Shea, E., Shoelson, S. E., Karplus, M., and Neuringer, L. J. (1989) Two-dimensional NMR and photo-CIDNP studies of the insulin monomer: Assignment of aromatic resonances with application to protein folding, structure, and dynamics. *Biochemistry* 28, 9855-9873.
- Wells, J. A., and Powers, D. B. (1986) *In vivo* formation and stability of engineered disulfide bonds in subtilisin. *J. Biol. Chem.* 261, 6564-6570.
- Wendoloski, J. J., Matthew, J. B., Weber, P. C., and Salemme, F. R. (1987) Molecular dynamics of a cytochrome c-cytochrome b₅ electron transfer complex. *Science* 238, 794-797.
- Whitford, D. (1992) The identification of cation-binding domains on the surface of microsomal cytochrome b₅ using ¹H-NMR paramagnetic difference spectroscopy. *Eur. J. Biochem.* 203, 211-223.
- Williams, E. J., Herskovits, T. T., and Laskowski, J., M. (1965) *J. Biol. Chem.* 240, 3574.
- Wittekind, M., Rajagopal, P., Branchini, B. R., Reizer, J., Saier, J., M.H., and Klevit, R. E. (1992) Solution structure of the phosphocarrier protein HPr from *Bacillus subtilis* by 2D-NMR spectroscopy. *Protein Science* 1, 1363-1376.
- Wüthrich, K. (1986) In *NMR of Proteins and Nucleic Acids*, (New York: John Wiley and Sons, Inc.).

Curriculum Vitae

Elizabeth Marie Storch

EDUCATION

- Ph.D. Medicinal Chemistry, University of Washington, Seattle
(1992-1998) Dissertation: *Experimental and Computational Investigations of the Stability and Dynamics of Cytochrome b₅*
 Thesis advisors: Dr. Bill Atkins and Dr. Valerie Daggett
- B.S. Chemistry, University of Washington, Seattle
(1988-1992)

RESEARCH and WORK EXPERIENCE

- (1992-1998) Research Assistant (Advisors: Dr. Bill Atkins and Dr. Valerie Daggett)
 Department of Medicinal Chemistry, U of W, Seattle
- Studied the solution structure and dynamics of cytochrome b₅ using molecular dynamics simulations, molecular modeling, protein engineering, purification, absorbance and fluorescence spectroscopies, gel electrophoresis, and MALDI-TOF mass spectrometry.
- (1993-1994) Teaching Assistant
 Department of Medicinal Chemistry, U of W, Seattle
- Responsible for teaching a study section in Medicinal Chemistry course series to fourth year Pharmacy students.
- (1991-1992) Research Assistant (Advisor: Dr. Allan Rettie)
 Department of Medicinal Chemistry, U of W, Seattle
- Studied the drug metabolism of (R)- and (S)-mephénytoin in human liver microsomes using HPLC, gas chromatography, synthesis, and EI-mass spectrometry.

(1989-1991) Research Assistant (Advisor: Dr. Elaine Faustman)
 Department of Toxicology, U of W, Seattle

Studied the teratogenic effects of various environmental chemicals in rat fetuses.

RESEARCH INTERESTS

Studying the relationship between protein structure and biological function using protein engineering, protein characterization, and molecular modeling.

AWARDS

1997-1998 Hope Barnes Graduate Fellowship

PUBLICATIONS

Storch, E.M. and Daggett, V. (1995) Molecular dynamics simulation of cytochrome b_5 : Implications for protein-protein recognition. *Biochemistry* 34, 9682-9693.

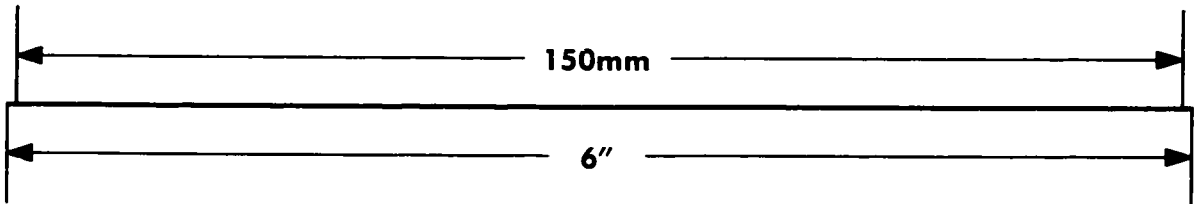
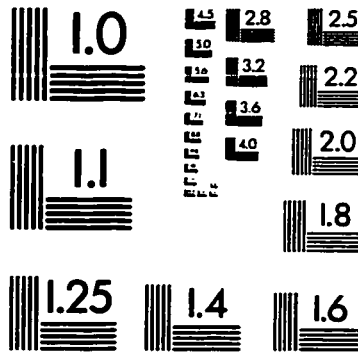
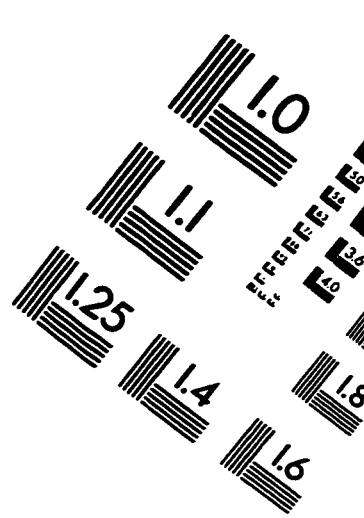
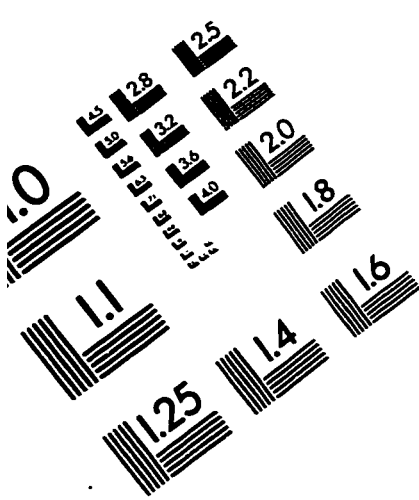
Storch, E.M. and Daggett, V. (1996) Structural consequences of heme removal: Molecular dynamics simulations of rat and bovine apocytochrome b_5 . *Biochemistry* 35, 11596-11604.

Wienkers, L.C., Wurden, C.J., **Storch, E.**, Kunze, K.L., Rettie, A.E., and Trager, W.F. (1996) Formation of (R)-8-hydroxywarfarin in human liver microsomes: A new metabolic marker for the (S)-mephenytoin hydroxylase, P450 2C19. *Drug Metabolism and Disposition* 24, 610-614.

Storch, E.M., Lim, K., Daggett, V, and Atkins, W.M. Engineering out motion: Introduction of a *de novo* disulfide bond and a salt bridge designed to close a putative dynamic cleft on the surface of cytochrome b_5 . *In preparation*.

Storch, E.M. and Atkins, W.M. Controlling the dynamics of a cleft on the surface of cytochrome b_5 through rational mutagenesis: A steady-state and time-resolved fluorescence study. *In preparation*.

IMAGE EVALUATION TEST TARGET (QA-3)



APPLIED IMAGE, Inc
1653 East Main Street
Rochester, NY 14609 USA
Phone: 716/482-0300
Fax: 716/288-5989

© 1993, Applied Image, Inc., All Rights Reserved

